THE THEORY OF PULSED NEUTRON EXPERIMENTS IN POLYCRYSTALLINE MODERATORS

Thesis by

Robert Conn

In Partial Fulfillment of the Requirements

For the Degree of

Doctor of Philosophy

California Institute of Technology

Pasadena, California

1968

(Submitted April 30, 1968)

ACKNOWLEDGMENTS

I would like to thank my thesis advisor, Dr. Noel Corngold, for the guidance he provided during the course of this research. In addition I express my gratitude to Dr. Jerome Shapiro for introducing me to the subject of pulsed neutrons and for several stimulating discussions concerning this research; and to Dr. Anthony Leonard for his assistance during the time this research was begun.

My graduate study at the Institute was supported, from 1964 to 1966, by the National Science Foundation through its graduate fellowship program, and, from 1966 to 1968, by the Atomic Energy Commission which provided a Special Fellowship in Nuclear Science and Engineering. Also, I want to acknowledge the support of the Ford Foundation which provided a research grant for the summer of 1965 and which made additional funds available to me through its forgivable loan program. To the administrators of these sources of support, I express my thanks.

ABSTRACT

This thesis is a theoretical investigation of pulsed neutron experiments in thermal, non-multiplying, polycrystalline moderators. A transport approximation is used to model the spatial dependence of the neutron distribution function.

The first part is concerned with the initial value problem for the Boltzmann equation describing the decay of thermal neutrons in a finite, polycrystalline system. The scattering kernel employed contains an isotropic, square-integrable component describing inelastic scattering and a term of the form $v\Sigma_{el}(v)\delta(\underline{v}'^2 - \underline{v}^2)$ that models elastic scattering. Laplace transform methods are applied to the Boltzmann equation which lead to an unsuspected structure in the transform variable plane. Discrete eigenvalue existence theorems are re-examined and the role of new continuum terms in the total solution are considered. The variation of the lowest eigenvalue with system size, i.e., the dispersion law, is thoroughly investigated. An alternate representation of the dispersion law is developed which aids in explaining experimental results.

In the second part of this thesis, a simplified model of the inelastic scattering kernel is used to investigate and expand the ideas in the first part and to examine the role of various continuum contributions to the total solution. The dispersion law is examined in some detail both analytically and numerically. Comparisons are made with experimental data and multi-group calculations in beryllium and graphite.

The implication of results for experiment and multi-group calculations are indicated throughout chapters II and III. Several results of major significance are examined together with suggestions for future work.

TABLE OF CONTENTS

I. INTRODUCTION

A. THE PULSED NEUTRON EXPERIMENT

A significant amount of both experimental and theoretical work has been done on pulsed neutron experiments since the technique was introduced by von Dardel[1,2] in 1954. Initially, the purpose of such experiments in non-multiplying media was to measure certain physical parameters of interest to reactor design such as the absorption rate and average diffusion coefficient. In recent years, motivation has been provided by a desire to better understand the approach of the neutron field to equilibrium.

The experiment itself consists of introducing a burst of neutrons into a system and measuring the resulting decay of the neutron density caused by absorption and leakage. Simple analysis leads one to believe that the asymptotic behavior in time is exponential. It also predicts that by measuring the decay constant as a function of system size, one can deduce the desired physical quantities. The concept of a buckling, given by $\pi^2/(\text{characteristic dimension})^2$, is introduced as a measure of the size of the system.

In non-polycrystalline moderators such as water, agreement between experiment and theory is very good. A recent comprehensive work[3] concludes that the agreement between observed and calculated time decay constants for water implies that scattering models incorporating the essential physical features of this scattering system are sufficient for pulsed neutron calculations. It is further concluded that once bucklings are assigned for various systems, it

would be unnecessary to perform experiments to obtain pertinent physical parameters since they could be calculated theoretically.

Results of work in polycrystalline moderators such as graphite and beryllium produce no such confidence. Agreement among experimenters is comparatively poor, and certain results appear to contradict theory. As far back as 1962, Beckurts[4] concluded that the situation in graphite is "less favorable" than that in water and that theoretical work would be necessary to show how these experiments can be evaluated.

B. REVIEW OF THEORETICAL WORK

The first theoretical analysis of pulsed neutron experiments was included in von Dardel's[1,2] original papers. He developed the idea that the equilibrium spectrum in a finite moderator would be diffusion cooled because of the preferential leakage of faster neutrons. Antonov et al.[5] derived an expansion of the fundamental eigenvalue as a power series in the buckling, B^2,

$$\lambda_o = \alpha_o + D_o B^2 - C B^4 + \ldots \qquad (I\text{-}1)$$

using two group diffusion theory. Nelkin[6], using perturbation theory, subsequently developed a similar expansion from the energy dependent transport equation. Analytic expressions for D_o and C clearly indicate their physical origin.

These initial theoretical efforts implicitly assumed that a fundamental discrete eigenvalue existed for every system size.

Lehner and Wing[7] first attacked this question for the one-velocity Boltzmann equation in slab geometry using the spectral theory of operators. They found that a discrete eigenvalue always exists for any slab thickness. However, the discrete spectrum consisting of a finite, non-void set of real eigenvalues coexists with a continuous spectrum occupying one half of the spectral plane. Van Norton[8] examined the one-velocity Boltzmann equation for spherical geometry and also found that a discrete mode exists for every sphere radius. In fact, he found only discrete spectra which form an infinite sequence of real numbers without an accumulation point in the finite plane. Jörgens[9] obtained similar results in spheres using the energy dependent Boltzmann equation but bounding the minimum neutron speed away from zero.

Corngold and Nelkin were the first to approach this problem using the full energy range. Corngold[10] employed asymptotic reactor theory to model the spatial dependence and a general, isotropic scattering kernel. Under these assumptions, he found that the discrete eigenvalues are bounded from above by the minimum value of the collision frequency, $v\Sigma_T(v)$, generally denoted λ^*. Furthermore, there exists a certain critical size with buckling $B^2 = B^{*2}$ such that for systems smaller than critical, no discrete eigenvalues exist. Nelkin[11] examined the velocity dependent Boltzmann equation in spherical geometry with exact boundary conditions but with a simple one-term degenerate scattering kernel. He also found that the discrete eigenvalues are bounded from above by λ^* and that the

discrete spectrum is empty when the sphere radius is smaller than some critical value. Theorists studying sound propagation encountered similar situations. For a recent discussion, see Sirovich and Thurber[12].

More recently, Albertoni and Montagnini[13] and Bednarz[65] were able to prove these same results for the exact energy dependent Boltzmann equation in bounded geometry and a rather general isotropic scattering kernel. Ukai[14] and Mockel[15] provided the necessary proofs for infinite slabs.

In all these analyses, the scattering kernel is assumed to be compact and the total cross section to be a smooth, non-increasing function of energy. Theory and experiment are in agreement where such assumptions are justified, e.g., water. However, neither assumption is true for polycrystalline systems. And it is here that theory and experiment appear to disagree. Figure 1 illustrates this disagreement. Experimenters apparently extract a discrete decay constant in systems smaller than critical[16-20]. Figure 1 illustrates the situation for beryllium in which $\lambda^* = 3800\ \text{sec}^{-1}$. A similar situation exists for graphite and beryllium oxide. As well, multi-group diffusion theory calculations employing the best scattering kernels available yield multi-group eigenvalue curves for polycrystals that differ markedly from those for water. This is demonstrated in figures 2 and 3 with the results of Ghatak and Honeck[21].

Kothari[22-24] has attempted to explain this condition by suggesting the observed decay constants are the eigenvalues of an

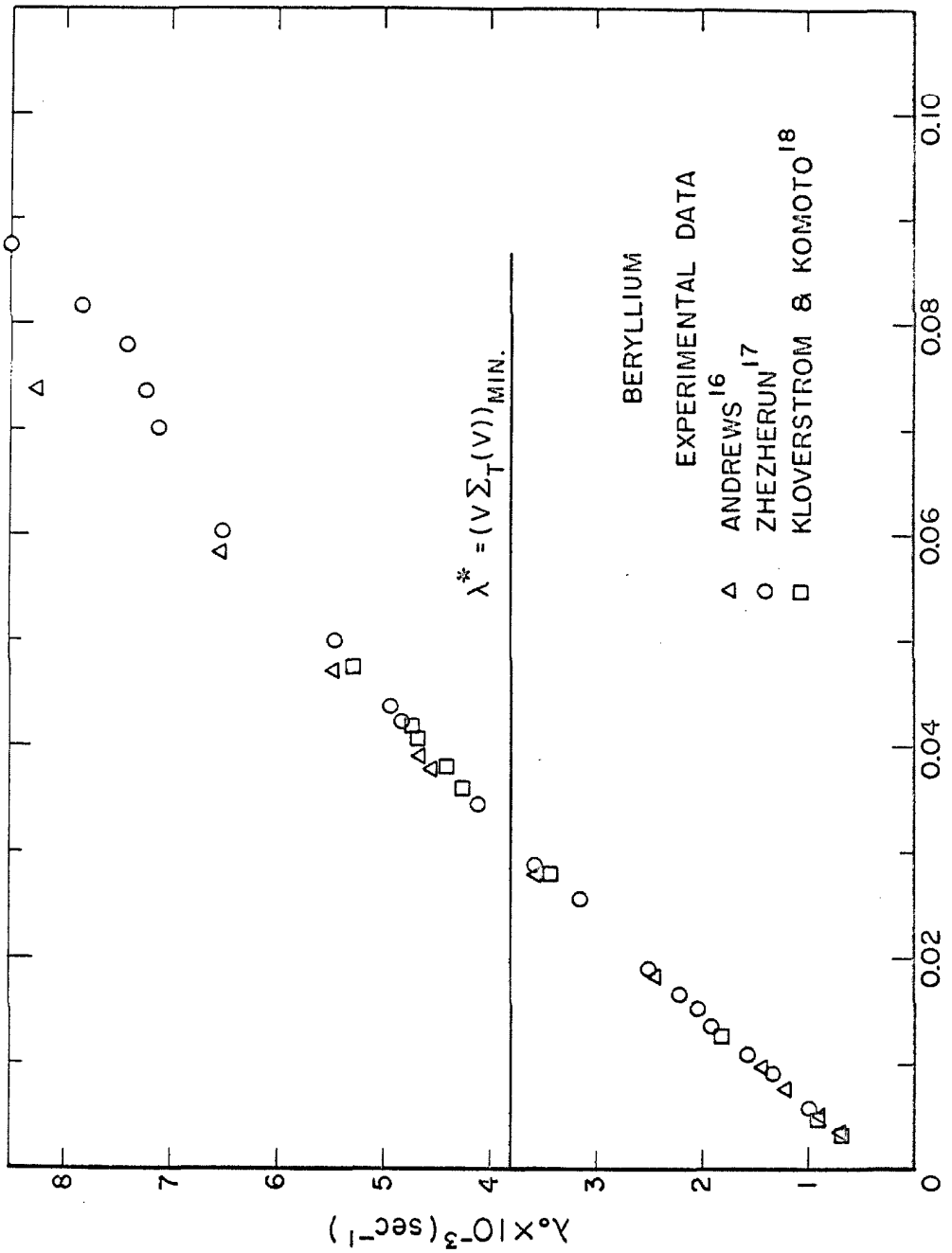

FIG. 1. Experimental data for beryllium. $\lambda^* = 3800$ sec^{-1}.

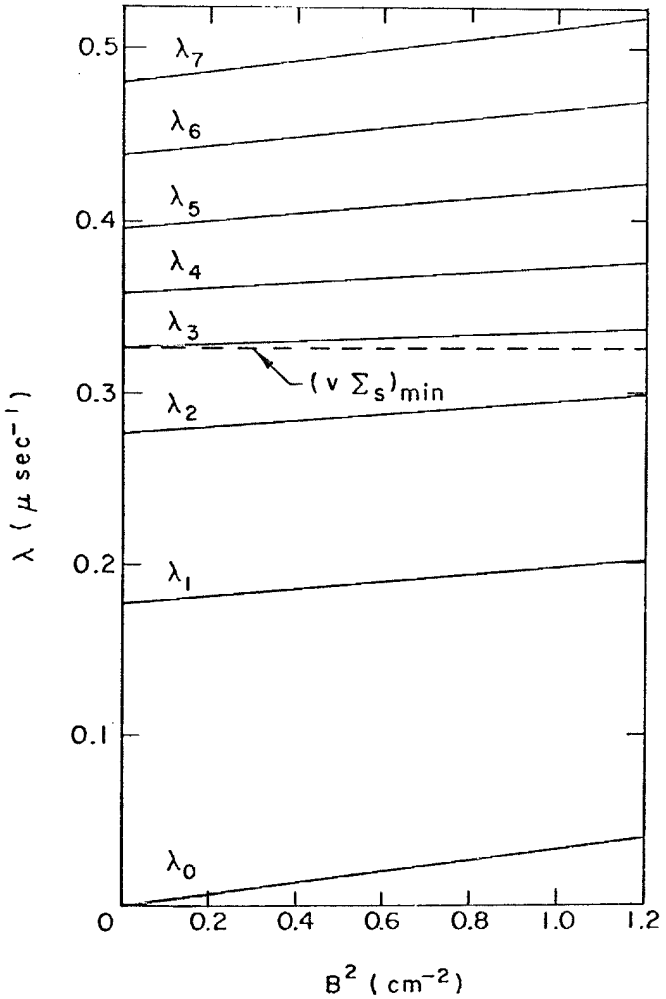

FIG. 2. Buckling dependence of the time eigenvalues in the multi-group calculation by Ghatak and Honeck[21] for water.

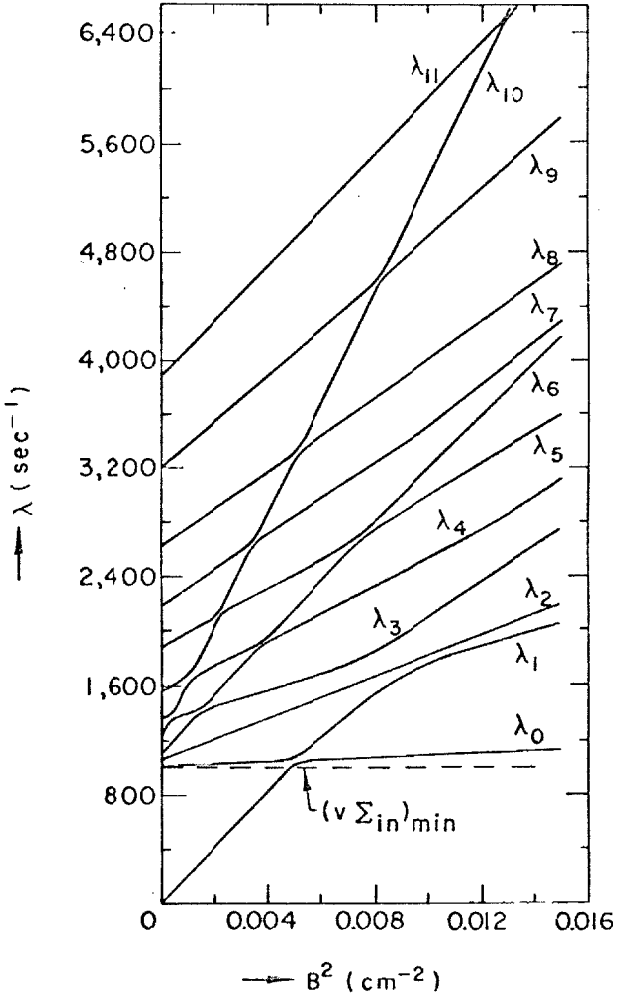

FIG. 3. Buckling dependence of the time eigenvalues in the multi-group calculation by Ghatak and Honeck[21] for graphite.

equation bounded in energy on the low energy side. This raises the eigenvalue bound such that the experimental data in beryllium lie below it. One should, however, be able to explain the discrepancy without resorting to such an assumption. Indeed, if the Boltzmann equation governs the experiment, we must explain the problem from a more general viewpoint.

Most recently, Corngold and Durgun[25] have approached the problem with diffusion theory and a modified kernel first proposed in general form by Corngold[26] which accounts for elastic scattering in polycrystals. The structure of their time transform plane is shown in figure 4 where overlapping branch cuts exist on the negative real axis. Areas do not arise because transport effects are not included. When discrete eigenvalues no longer exist, they find a peak in the integrand of the line integral about the cuts. The result is a solution which appears to decay exponentially for typical measuring times with a "pseudo-fundamental" decay constant. However, the line integral contribution was not calculated. They also develop an extended λ_o vs. B^2 curve which has a discontinuous slope at $\lambda_o = \lambda^*$. This effect appears to be peculiar to diffusion theory.

Borysiewicz and Mika[27] have considered the energy dependent Boltzmann equation including isotropic elastic scattering. They find that including elastic scattering does not change any of the results already obtained for square-integrable kernels[13]. However, their analysis implicitly assumes $v\Sigma_T(v)$ has no upward discontinuities such as those which exist for polycrystals. Including such

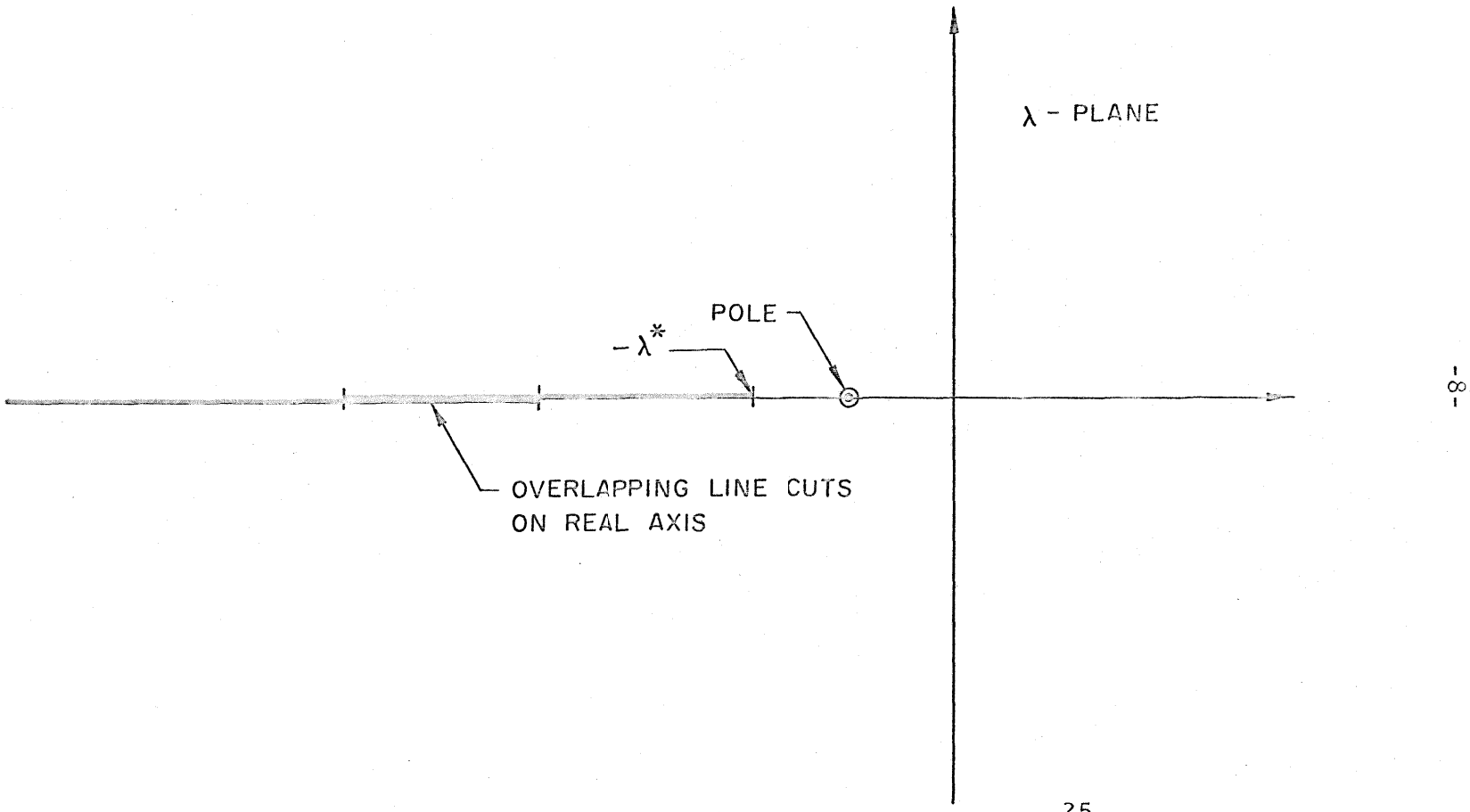

FIG. 4. The Laplace transform or λ-plane found by Corngold and Durgun[25] using diffusion theory.

discontinuities will alter the spectrum of the Boltzmann operator.

The works discussed here have recently been thoroughly reviewed by Kuščer[28] who includes a very complete bibliography.

C. MOTIVATION FOR THIS THESIS

The motivation, then, for this thesis is to gain a more thorough understanding of pulsed neutron experiments in polycrystals and, as well, a greater appreciation of the multi-group computer calculations that have been performed.

The aim is to include transport effects with the asymptotic reactor theory (or $e^{\underline{iB}\cdot\underline{r}}$) model of the spatial dependence. This assumption has been of paramount importance to the field because of the physical insights it has allowed. Also, particular attention is placed on maintaining certain physical aspects of neutron scattering in polycrystals. This includes a non-square-integrable kernel and a discontinuous total cross section.

In recent years, it has become fashionable to approach problems of this nature with the spectral theory of operators. However, as posed, the initial value problem for the Boltzmann equation can be handled in a straightforward manner with integral transform techniques. Therefore, rather than examine the Boltzmann operator for various types of eigenvalue spectra, transforms are used and the analyticity of the resulting transformed density is considered. However an attempt is made to suggest which parts of the transform plane are in the spectrum of the operator. Hence, the thesis employs

transform techniques and no proofs relating to the spectrum of the operator are included.

The role of discrete eigenvalues is of particular importance and we will examine the questions of when and where they exist, and how they vary with system size. Consideration is given to the connection between certain physical parameters, the dispersion law, $\lambda_o(B^2)$, and the structure of multi-group computer results. The various continuum terms in the total solution are examined together with their relationship to one another and to the discrete mode.

Chapter II is devoted to the analysis of the general problem with a kernel that includes both inelastic and elastic scattering. Chapter III employs a modified degenerate kernel model due to Corngold to evaluate both the dispersion law and the continuum contributions in the total solution. The importance of results for experiment and computer analysis are scattered throughout the thesis and, as well, in the summary and conclusions.

II. GENERAL THEORY

A. FORMULATION OF THE PROBLEM

The basic equation describing the behavior of neutrons in a homogeneous moderating system is the linearized Boltzmann equation[29]

$$\left(\frac{\partial}{\partial t} + \underline{v}\cdot\nabla + v\Sigma_T(v)\right)n(\underline{r},\underline{v},t) = \int v'\Sigma(\underline{v}'\rightarrow\underline{v})n(\underline{r},\underline{v}',t)d^3v' + S(\underline{r},\underline{v},t). \tag{II-1}$$

$n(\underline{r},\underline{v},t)$ is the neutron density or neutron distribution function and depends on position $\underline{r}$, velocity $\underline{v}$, and time t. $S(\underline{r},\underline{v},t)$ is a source distribution function, $\Sigma_T(v)$ is the macroscopic total cross section, and $v'\Sigma(\underline{v}'\rightarrow\underline{v})$ is the scattering kernel describing the rate of scattering from d^3v' about $\underline{v}'$ to d^3v about $\underline{v}$.

We are interested in the solution of the initial value problem for equation II-1 in a finite, polycrystalline moderator. This implies a source term of the form

$$S(\underline{r},\underline{v},t) = s(\underline{r},\underline{v})\delta(t) \tag{II-2}$$

where δ is the Dirac delta function. As well, the system is assumed to be in a vacuum implying particles escaping from the surface do not return. This supplies the boundary condition for a convex body,

$$n(\underline{r}_s,\underline{v},t) = 0, \quad t > 0 \quad \text{and} \quad \hat{e}_s\cdot\underline{v} < 0 \tag{II-3}$$

where $\hat{e}_s$ is the outward normal at the surface point $\underline{r}_s$.

We now assume a solution of the form

$$n(\underline{r},\underline{v},t) = \varphi(\underline{B},\underline{v},t)\,\psi_{asy}(\underline{B},\underline{r}) \tag{II-4a}$$

where $\underline{B}$ is the wave vector and

$$\psi_{asy}(\underline{B},\underline{r}) = e^{i\underline{B}\cdot\underline{r}} \tag{II-5}$$

This solution is separable in space and energy and we assume that a single spatial mode is adequate to describe the neutron density. This amounts to neglecting spatial transients near the boundary of the system and eliminates the role of the boundary condition II-3. This general approach is referred to as asymptotic reactor theory[29]. In effect, we are replacing the problem of the decay of a thermalized pulse in a finite, homogeneous system by a similar problem in an infinite medium in which the neutron flux vanishes at an extrapolated boundary of the system. The spatial function $\psi_{asy}(\underline{B},\underline{r})$ is the fundamental solution of the wave equation

$$\nabla^2\psi_{asy}(\underline{B},\underline{r}) + B^2\psi_{asy}(\underline{B},\underline{r}) = 0 \tag{II-6}$$

subject to the boundary condition that $\psi_{asy}(\underline{B},\underline{r})$ vanish at the extrapolated surface of the system, i.e., the distance from the boundary where the analytic continuation of the asymptotic solution is zero. For example, the buckling of an infinite slab of width 2d is

$$B^2 = \left[\frac{\pi}{2(d+z_o)}\right]^2 \qquad \text{(II-7)}$$

where z_o is the extrapolated endpoint.

The comparison of the infinite medium theory to be used in this thesis with experimental results depends on the validity of the procedure for assigning an equivalent infinite medium buckling to a finite system. Several investigations (for a review, see chapter 5 of reference 30) indicate it is likely that the usual interpretation of experimental results in terms of infinite medium parameters will be accurate if the extrapolation distance is carefully defined when assigning bucklings to the systems considered.

An additional motivation for assuming the applicability of asymptotic reactor theory is that it has led to important physical consequences that were later confirmed for the Boltzmann equation with the exact boundary conditions II-3. As an example, Corngold[10] predicted, using asymptotic reactor theory, that there exists a maximum B^2, denoted B^{*2}, such that for $B^2 > B^{*2}$, no discrete time eigenvalues exist. This was later confirmed for the Boltzmann equation with exact boundary conditions by Albertoni and Montagnini[13] and Bednarz[65]. Thus, we take the approach that the assumption of asymptotic reactor theory appears to retain enough transport character to yield correct physical results while reducing the problem to tractable form.

We also assume the source has the form

$$S(\underline{r},\underline{v},t) = Q(\underline{B},\underline{v})\delta(t)e^{i\underline{B}\cdot\underline{r}} \qquad \text{(II-4b)}$$

and that, again, a single buckling mode is sufficient. Barnard et al.[67] have shown II-4b to be an acceptable approximation if we replace $\delta(t)$ by $\delta(t - t_s)$, where t_s is the slowing down time for neutrons with final energies in the range E_s to E_s/α. Here, $E_s \sim .3$ ev, $\alpha = \left(\frac{A-1}{A+1}\right)^2$ and A is the atomic weight of the moderator. At the time, t_s, the neutron population in the higher spatial modes is negligible compared with the population in the fundamental mode. (Barnard et al.[67] show that the ratio of fast non-leakage probabilities[51] during slowing down, $e^{-(B_n^2 - B_o^2)\tau}$, is of the order 10^{-7}. Here, τ is the Fermi age[51].)

Thus, shifting the time origin so that $t_s = 0$, and substituting equations II-4a and II-4b, the Boltzmann equation becomes

$$\left(\frac{\partial}{\partial t} + v\Sigma_T(v) + i\underline{B}\cdot\underline{v}\right)\varphi(\underline{B},\underline{v},t) = \int v'\Sigma(\underline{v}' \rightarrow \underline{v})\varphi(\underline{B},\underline{v}',t)d^3v' + Q(\underline{B},\underline{v})\delta(t) \tag{II-8}$$

B. THE SCATTERING KERNEL

The scattering kernel in this equation is of primary importance. One of its basic general properties is the detailed balance condition[30]

$$v'\Sigma(\underline{v}' \rightarrow \underline{v})M(v') = v\Sigma(-\underline{v} \rightarrow -\underline{v}')M(v) \tag{II-9}$$

where $M(v)$ is the Maxwellian distribution. Kernels for the polycrystalline forms of graphite and beryllium are distinguished by the predominant amount of coherent elastic or Bragg scattering of neutrons in the thermal energy range. Such scattering is represented by δ-functions in energy and angle which causes the kernel to become

non-square-integrable. Hence, it is natural to separate the kernel into two parts,

$$v'\Sigma(\underline{v}'\rightarrow\underline{v}) = v'\Sigma_{inel}(\underline{v}'\rightarrow\underline{v}) + v'\Sigma_{el}(\underline{v}'\rightarrow\underline{v}) \qquad \text{(II-10)}$$

where the first term describes all inelastic interactions and the second all elastic scattering. The elastic kernel contains δ-functions and will be called the singular part of the kernel. The results of Dorfman[31] and Kuščer and Corngold[32] indicate that the inelastic term $v'\Sigma_{inel}(\underline{v}'\rightarrow\underline{v})$, or one of its iterates, is square-integrable provided inelastic coherent scattering is neglected. Thus, the incoherent approximation[33], in which one neglects all interference effects and replaces σ_b^{inc} by $\sigma_b^{inc} + \sigma_b^{coh}$, is used to construct kernels describing inelastic scattering in polycrystals. σ_b^{inc} and σ_b^{coh} are the bound atom incoherent and coherent cross sections, respectively.

We will further assume that all scattering is isotropic. This assumption is generally made in such analyses and, hopefully, will not alter the basic qualitative results.

Thus, we have generated a "super-incoherent," isotropic scattering kernel for slow neutron scattering in polycrystals given by

$$v'\Sigma(\underline{v}'\rightarrow\underline{v}) = \frac{v'\Sigma_{inel}(v',v)}{4\pi} + \frac{v\Sigma_{el}(v)}{4\pi}\,\delta(\underline{v}'^2 - \underline{v}^2) \qquad \text{(II-11)}$$

Kernels of this form have been discussed by Corngold[26].

An additional feature of polycrystalline systems is the existence of a cutoff speed at the Bragg cutoff, v_B, such that for $v < v_B$, the elastic, coherent scattering cross section is zero. To understand this

feature, recall that the coherent scattering of neutrons results from the periodic arrangement of nuclei in a lattice. The term coherent implies neutron waves scattered from one lattice site interfere with waves scattered at other sites. When the neutron wavelength becomes greater than twice the lattice spacing, elastic coherent scattering can no longer occur. The effect is to cause the total cross section to exhibit a major discontinuity at the Bragg cutoff.

The expression[34] for the elastic, coherent scattering kernel in polycrystals is

$$\Sigma_{el,coh}(\underline{v}' \rightarrow \underline{v}) = \delta(E' - E) \frac{\pi \Sigma_{coh}}{4 v_c} \sum_{\tau} \frac{e^{-\tau^2 W}}{\tau^2} |F_{\underline{\tau}}|^2 \delta(\tau - 2k_o \sin \frac{\theta}{2}) \tag{II-12}$$

where $\underline{\tau}$ is the reciprocal lattice vector[68]; v_c is the volume of the unit cell; $\underline{k}$ is the momentum transfer vector; $|k| = 2k_o \sin \frac{\theta}{2}$; θ is the scattering angle; Σ_{coh} is the zero energy bound atom coherent cross section; F_τ is the structure factor for scattering from a unit cell; and

$$W = \frac{\hbar}{2M} \int_o^{\omega_{max}} d\omega \frac{f(\omega)}{\omega} \coth \frac{\omega}{2kT} \quad . \tag{II-13}$$

Details about W are given by Young and Koppel[34]. The term polycrystal implies averaging over the various directions of $\underline{\tau}$. The total coherent, elastic scattering cross section is obtained by integrating the kernel II-12 over all scattering angles and over E' yielding

$$\Sigma_{el,coh}(v) = \Sigma_{coh} \frac{(2\pi)^2 \hbar^2}{8mE} \sum_{\tau}^{\frac{\tau}{2} < \frac{\sqrt{2mE}}{\hbar}} \frac{e^{-\tau^2 W}}{\tau} |F_{\underline{\tau}}| . \qquad \text{(II-14)}$$

Thus, when $E < \frac{\hbar^2 \tau_{min}^2}{8m}$, the sum over τ does not exist and $\Sigma_{el,coh}(v) = 0$. In this inequality, τ_{min} is the maximum interplanar distance and

$$E_B = \frac{\hbar^2 \tau_{min}^2}{8m} \qquad \text{(II-15)}$$

yields the Bragg cutoff energy. Notice that other discontinuities appear as the incident neutron energy increases. Between discontinuities, $\Sigma_{el,coh}(v)$ varies as $1/E$. Figure 5 illustrates this behavior in graphite together with the results of theoretical calculations of various cross sections[35]. The non-physical assumption that $\Sigma_{el}(v)$ is continuous and monotonic in v has led to conclusions[26,27] different from those of this thesis and emphasizes the importance of retaining the major characteristics of the scattering cross sections of polycrystals.

The assumption of isotropic elastic scattering effectively means that we expand the sum over τ in Legendre polynomials and retain only the P_o component. Young and Koppel[34] have calculated the P_o and P_1 components of the elastic, coherent scattering kernel for beryllium and found that for more than two reciprocal lattice vectors in the sum II-12, the P_1 component is small compared to the P_o part. Hence, over the bulk of the energy range, we expect the isotropic elastic scattering assumption to be good. We could now replace the sum over reciprocal lattice vectors by an integral and

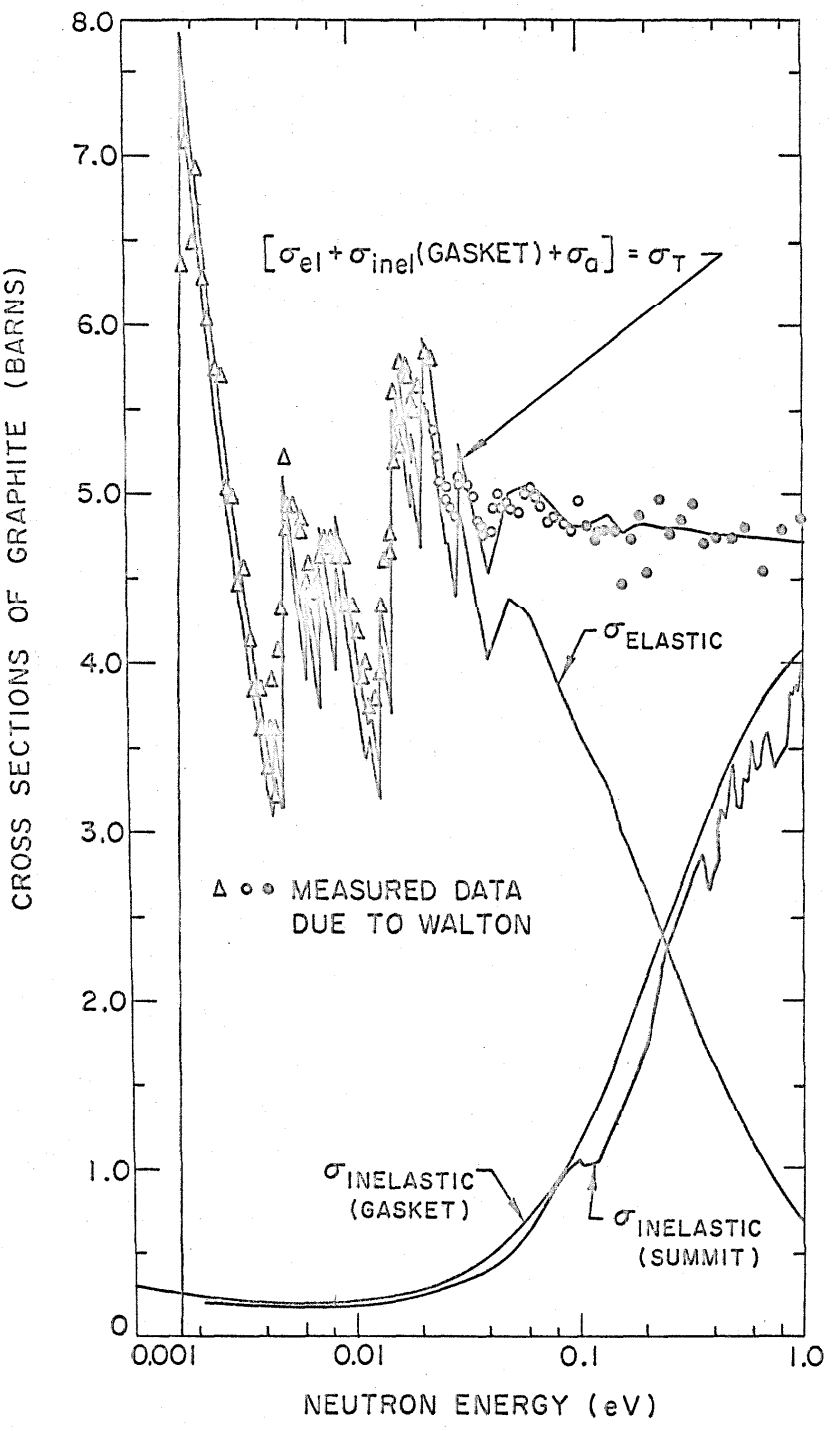

FIG. 5. Experimental and calculated cross sections for graphite.

obtain the incoherent approximation to elastic, coherent scattering. This approximation is used extensively in multi-group calculations[21,35].

Throughout most of this thesis, only the major discontinuity in $\Sigma_T(v)$ at the Bragg cutoff v_B is included. The other minor discontinuities have no major qualitative effect on the conclusions.

A final comment must be made about the total cross section behavior below the Bragg cutoff ($v < v_B$). There, we shall take $\Sigma_T(v)$ proportional to $1/v$. This is referred to as the "λ-law" because it implies the cross section is directly proportional to the neutron wavelength. For neutrons below the cutoff, the main inelastic scattering process is one where the neutrons absorb energy from the lattice and thus gain energy. The scattered neutron being fast compared to the incident neutron leads to the $1/v$ behavior. The "λ-law" is illustrated in figure 6a for graphite. For beryllium, however, figure 6b shows that the cross section deviates slightly from $1/v$ just below the cutoff because there remains a possibility of energy transfer <u>from</u> the neutron <u>to</u> the lattice.

C. ANALYSIS OF BOLTZMANN EQUATION

The Boltzmann equation II-8 with the scattering kernel II-11 becomes

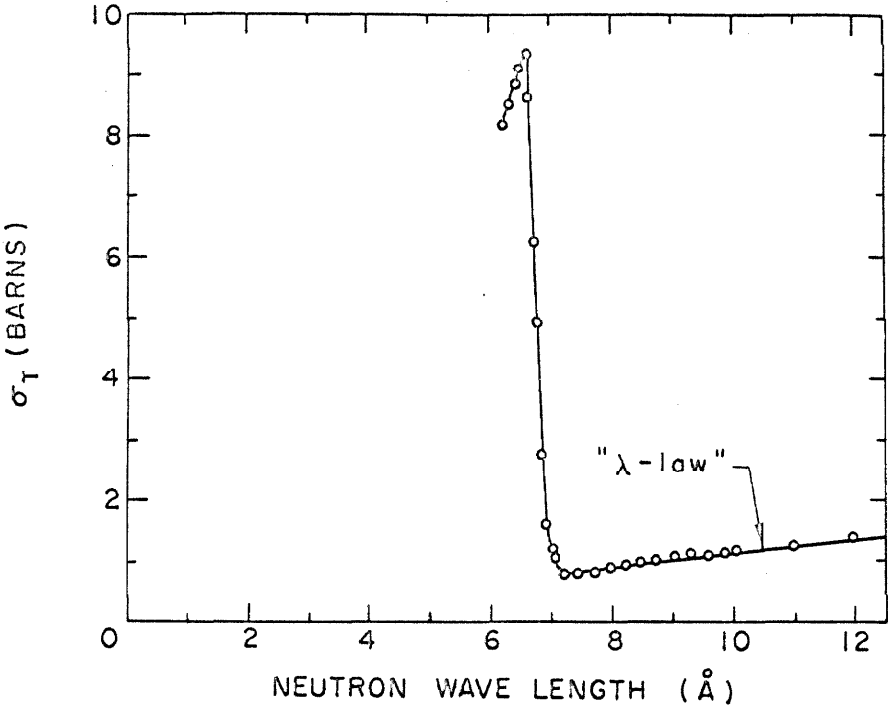

FIG. 6a. The total cross section dependence on the incident neutron wavelength in graphite[61] illustrating the "λ-law."

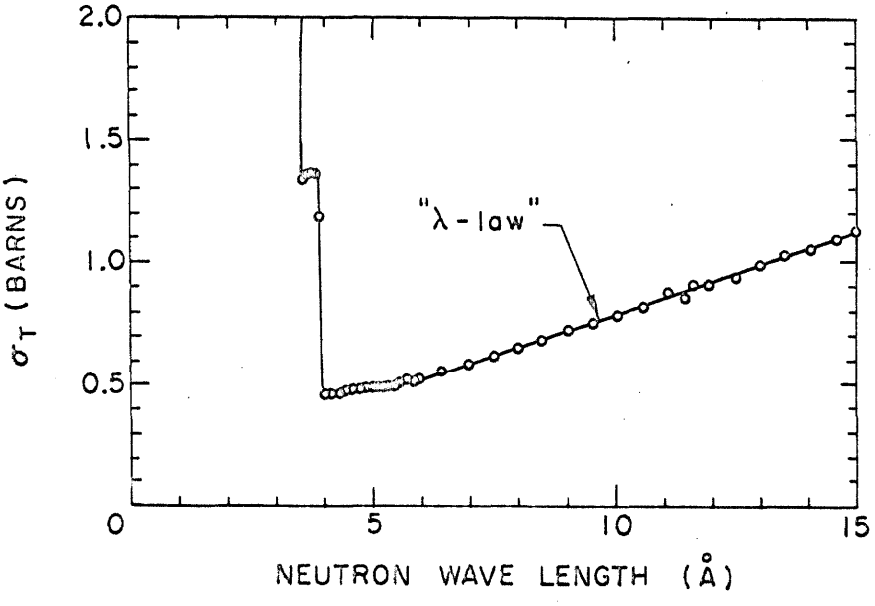

FIG. 6b. The total cross section dependence on the incident neutron wavelength in beryllium[61].

$$\left(\frac{\partial}{\partial t} + v\Sigma_T(v) + iBv\mu\right)\varphi(B,v,\mu,t)$$

$$= \frac{1}{2}\int_o^\infty \int_{-1}^1 v'\Sigma_{inel}(v',v)\varphi(B,v',\mu',t)\, dv'\, d\mu'$$

$$+ \frac{v\Sigma_{el}(v)}{2}\int_{-1}^1 \varphi(B,v,\mu',t)\, d\mu' + Q(v,\mu)\delta(t) \qquad \text{(II-16)}$$

where $\mu \equiv \left(\frac{\underline{B}\cdot\underline{v}}{Bv}\right)$. This equation can be written in a more compact form by defining the operators

$$S_i \equiv \frac{1}{2}\int_o^\infty \int_{-1}^1 v'\Sigma_{inel}(v',v)\, dv'\, d\mu'. \qquad \text{(II-17)}$$

$$S_e \equiv \frac{v\Sigma_{el}(v)}{2}\int_{-1}^1 d\mu'. \qquad \text{(II-18)}$$

$$A_m \equiv -(v\Sigma_T(v) + iBv\mu) \qquad \text{(II-19)}$$

$$A \equiv S_i + S_e + A_m \qquad \text{(II-20)}$$

Then equation II-16 becomes

$$\frac{\partial\varphi}{\partial t} = A\varphi + Q(v,\mu)\delta(t) \qquad \text{(II-21)}$$

At this point, one could proceed in either of two ways. One method is to use the spectral theory of operators and functional analysis in an effort to solve II-21. Thus, we Laplace transform in time, solve the resulting inhomogeneous equation using the resolvent of A, and present the solution as the Bromwich inversion integral (see

Kuščer[28])

$$\varphi(B,v,\mu,t) = \lim_{\gamma\to\infty} \frac{1}{2\pi i}\int_{a-i\gamma}^{a+i\gamma} e^{\lambda t}(\lambda I - A)^{-1} Q(v,\mu)\, d\lambda \,. \qquad \text{(II-22)}$$

I is the identity operator and "a" lies to the right of the spectrum of A. This approach requires that we consider the linear operator A as defined on a Hilbert space $\mathcal{L}_2$. One works in such a space primarily for mathematical convenience (we know the theorems there). As well, the detailed balance condition II-9 makes it possible to symmetize the scattering kernel in the Boltzmann equation II-1. In such a space, we can associate with A an eigenvalue spectrum the complement of which is the resolvent set. A detailed discussion of this approach is given in reference 28.

Alternatively, we can Laplace transform II-21 and examine the analyticity of the resulting transformed density. This approach is more straightforward and is employed throughout the remainder of the thesis.

Thus, define the Laplace transform of $\varphi(B,v,\mu,t)$ as

$$\tilde{\varphi}(B,v,\mu,\lambda) = \int_0^\infty e^{-\lambda t}\varphi(B,v,\mu,t)\, dt \qquad \text{(II-23)}$$

and operate with it on equation II-21. The result is

$$\lambda\tilde{\varphi}(B,v,\mu,\lambda) = A\tilde{\varphi} + Q(v,\mu)\,. \qquad \text{(II-24)}$$

Define the transformed scalar density as

$$\tilde{\psi}(B,v,\lambda) \equiv \int_{-1}^{1} \tilde{\varphi}(B,v,\mu,\lambda)\, d\mu \,. \qquad \text{(II-25)}$$

Explicitly, equation II-24 is

$$(\lambda + v\Sigma_T(v) + iBv\mu)\tilde{\varphi}(B,v,\mu,\lambda)$$

$$= \frac{1}{2}\int_0^\infty v'\Sigma_{inel}(v',v)\,\tilde{\psi}(B,v',\lambda)\,dv' + \frac{v\Sigma_{el}(v)}{2}\,\tilde{\psi}(B,v,\lambda) + Q(v,\mu) \tag{II-26}$$

Assume $\lambda + v\Sigma_T(v) + iBv\mu \neq 0$, divide by it and integrate over μ to obtain

$$\tilde{\psi}(B,v,\lambda) = \frac{T(B,v,\lambda)}{\Gamma_e(B,v,\lambda)}\left\{\int_0^\infty v'\Sigma_{inel}(v',v)\tilde{\psi}(B,v',\lambda)\,dv' + 2Q(v,\mu)\right\} \tag{II-27}$$

where

$$T(B,v,\lambda) \equiv \frac{1}{Bv}\tan^{-1}\frac{Bv}{\lambda + v\Sigma_T(v)} \tag{II-28}$$

and

$$\Gamma_e(B,v,\lambda) \equiv 1 - \frac{\Sigma_{el}(v)}{B}\tan^{-1}\frac{Bv}{\lambda + v\Sigma_T(v)} \quad . \tag{II-29}$$

Here, we employ the principal branch of the arctangent function. Equation II-27 is an inhomogeneous Fredholm integral equation for the angle integrated transformed density $\tilde{\psi}(B,v,\lambda)$. Examining this equation will allow a determination of the analyticity properties of $\tilde{\psi}(B,v,\lambda)$ and, as well, detailed information concerning the associated eigenvalue problem.

D. STRUCTURE OF THE TRANSFORM PLANE

As a function of λ, $\tilde{\psi}(B,v,\lambda)$ is not analytic at those values of λ for which the homogeneous form of equation II-27 has non-trivial solutions. These values of λ are the discrete eigenvalues of the problem and correspond to the discrete spectrum of the operator A. As well, $\tilde{\psi}(B,v,\lambda)$ is not analytic at the singular points of $T(B,v,\lambda)$ and at the zeros of $\Gamma_e(B,v,\lambda)$.

We can best examine the function $T(B,v,\lambda)$ by rewriting it as it was defined, namely

$$T(B,v,\lambda) = \frac{1}{2}\int_{-1}^{1} \frac{d\mu}{\lambda + v\Sigma_T(v) + iBv\mu} \quad . \tag{II-30}$$

The integral over μ defines a function analytic in the λ plane except for the set defined by

$$\lambda + v\Sigma_T(v) + iBv\mu = 0; \quad v \in [0,\infty), \; \mu \in [-1,1] \; . \tag{II-31}$$

This reflects the assumption made to obtain equation II-27. Since the inelastic kernel is compact, $S_i\tilde{\psi}(B,v,\lambda)$ is analytic wherever $\tilde{\psi}$ is. Hence, we find $\tilde{\psi}(B,v,\lambda)$ is not analytic wherever equation II-31 is satisfied.

The presence of $1/\Gamma_e(B,v,\lambda)$ in II-27 implies $\tilde{\psi}$ is also not analytic at those values of λ satisfying

$$\Gamma_e(B,v,\lambda) = 0 \qquad v \in [v_B^{+},\infty) \quad . \tag{II-32}$$

The range of v is restricted because $\Sigma_{el}(v) \equiv 0$ for $v < v_B$. For

fixed v, II-32 is exactly the form of the one-velocity dispersion law[36] reflecting the one-velocity nature of elastically scattered neutrons. Solving II-32 for λ yields

$$\lambda \equiv -\lambda_e(B,v) = -v\left(\Sigma_T(v) - \frac{B}{\tan\left(\frac{B}{\Sigma_{el}(v)}\right)}\right) \qquad \text{(II-33)}$$

It is readily shown that

$$\min_{v\in[v_B^+,\infty)} \lambda_e(B,v) = \lambda_e(B,v_B) \equiv \lambda_{el} \,. \qquad \text{(II-34)}$$

In other words, that point of the set defined by II-33 with least real part occurs when $\Sigma_T(v)$ and $\Sigma_{el}(v)$ are evaluated just above the Bragg cutoff. λ_{el} will play an important role in determining the shape of the dispersion curve (the variation of the smallest discrete eigenvalue with buckling, B^2).

The discrete eigenvalues, $-\lambda_o$, are physically expected to have negative real parts, i.e., $\mathrm{Re}(\lambda_o) \geq 0$. As well, in Appendix A, we symmetize the kernel and prove that only real eigenvalues exist. Furthermore, there is numerical evidence[21,41,43,44] that, at most, one discrete eigenvalue exists with magnitude less than λ^* when the kernel employed describes neutron scattering in the polycrystalline forms of graphite and beryllium.

Equations II-31 and II-32 together with the restrictions described above imply the λ-plane structure of figure 7. This figure is drawn to scale based upon parameters for graphite. It is general terminology in the field to refer to the line cuts and area as continuum since such

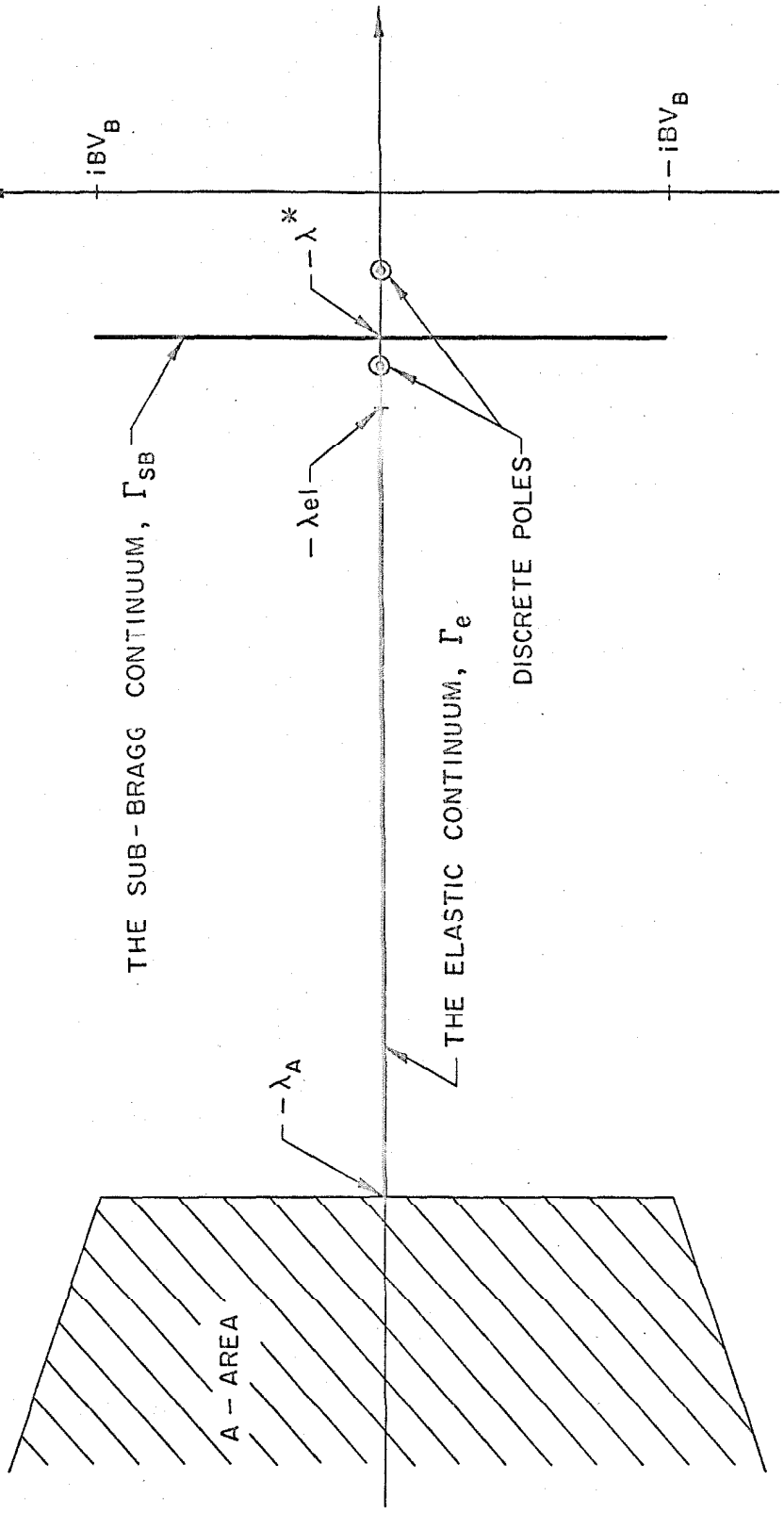

FIG. 7. The Laplace transform or λ-plane structure for polycrystals.

sets correspond to the continuous spectrum in spectral theory. The vertical line cut at $\mathrm{Re}\,(\lambda) = -\lambda^* = -\min_{v \in [0,\infty)} (v\,\Sigma_T(v))$ is a result of the constant collision frequency below the Bragg cutoff. It is thus called the "sub-Bragg" continuum, Γ_{SB}. It is disjoint from the area because $\Sigma_T(v)$ is discontinuous at v_B. The area to the left of $-\lambda_A$ is the set defined by II-15 for $v > v_B$ and reflects the nature of $\Sigma_T(v)$ above the Bragg cutoff. This area can become fragmented if we account for the other, smaller, discontinuities in $\Sigma_T(v)$ occurring at $v > v_B$ and caused by higher order Bragg reflections. The set eminating from the area is defined by II-31, depends critically on $\Sigma_{el}(v)$, and thus is referred to as the elastic continuum, Γ_e.

It is both interesting and instructive to compare this new λ-plane with those obtained in previous theoretical efforts. Figure 8 results from using asymptotic reactor theory and continuous, non-increasing cross sections[10]. The area reflects a condition analogous to II-15. As mentioned earlier, the separation of Γ_{SB} and the area in figure 7 results from the discontinuity in $\Sigma_T(v)$. Figure 8 contains no analogy to Γ_e because there is no elastic scattering. The λ-plane for diffusion theory with discontinuous cross section and elastic scattering was presented in figure 4.

The structure of the λ-plane in figure 7 is based, in part, on the assumption of constant collision frequency below the Bragg cutoff. Figure 6a shows this to be an excellent assumption for graphite. However, we might well ask what effect deviations from this behavior, as in figure 6b, have on the λ-plane structure. The effect is to expand

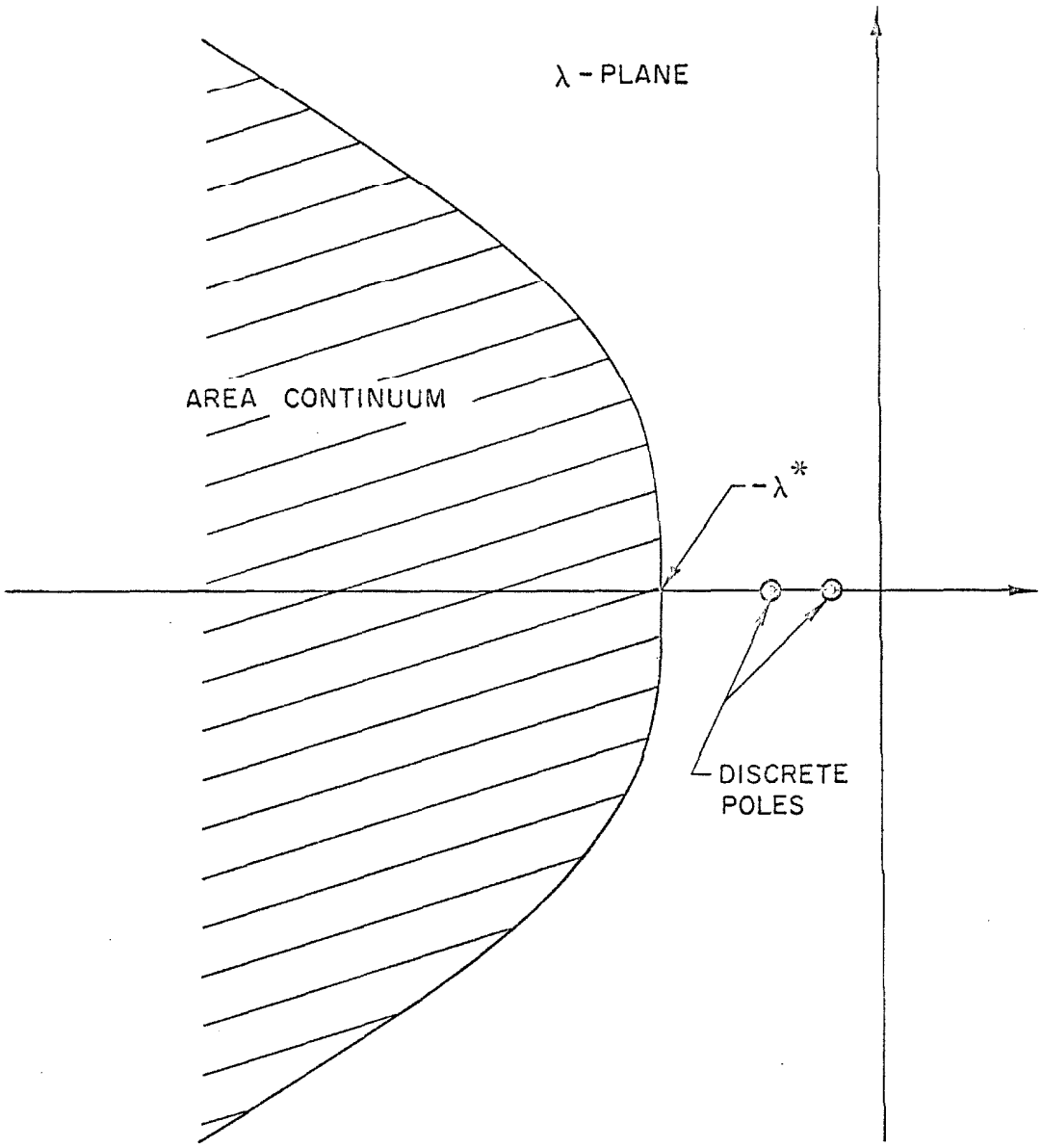

FIG. 8. The λ-plane which results with smooth cross sections and asymptotic reactor theory.[11]

the line cut Γ_{SB} into the narrow area in figure 9. The right side still has $Re(\lambda) = -\lambda^*$ but the left is given by $Re(\lambda) = -v_B(\Sigma_i(v_B) + \Sigma_a(v_B))$. In addition, the edge of the elastic continuum, $-\lambda_{el}$, now equals $-v_B(\Sigma_i(v_B) + \Sigma_a(v_B))$ at $B^2 = 0$ instead of λ^*.

E. DISCRETE EIGENVALUES

If we recall the conditions on the discrete eigenvalues and examine figure 7, we see it is possible for discrete eigenvalues to exist between the origin and Γ_{SB} and, in addition, in the gap on the negative real axis between Γ_{SB} and Γ_e. These latter eigenvalues will have magnitude greater than λ^* and be bounded from above, for fixed B^2, by the edge of the elastic continuum. This is in contrast with part of the "maximum B^2" theorem of Corngold[10] which states that λ^* is an upper bound to the magnitude of any discrete eigenvalue. However, he implicitly assumed smooth, non-increasing cross sections and did not explicitly account for elastic scattering. This illustrates the importance of maintaining the physical nature of scattering in polycrystals. A maximum B^2 theorem can be proven but it yields a much larger value for the critical buckling. The proof yields a method for determining the large B^2 behavior of the discrete eigenvalues.

Theorem: There exists a maximum B^2, say B^{**2}, such that for $B^2 > B^{**2}$, no discrete eigenvalues exist outside the continuum regions of the λ-plane. In addition, all such eigenvalues are bounded in magnitude from above by λ_A, the edge of the area continuum.

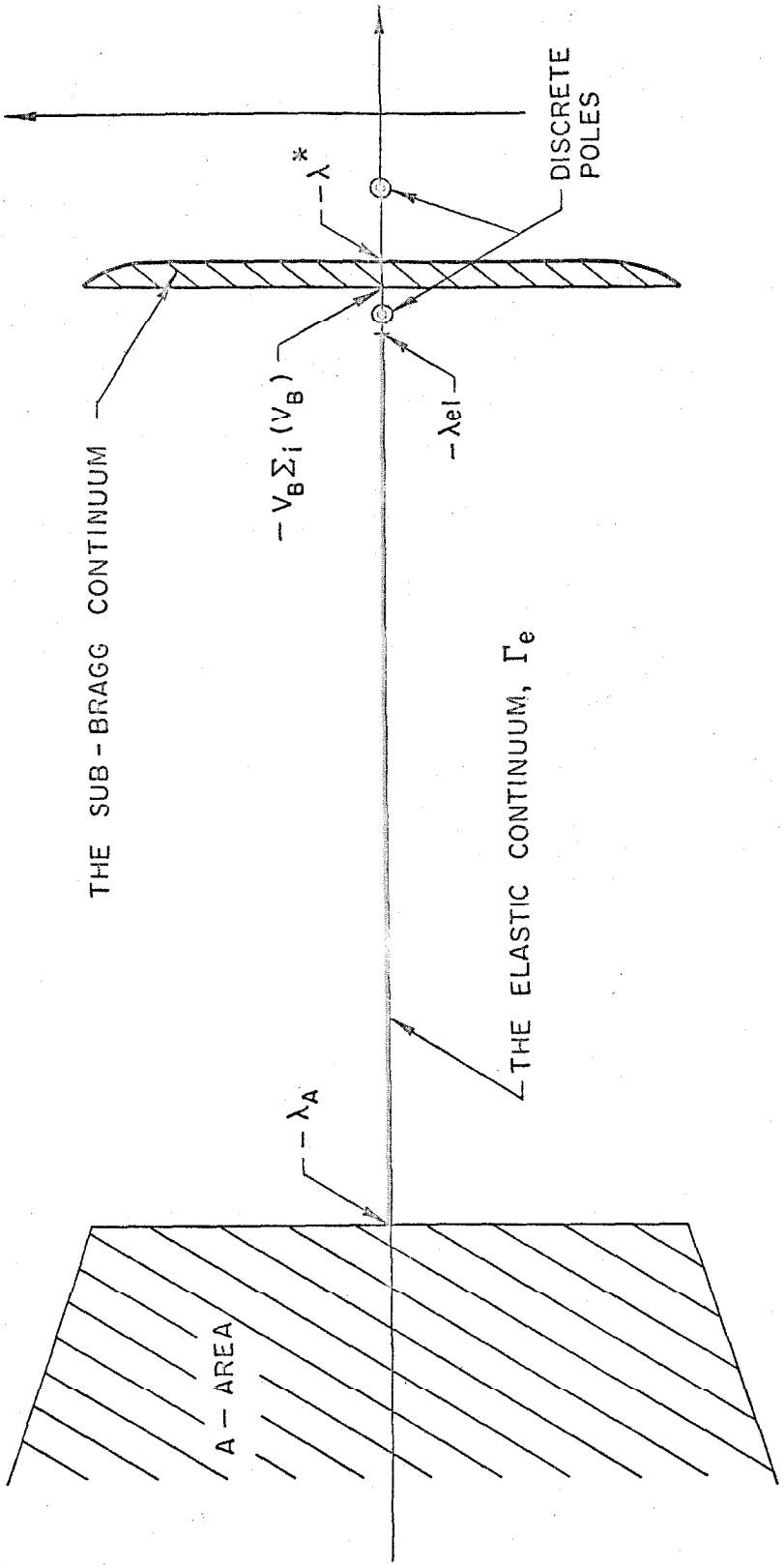

FIG. 9. The λ-plane structure analogous to figure 7 illustrating the effect of a variation from the "λ-law."

Proof: The implicit eigenvalue equation for $-\lambda_o, \lambda_o \geq 0$, is

$$\tilde{\psi}_H(B,v,\lambda_o) = \frac{T(B,v,-\lambda_o)}{\Gamma_e(B,v,-\lambda_o)} \int_o^\infty v'\Sigma_{inel}(v',v)\tilde{\psi}_H(B,v',\lambda_o)\, dv' \qquad \text{(II-35)}$$

The proof follows the general outline given by Corngold[10]. To obtain a dispersion law, we assume the eigenfunction, $\tilde{\psi}_H(B,v,\lambda_o)$, is normalizable, i.e. $\int_o^\infty v\Sigma_i(v)\psi_H(B,v,\lambda_o)\, dv \neq 0$. Multiply II-35 by $v\Sigma_i(v)$, integrate over v, and normalize the left-hand side to one. This gives

$$1 = \frac{1}{B}\left\{\int_o^{v_B} \Sigma_i(v) \tan^{-1}\left(\frac{Bv}{-\lambda_o+\lambda^*}\right) dv \int_o^\infty v'\Sigma_{inel}(v',v)\tilde{\psi}_H(B,v',\lambda_o)\, dv' \right.$$

$$\left. + \int_{v_B}^\infty \frac{\Sigma_i(v) \tan^{-1}\left(\frac{Bv}{-\lambda_o+v\Sigma_T(v)}\right)}{\Gamma_e(B,v,-\lambda_o)} dv \int_o^\infty v'\Sigma_{inel}(v',v)\tilde{\psi}_H(B,v',\lambda_o)\, dv' \right\} \qquad \text{(II-36)}$$

$\Sigma_i(v)$ is the macroscopic inelastic cross section. The functional $\Lambda(\lambda,B;\tilde{\psi}_H)$ defined by

$$\Lambda(\lambda,B;\tilde{\psi}_H) = 1 - \int_o^\infty \frac{v\Sigma_i(v)T(B,v,\lambda)}{\Gamma_e(B,v,\lambda)} dv \int_o^\infty v'\Sigma_{inel}(v',v)\tilde{\psi}_H(B,v',-\lambda)\, dv' \qquad \text{(II-37)}$$

is commonly called the dispersion function.

Equation II-36 can be re-written as

$$1 = \frac{1}{B}\int_o^\infty v\Sigma_i(v)\tilde{\psi}_H(B,v,\lambda_o)\left\{g_b(B,v,\lambda_o) + g_u(B,v,\lambda_o)\right\} dv \qquad \text{(II-38)}$$

where

$$g_b(B,v,\lambda_o) = \int_o^{v_B} \frac{\Sigma_i(v')}{\Sigma_i(v)} \Sigma_{inel}(v,v') \tan^{-1}\left(\frac{Bv'}{-\lambda_o+\lambda^*}\right) dv' \qquad \text{(II-39)}$$

and

$$g_u(B,v,\lambda_o) = \int_{v_B}^{\infty} \frac{\Sigma_i(v')}{\Sigma_i(v)} \Sigma_{inel}(v,v') \frac{\tan^{-1}\left(\frac{Bv'}{-\lambda_o+v'\Sigma_T(v')}\right)}{\Gamma_e(B,v',-\lambda_o)} dv' \qquad \text{(II-40)}$$

Equation II-38 is a necessary condition for the existence of a non-trivial solution of equation II-35. Our aim is to show that both $g_b(B,v,\lambda_o)$ and $g_u(B,v,\lambda_o)$ can be bounded independent of B^2. If $|g_b(B,v,\lambda_o)| < K_1$ and $|g_u(B,v,\lambda_o)| < K_2$ for K_1 and K_2 independent of B^2, then

$$1 = \frac{1}{B}\int_o^{\infty} v\Sigma_i(v)\tilde{\psi}_H(B,v,\lambda_o)\left\{g_b(B,v,\lambda_o) + g_u(B,v,\lambda_o)\right\} dv$$

$$\leq \frac{(K_1+K_2)}{B}\int_o^{\infty} v\Sigma_i(v)\tilde{\psi}_H(B,v,\lambda_o)\, dv \qquad \text{(II-41)}$$

$$1 \leq \frac{(K_1+K_2)}{B} . \qquad \text{(II-42)}$$

Therefore, for sufficiently large B^2, equation II-38 will not be satisfied.

Corngold's original arguments[10] remain applicable to $g_b(B,v,\lambda_o)$ and yield

$$g_b(B,v,\lambda_o) \leq |g_b(B,v,\lambda_o)| \leq \frac{\pi}{2}\int_o^{v_B} \frac{\Sigma_i(v')}{\Sigma_i(v)} \Sigma_{inel}(v,v')\, dv' \equiv \frac{\pi}{2} g_{1b}(v) < K_1 .$$

(II-43)

He has shown that K_1 is independent of B^2. If $g_u(B,v,\lambda_o)$ did not have the factor $1/\Gamma_e(B,v,-\lambda_o)$ in the integrand, his original proof would remain unaltered. However, this factor implies $g_u(B,v,\lambda_o)$ cannot be bounded independent of B^2 unless $B^2 > [\pi\Sigma_{el}(v_B)/2]^2$.

To understand this condition, examine $\Gamma_e(B,v,-\lambda_o)$ in closer detail. We know that its zeros, given by equation II-30, satisfy $\lambda_e(B,v) + v\Sigma_T(v) > 0$ for fixed B^2. Furthermore, II-30 implies that the inequality $\frac{B}{\Sigma_{el}(v)} < \frac{\pi}{2}$ must be satisfied. We know from equation II-34 that $\min_{v\in[v_B^+,\infty)} \lambda_e(B,v) = \lambda_e(B,v_B) = \lambda_{el}$ where λ_{el} depends on B^2. Therefore, any discrete eigenvalue on the real axis in the gap between Γ_{SB} and Γ_e is bounded from above by λ_{el}. As B^2 increases, but with $B^2 < \left(\frac{\pi\Sigma_{el}(v_B)}{2}\right)^2$, the necessary condition II-38 can be satisfied by letting $(\lambda_{el} - \lambda_o)$ be as small as is necessary. The function $\Gamma_e(B,v,-\lambda_o)$ decreases with decreasing $\lambda_{el} - \lambda_o$, expecially near v_B. To satisfy equation II-38, for fixed B^2, we decrease $(\lambda_{el} - \lambda_o)$ and thus increase $g_u(B,v,\lambda_o)$ until II-38 is obeyed. This yields the large B^2 behavior of λ_o, namely, λ_o tends asymptotically to λ_{el} with increasing B^2.

When $B^2 > \left(\frac{\pi\Sigma_{el}(v_B)}{2}\right)^2$, $(\Sigma_{el}(v_B) = \max_{v\in(v_B,\infty)} \Sigma_{el}(v))$, we replace $\Gamma_e(B,v,-\lambda_o)$ by 1. Now only λ_A bounds λ_o and λ_A is independent of B^2. Therefore, Corngold's original arguments allow $g_u(B,v,\lambda_o)$ to be bounded by some K_2, independent of B^2. Thus, given any $B^2 > \left(\frac{\pi\Sigma_{el}(v_B)}{2}\right)^2$, there exists finite constants, K_1 and

K_2, independent of B^2, such that $|g_b(B,v,\lambda_o)| < K_1$ and $|g_u(B,v,\lambda_o)| < K_2$ and

$$\frac{1}{B}\int_o^\infty v\Sigma_i(v)\psi_H(B,v,\lambda_o)\Big(g_b(B,v,\lambda_o) + g_u(B,v,\lambda_o)\Big)\,dv < \frac{(K_1+K_2)}{B} \qquad \text{(II-44)}$$

This implies there exists a B^2, say B^{**2}, such that for any $B^2 > B^{**2}$, no discrete eigenvalues exist. This completes the proof.

Since λ_o tends to λ_{el}, λ_{el} tends to λ_A, and $B/\Sigma_{el}(v_B)$ tends to $\pi/2$ with increasing B^2, we expect $|\lambda_o - \lambda_{el}|$ to be very small at $B = \pi\Sigma_{el}(v_B)/2$. Taking $(B^{**})^2$ equal to $\pi\Sigma_{el}(v_B)/2$ predicts polycrystalline system sizes of the order of a mean free path. This is what is obtained for a water system. Since λ_A depends only on neutrons above the Bragg cutoff, this is reasonable. If, in fact, λ_A were the minimum collision frequency, we would have a "water-like" system.

F. PROPERTIES OF THE EDGE OF THE ELASTIC CONTINUUM

We have shown that λ_{el} bounds the discrete eigenvalues when $\lambda_A > \lambda_{el}$. To obtain the behavior of λ_{el} for small B^2, expand II-33 about $B^2 = 0$.

$$\lambda_{el} = v_B\left\{\Big(\Sigma_i(v_B) + \Sigma_a(v_B)\Big) + \frac{1}{3\Sigma_{el}(v_B)}\,B^2 + O(B^4)\right\} \qquad \text{(II-45)}$$

When the "λ-law" is satisfied for all $v < v_B$, λ_{el} becomes

$$\lambda_{el} = \lambda^* + \frac{v_B B^2}{3\,\Sigma_{el}(v_B^+)} + O(B^4) \qquad \text{(II-46)}$$

Thus, for small B^2, λ_{el} is similar to the bound proposed by Kothari[22] using a bounded energy variable. Corngold and Durgun[25] also proposed a line similar to II-46 using the full energy range and diffusion theory. We can obtain their bound by letting $D(v) = 1/3\,\Sigma_T(v)$, where $D(v)$ is a diffusion coefficient. Then II-46 becomes

$$\lambda_{el} = \lambda^* + v_B D(v_B) B^2 \left\{ 1 + \frac{\Sigma_i(v_B) + \Sigma_a(v_B)}{\Sigma_{el}(v_B)} \right\} + O(B^4) \qquad \text{(II-47)}$$

Since $\Sigma_i(v_B) + \Sigma_a(v_B) << \Sigma_{el}(v_B)$ in polycrystals, we have the diffusion theory result by setting the bracket coefficient of $v_B D(v_B) B^2$ equal to 1.

We have investigated the effects of anisotropic elastic scattering on λ_{el} by expanding the elastic, coherent scattering kernel in Legendre polynomials. In appendix D, we show, for any order expansion $N > 1$ that, to order B^2, the elastic continuum outside the area is given by

$$\lambda_e(B,v) = v\Sigma_i(v) + \frac{v}{3\,\Sigma_{el}(v)} \left[1 + \frac{\Sigma_{el}(v)_{P_1}}{\Sigma_{el}(v) + \Sigma_{el}(v)_{P_1}} \right] B^2 + O(B^4) \qquad \text{(II-48)}$$

$\Sigma_{el}(v)_{P_1}$ is the P_1 component of the elastic, coherent scattering cross section. Thus, the edge of the elastic continuum including anisotropic elastic scattering is

$$\lambda_{el} = v_B \Sigma_i(v_B) + \frac{v_B}{3\,\Sigma_{el}(v_B)} \left[1 + \frac{\Sigma_{el}(v_B)_{P_1}}{\Sigma_{el}(v_B) + \Sigma_{el}(v_B)_{P_1}} \right] B^2 + O(B^4) \,. \tag{II-49}$$

G. THE ROLE OF λ^*

We have, as yet, not considered the effect of λ^* on the dispersion curve, $\lambda_o(B^2)$. Since Γ_{SB} is a vertical cut in the λ-plane with real part equal to $-\lambda^*$, $\lambda_o(B^2)$ will not vary continuously through λ^*. The separation in B^2 of $\lambda_o(B^2)$ at λ^* can be estimated as follows: Consider the symmetrized eigenvalue problem

$$\chi(B,v,\lambda_o) = \frac{T(B,v,-\lambda_o)}{\Gamma_e(B,v,-\lambda_o)} \int_o^\infty k(v',v)\chi(B,v',\lambda_o)\,dv' \tag{II-50}$$

where

$$\chi(B,v,\lambda_o) = \frac{\tilde{\psi}_H(B,v,\lambda_o)}{\sqrt{M(v)}} \,, \tag{II-51}$$

$$k(v',v) = v'\Sigma_{inel}(v',v) \sqrt{\frac{M(v')}{M(v)}} \,, \tag{II-52}$$

$M(v)$ is the Maxwellian distribution function, and

$$k(v',v) = k(v,v') \tag{II-53}$$

by the detailed balance condition II-9. We know that $v\Sigma_T(v) = \lambda^*$ and $\Gamma_e(B,v,\lambda) = 1$ when $v < v_B$. Also

$$\lim_{\lambda_o \to \lambda^{*\pm}} \left\{ \tan^{-1}\left(\frac{Bv}{-\lambda_o + \lambda^*}\right) \right\} = \mp \frac{\pi}{2} \quad . \tag{II-54}$$

Let $\lambda_o^-(B^2)$ denote the fundamental eigenvalue and have magnitude less than λ^*. Let $\lambda_o^+(B^2)$ represent the segment of the dispersion curve which is greater than λ^*. The function $T(B,v,\lambda)$ in equation II-50 satisfies the inequalities $T(B,v,-\lambda_o^{\pm}(B^2)) \lesseqgtr 0$ when $v < v_B$. Define B^{*2} as that buckling for which $\lambda_o^-(B^2) = \lambda^*$ and B_+^2 as that buckling for which $\lambda_o^+(B^2) = \lambda^*$. We then have the two equations

$$\frac{\Gamma_e(B_+,v,-\lambda^*)}{T(B_+,v,-\lambda^*)} \chi(B_+,v,\lambda^*) = \int_o^\infty k(v',v)\chi(B_+,v',\lambda^*)\, dv' \tag{II-55}$$

and

$$\frac{\Gamma_e(B^*,v,-\lambda^*)}{T(B^*,v,-\lambda^*)} \chi(B^*,v,\lambda^*) = \int_o^\infty k(v',v)\chi(B^*,v',\lambda^*)\, dv' \,. \tag{II-56}$$

Multiply II-55 by $\chi(B^*,v,\lambda^*)$, II-56 by $\chi(B_+,v,\lambda^*)$, integrate over all v, subtract, and use II-53 to find

$$\int_o^\infty \chi(B_+,v,\lambda^*)\chi(B^*,v,\lambda^*) \left\{ \frac{\Gamma_e(B_+,v,-\lambda^*)}{T(B_+,v,-\lambda^*)} - \frac{\Gamma_e(B^*,v,-\lambda^*)}{T(B^*,v,-\lambda^*)} \right\} dv = 0 \tag{II-57}$$

Since we expect B_+^2 to be close to B^{*2}, expand $\dfrac{\Gamma_e(B_+,v,-\lambda^*)}{T(B_+,v,-\lambda^*)}$ about B^{*2}. Neglecting higher order terms yields

$$(B_+ - B^*) = \frac{\frac{2}{\pi}\int_o^{v_B} v\chi(B_+,v,\lambda^*)\chi(B^*,v,\lambda^*)\,dv}{\int_{v_B}^{\infty} v\chi(B_+,v,\lambda^*)\chi(B^*,v,\lambda^*)\frac{\partial}{\partial B^2}\left\{\frac{\Gamma_e(B,v,-\lambda^*)}{T(B,v,-\lambda^*)}\right\}_{B=B^*} dv}$$

$$+ O(B^+ - B^*)^2 . \qquad \text{(II-58)}$$

The derivative with respect to B^2 in II-58 is positive for all v. As well, when $\lambda_o^-(B^2) = \lambda^*$ is the fundamental eigenvalue, we have that $\chi(B^*,v,\lambda^*)$ is real and positive for all v. Physically, this follows from the fact that $\chi(B^*,v,\lambda^*)$ is the limit of functions which dominate the solution at long times and are thus real and positive. Mathematically, this results from the Perron-Frobenius theorem[32]. Therefore, the sign of $(B_+ - B^*)$ is determined by the dependence of $\chi(B_+,v,\lambda^*)$ on v.

An estimate of the velocity dependence of $\chi(B_+,v,\lambda^*)$ is obtained by approximating the inelastic scattering kernel with a one-term degenerate kernel (a kernel that is the product of a function of v and a function of v'). In chapter III, we show that this approximation implies $\chi(B_+,v,\lambda^*)$ is positive for $v > v_B$ and negative for $v < v_B$. Under these conditions, $B_+ - B^*$ is negative. This means that just prior to the disappearance of the fundamental mode at λ^*, another eigenvalue appears with value λ^* and increases from there with increasing B^2.

By combining these results with the large B^2 behavior predicted in the maximum buckling theorem, we obtain a dispersion curve

of the form

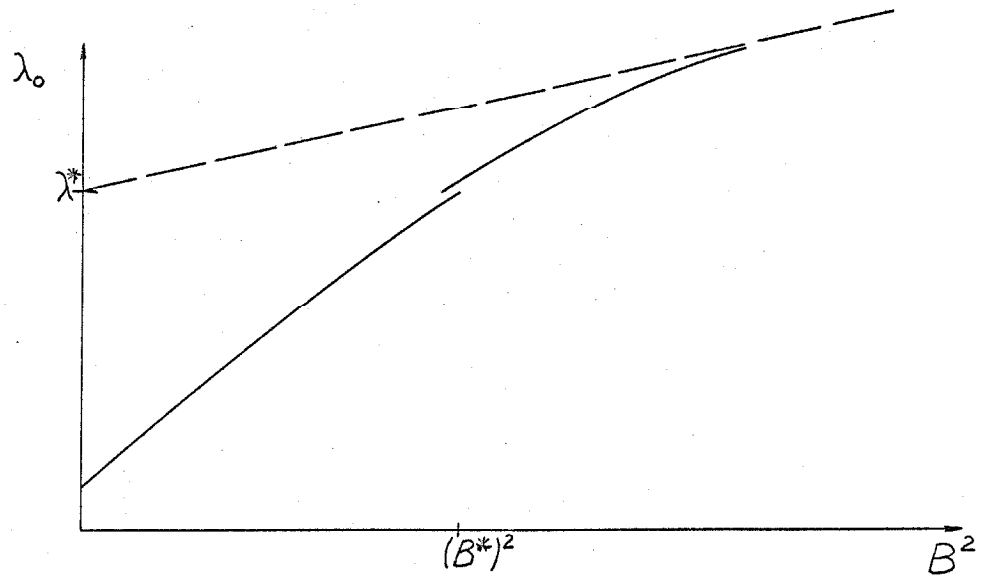

The dashed line is λ_{el} as a function of B^2.

The expression for the jump $(B^+ - B^*)$ is proportional to the ratio of an average square density of particles below to above the Bragg cutoff and, as such, is expected to be small[66].

In analyzing experimental data, it is conventional procedure to fit the measured dispersion curve with a power series

$$\lambda_o(B^2) = \lambda_o(B^2=0) + D_o B^2 - CB^4 + FB^6 \mp \ldots \qquad \text{(II-58a)}$$

By least square fitting, one attempts to arrive at values of the expansion coefficients. Nelkin[6] demonstrated with transport theory that such an expansion is derivable from perturbation theory by expanding the fundamental eigenvalue in a Maclaurin series in B^2. The results of the previous paragraphs show explicitly that Nelkin's derivation is

invalid for λ_o beyond λ^*. That is, even though discrete eigenvalues exist with magnitude greater than λ^* in the primary λ-plane, the coefficients in the expansion II-58a have a physical interpretation only when $\lambda_o < \lambda^*$.

H. PROPERTIES OF THE TOTAL SOLUTION

One may now ask whether the solution itself is a continuous function of the buckling. The fact that the dispersion curve is discontinuous at λ^* does not imply that the total solution is discontinuous. In appendix E, the continuity of the solution in B^2 is shown from direct examination of the Boltzmann equation. Furthermore we do not expect, physically, that altering system size will lead to a suddenly different response function. Certainly experimenters do not appear to observe such a jump near λ^* in, for example, beryllium. In chapter III, the continuity in B^2 is shown by the alternate approach of solving for the transformed density and inverting. In fact, we can explicitly demonstrate here the technique which, in this alternate approach, makes the conclusion manifest. It involves the analytic continuation of the dispersion relation II-37 from the right to the left of the sub-Bragg continuum. First, however, let us examine the various contributions in the "physical" plane (common terminology for the zeroth or primary Riemann sheet) to the total solution.

A representation of the solution in the physical plane can be derived by deforming the Bromwich inversion contour for the Laplace transform. The original inversion path lies to the right of all

singularities of $\tilde{\psi}(B,v,\lambda)$ or $\tilde{\varphi}(B,v,\mu,\lambda)$. Those portions of the λ-plane for which $\tilde{\psi}$ is not analytic are given by the solutions of II-31, II-33, and II-35. With this information, we can deform the contour as shown in figure 10. Thus the total solution will consist of continuum and discrete parts, i.e., line integrals about the sub-Bragg, elastic, and area continuums and about the discrete poles. Writing this solution out,

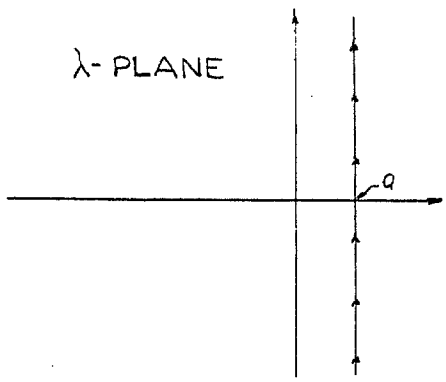

$$\psi(B,v,t) = \lim_{\delta\to\infty} \frac{1}{2\pi i}\int_{a-i\delta}^{a+i\delta} \tilde{\psi}(B,v,\lambda)e^{\lambda t}\, d\lambda \qquad \text{(II-59a)}$$

$$\psi(B,v,t) = \sum_{i=1}^{N} \tilde{\psi}_i(B,v)e^{-\lambda_i t} + \frac{1}{2\pi i}\left\{\int_{\partial A} + \int_{\partial \Gamma_e} + \int_{\partial \Gamma_{SB}}\right\} \tilde{\psi}(B,v,\lambda)e^{\lambda t}\, d\lambda \qquad \text{(II-59b)}$$

Corngold has shown that the integrands of the integrals about Γ_{SB} and the area exhibit the wave-like behavior that one expects when going beyond simple diffusion theory. Note that parameterizing the integrals about Γ_{SB} by $\lambda = -\lambda^* \pm iB\alpha$ implies $e^{\lambda t} = e^{-\lambda^* t} e^{\pm iB\alpha}$. That is, the damping factor $e^{-\lambda^* t}$ appears in front of the contribution from Γ_{SB} reflecting the constant collision frequency of the sub-Bragg neutrons involved.

On the other hand, the contribution from Γ_e cannot exhibit wave-like behavior. This term is more transparent in the form

$$\frac{1}{2\pi i}\int_{\partial\Gamma_e} e^{\lambda t}\tilde{\psi}(B,v,\lambda)\,d\lambda = \frac{1}{2\pi i}\int_{-\lambda_{el}}^{-\lambda_A} dp\, e^{pt}\{\tilde{\psi}^{+}(B,v,p) - \tilde{\psi}^{-}(B,v,p)\} \tag{II-60}$$

We previously noted that the solutions of $\Gamma_e(B,v,\lambda) = 0$, namely, the set Γ_e, represent decay constants for neutrons behaving in a one-velocity manner. These neutrons are singular in this velocity-dependent formalism. Thus, we see clearly that the continuum contribution from Γ_e concerns elastically scattered neutrons. The coefficient of e^{pt} acts to couple the various singular modes through inelastic scattering collisions.

Considering all the various contributions, the continuity of $\tilde{\psi}$ with B^2 involves the interplay of the discrete mode and sub-Bragg continuum as the pole tends towards Γ_{SB}. An alternate approach, however, is available for the examination of this question.

I. ANALYTIC CONTINUATION OF THE DISPERSION LAW

We can alternatively attempt to find a representation in which the continuity of the solution in B^2 is manifest. Such a representation is provided by contour deformation together with the analytic continuation of $\tilde{\varphi}(B,v,\mu,\lambda)$ or $\tilde{\psi}(B,v,\lambda)$ through Γ_{SB}. Such a contour is illustrated in figure 11 where one no longer has a cut that crosses the real axis at $-\lambda^*$. Thus, we expect the eigenvalues to vary continuously with B^2. The explicit construction of such a continuation is performed in chapter III. However, because the collision frequency is constant for $v < v_B$, we can demonstrate the

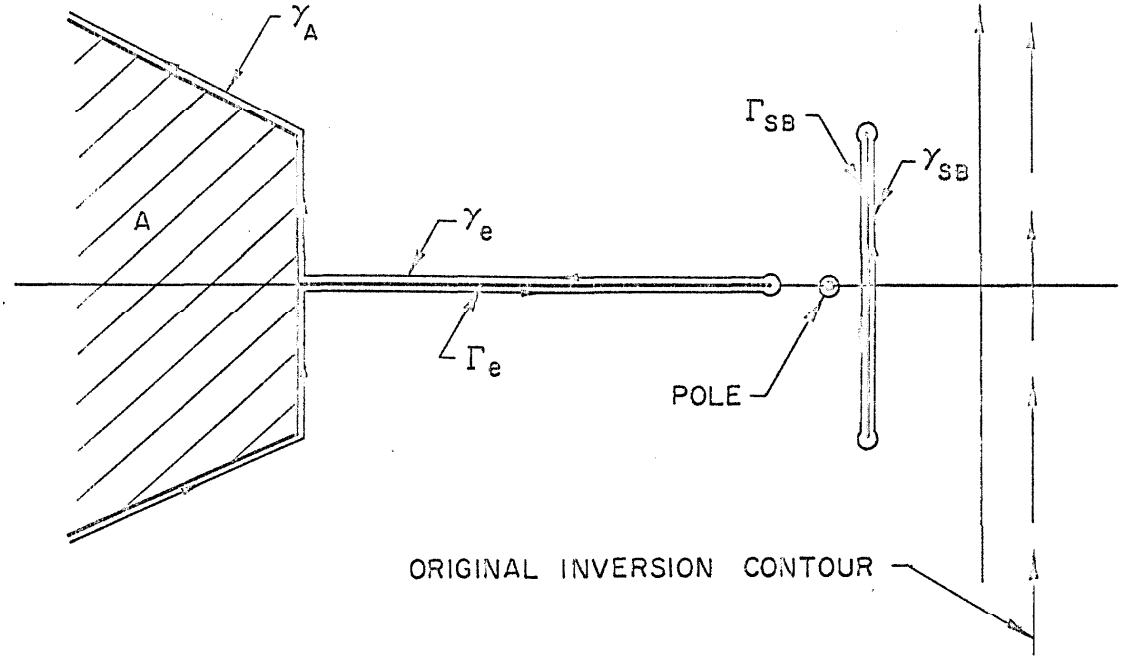

FIG. 10. The deformed contour in the primary λ-plane.

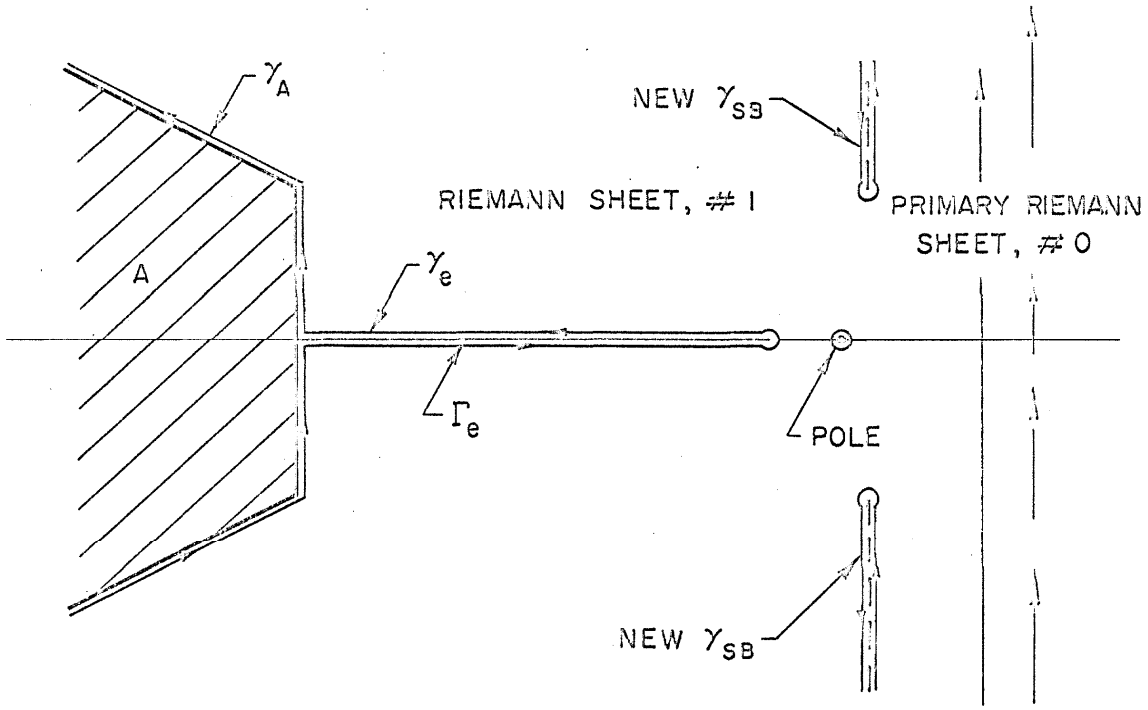

FIG. 11. The deformed contour employed with the analytic continuation of the solution.

explicit analytic continuation of the dispersion relation II-37. This allows the dispersion curve to be extended in a continuous manner past λ^*.

Define $\mathcal{E}(v^2)$ as

$$\mathcal{E}(v^2) = \frac{1}{2}\int_o^\infty v'\Sigma_{inel}(v',v)\tilde{\psi}_H(B,v',\lambda)\,dv' \tag{II-61}$$

Then the dispersion relation II-37 becomes

$$\Lambda(\lambda,B;\tilde{\psi}_H) = 1 - \int_o^{v_B}\int_{-1}^{1} \frac{v^2\mathcal{E}(v^2)\,dv\,d\mu}{\lambda+\lambda^*+iBv\mu}$$

$$-\int_{v_B}^\infty \int_{-1}^{1} \frac{v^2\mathcal{E}(v^2)\,dv\,d\mu}{\Gamma_e(B,v,\lambda)(\lambda+v\Sigma_T(v)+iBv\mu)}$$

$$= 0 \tag{II-62}$$

Define

$$\Lambda_1(\lambda,B;\mathcal{E}) = \int_o^{v_B}\int_{-1}^{1}\int_o^{2\pi} \frac{v^2\mathcal{E}(v^2)\,dv\,d\mu\,d\varphi}{2\pi(\lambda+\lambda^*+iBv\mu)} \tag{II-63}$$

A more transparent form of Λ_1 is obtained by transforming to cylindrical coordinates.

$$\Lambda_1(\lambda,B;\mathcal{E}) = \int_{-v_B}^{v_B} \frac{\mathcal{E}_1(z)\,dz}{\lambda+\lambda^*+iBz} \tag{II-64}$$

where

$$\mathcal{E}_1(z) = \int_o^{\sqrt{r^2+z^2}} \mathcal{E}(r^2+z^2)\,r\,dr \tag{II-65}$$

and $v^2 = r^2 + z^2$. The functional

$$\Lambda_2(\lambda,B;\mathcal{E}) = \int_{v_B}^{\infty}\int_{-1}^{1} \frac{v^2\mathcal{E}(v^2)\,dv\,d\mu}{\Gamma_e(B,v,\lambda)(\lambda+v\Sigma_T(v)+iBv\mu)} \quad \text{(II-66)}$$

is analytic outside Γ_e and the area of figure 7 and, in particular, for $\lambda \in \Gamma_{SB}$. On the other hand, $\Lambda_1(\lambda,B;\mathcal{E})$, defined by a Cauchy integral, is analytic in the λ-plane cut by Γ_{SB}. That is, it is a sectionally holomorphic functional[37]. Parameterizing λ as $\lambda = -\lambda^* - iB\nu$ yields

$$\Lambda_1(\lambda(\nu),B;\mathcal{E}) = \frac{1}{iB}\int_{-v_B}^{v_B} \frac{\mathcal{E}_1(z)\,dz}{z-\nu} \quad \text{(II-67)}$$

Therefore, in the ν-plane, $\Lambda_1(\lambda(\nu),B;\mathcal{E})$ is analytic except for the set on the real axis, $[-v_B,v_B]$. We assume that $\mathcal{E}_1(z)$ obeys a suitable Hölder condition[37] in z. The Plemelj formulas then allow an evaluation of $\Lambda_1(\lambda(\nu),B;\mathcal{E})$ on either side of the cut, Γ_{SB}. Thus, as $\nu \to \zeta^{\pm}$, $\zeta \in (-v_B,v_B)$, we have

$$\Lambda_1^{\pm}(\lambda(\zeta),B;\mathcal{E}) = \frac{1}{iB}\int_{-v_B}^{v_B} \frac{\mathcal{E}_1(z)\,dz}{z-\zeta} \pm \frac{\pi}{B}\mathcal{E}_1(\zeta) \quad \text{(II-68)}$$

The symbol $\int$ denotes the Cauchy principle value integral. From this, we can construct the analytic continuation of $\Lambda_1(\lambda,B;\mathcal{E})$ across Γ_{SB}. It is given by

$$\Lambda_{1c}(\lambda,B;\mathcal{E}) = \int_{-v_B}^{v_B} \frac{\mathcal{E}_1(z)\,dz}{\lambda+\lambda^*+iBz} + \frac{2\pi}{B}\mathcal{E}_1\left(\frac{\lambda+\lambda^*}{iB}\right) \quad \text{(II-69)}$$

Using the diagram on the right, we can summarize the procedure as follows: $\Lambda_1(\lambda,B;\mathcal{E})$ is analytic in the domain D_1 and continuous in $D_1 \cup \Gamma_{SB}$. $\Lambda_{1c}(\lambda,B;\mathcal{E})$ is analytic in the domain D_2 and continuous in $D_2 \cup \Gamma_{SB}$. Furthermore, $\Lambda_{1c}(\lambda,B;\mathcal{E}) = \Lambda_1(\lambda,B;\mathcal{E})$ for $\lambda \in \Gamma_{SB}$. Therefore, $\Lambda_{1c}(\lambda,B;\mathcal{E})$ is the analytic continuation of $\Lambda_1(\lambda,B;\mathcal{E})$ from D_1 to D_2 and vice versa[38].

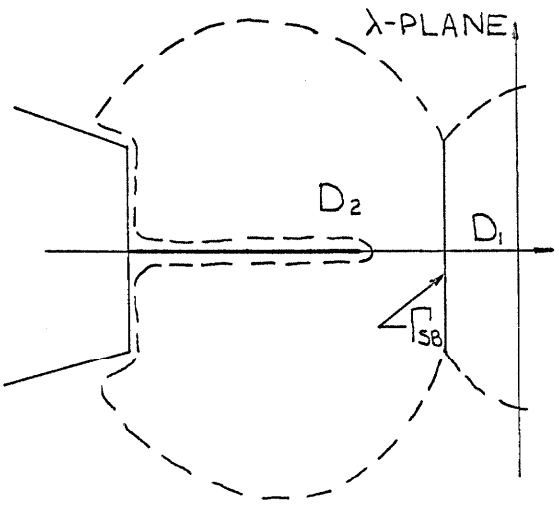

With this, the analytic continuation of the dispersion law is

$$\Lambda_c(\lambda,B;\mathcal{E}) = 1 - \Lambda_{1c}(\lambda,B;\mathcal{E}) - \Lambda_2(\lambda,B;\mathcal{E}) \qquad \text{(II-70)}$$

Hence, we can extend the dispersion curve, $\lambda_o(B^2)$, in a continuous manner past λ^* by using the eigenvalues of the analytically continued dispersion law when $B^2 > B^{*2}$.

One can conjecture that since experimenters observe no discontinuity in their response function as B^2 passes B^{*2} and report what they feel are valid decay constants, the discrete eigenvalue measured is the eigenvalue of the analytically continued dispersion law. This is physically reasonable since the sub-Bragg continuum in either representation is excited by sub-Bragg neutrons which are smaller in number at early times. Hence, we expect it to be small compared with the discrete mode. However, we must realize that in either representation, when no eigenvalues exist with magnitude less than λ^*, there is always

a continuum contribution to the right of the discrete poles that dominates at very long times.

For the remainder of our analysis, we proceed to chapter III in which a simple model of the inelastic scattering kernel is utilized to find explicit solutions for $\tilde{\varphi}(B,v,\mu,\lambda)$ and $\tilde{\psi}(B,v,\lambda)$. This will allow a detailed investigation of the ideas in chapter II.

III. ANALYSIS WITH A MODELED KERNEL

A. DISCUSSION OF THE MODELED KERNEL

In this chapter, a simplified model of the inelastic scattering kernel is used to examine in greater detail the conclusions of chapter II. As well, we will investigate the contributions from the various continuum parts of the total solution. Of particular interest is the buckling range $B^2 > B^{*2}$ where the relation between theory and experiment has not been clear.

The modeled kernel is called a one-term or simple degenerate kernel and is given by

$$v'\Sigma_{inel}(v',v) = \frac{1}{\overline{\Sigma}} v'\Sigma_i(v')v\Sigma_i(v)M(v) \qquad \text{(III-1)}$$

where

$$\overline{\Sigma} = \int_o^\infty v\Sigma_i(v)M(v)\, dv \,. \qquad \text{(III-2)}$$

Mathematically, this approximation is the truncation after one term of a degenerate kernel expansion of the inelastic scattering kernel. Such an expansion is valid because Kuščer and Corngold have shown that the symmetrized form of the inelastic, isotropic scattering kernel for solids in the incoherent approximation[1] is square-integrable for low and intermediate values of (v,v'). Since the kernel must reduce to the monatomic gas kernel at high (v,v') (where we know the kernel's third iterate is square-integrable[31]) they conclude that the symmetrized

---

[1] Solids in which inelastic coherent scattering is negligible.

form of S_1 (defined by equation II-17) is completely continuous. But a suitable definition of a completely continuous operator[67] is one which can be uniformly approximated by an expansion in projection operators, i.e., an operator whose kernel can be represented by a sequence of degenerate kernels.

Expansion of kernels as a sum of products separable in v' and v are used by Tricomi[40] who calls them Pincherle-Goursat kernels. He shows that a Fredholm integral equation whose kernel is the sum of n products separable as above can be reduced to an algebraic system of n linear equations in n unknowns.

The approximate kernel III-1 preserves the total cross section and obeys detailed balance. It also simplifies the mathematical problem by allowing a closed form solution to be obtained and tractable expressions for the dispersion relation and continuum contributions. As well, since the modeled kernel III-1 is square integrable, the continuum regions of the λ-plane obtained with III-1 will be identical to those obtained with the general inelastic kernel of chapter II.

A disadvantage of such modeling is that higher moments of the general inelastic kernel are not preserved. Furthermore, a synthetic kernel can be regarded as a perfect thermalizer because a single collision is sufficient to completely thermalize a neutron. Thus, one expects dispersion curves to be less "diffusion cooled" than those calculated with more general kernels. Correspondingly, asymptotic energy spectra calculated with this model will appear too Maxwellian in leaky systems. A comprehensive study of degenerate kernels in

neutron thermalization has been performed by Shapiro and Corngold[41].

For systems with no elastic scattering, the synthetic kernel has been employed by many authors to gain insight into numerous problems in neutron transport theory. As examples, Corngold et al.[39] used it to extract information about the spectrum of the space-independent Boltzmann operator. Williams[42] was able to solve the energy-dependent Milne problem using III-1 and the Weiner Hopf technique. Nelkin[11] examined the discrete time eigenvalue spectrum of the Boltzmann operator in spherical geometry while Arkuszewski[69] examined the effects of absorption on diffusion lengths. Recently, Dorning[3] used a synthetic kernel to derive information about the behavior of discrete time eigenvalues for water assemblies. In addition, models of this type, such as the Krook model, have found extensive use in the kinetic theory of gases.

By including a model of elastic scattering, the approximation III-1 implies a modified synthetic kernel given by

$$v'\Sigma_s(v',v) = \frac{1}{\Sigma} v'\Sigma_i(v')v\Sigma_i(v)M(v) + v\Sigma_{el}(v)\delta(\underline{v}'^2 - \underline{v}^2) \quad . \qquad \text{(III-3)}$$

As mentioned previously, Corngold and Durgun[25] used III-3 and diffusion theory to investigate pulsed neutron experiments in polycrystals. However, because of the diffusion theory approximation, they were led to consider "peaks" in the continuum integrand with corresponding "widths" when $B^2 > B^{*2}$. We now know from chapter II that discrete eigenvalues can exist for $B^2 > B^{*2}$ so that there are no associated widths.

B. SOLUTION OF THE MODELED BOLTZMANN EQUATION

Subject to modeling with III-3, the Boltzmann equation becomes

$$\left(\frac{\partial}{\partial t} + v\Sigma_T(v) + iBv\mu\right)\varphi(B,v,\mu,t)$$

$$= \frac{v\Sigma_i(v)M(v)}{2\overline{\Sigma}} \int_0^\infty\int_{-1}^1 v'\Sigma_i(v')\varphi(B,v',\mu',t)\, dv'\, d\mu'$$

$$+ \frac{v\Sigma_{el}(v)}{2} \int_{-1}^1 \varphi(B,v,\mu',t)\, d\mu' + Q(B,\underline{v})\delta(t) \quad . \qquad \text{(III-4)}$$

By Laplace transforming III-4 and using the definitions II-20 and II-22 with

$$f(\lambda,B) = \int_0^\infty\int_{-1}^1 v'\Sigma_i(v')\tilde{\varphi}(B,v',\mu',\lambda)\, dv'\, d\mu' \qquad \text{(III-5)}$$

we obtain

$$(\lambda + v\Sigma_T(v) + iBv\mu)\tilde{\varphi}(B,v,\mu,\lambda) = \frac{v\Sigma_i(v)M(v)f(\lambda,B)}{2\overline{\Sigma}} + \frac{v\Sigma_{el}(v)\tilde{\psi}(B,v,\lambda)}{2}$$

$$+ Q(B,v,\mu) \qquad \text{(III-6)}$$

Assume $\lambda + v\Sigma_T(v) + iBv\mu \neq 0$, divide by it, and integrate over μ to find

$$\tilde{\psi}(B,v,\lambda) = \frac{T(B,v,\lambda)}{\Gamma_e(B,v,\lambda)} \frac{v\Sigma_i(v)M(v)}{\overline{\Sigma}} f(\lambda,B) + \frac{S(B,v,\lambda)}{\Gamma_e(B,v,\lambda)} \quad . \qquad \text{(III-7)}$$

Here, we have implicitly assumed $\Gamma_e(B,v,\lambda) \neq 0$ and defined $S(B,v,\lambda)$ by

$$S(B,v,\lambda) = \int_{-1}^{1} \frac{Q(B,v,\mu)\, d\mu}{\lambda + v\Sigma_T(v) + iBv\mu} \quad . \tag{III-8}$$

Now multiply III-7 by $v\Sigma_i(v)$, integrate over all v, and use III-5 to obtain

$$f(\lambda,B)\left\{1 - \int_o^\infty \frac{v^2\Sigma_i(v)^2 M(v)}{\overline{\Sigma}} \frac{T(B,v,\lambda)}{\Gamma_e(B,v,\lambda)}\, d\lambda\right\} = \int_o^\infty \frac{v\Sigma_i(v)S(B,v,\lambda)\, dv}{\Gamma_e(B,v,\lambda)} \quad . \tag{III-9}$$

This last equation can be simplified by defining

$$S(\lambda,B) = \int_o^\infty \frac{v\Sigma_i(v)S(B,v,\lambda)}{\Gamma_e(B,v,\lambda)}\, dv \tag{III-10}$$

and

$$\Lambda(\lambda,B) = 1 - \int_o^\infty \frac{v^2\Sigma_i^2(v)M(v)}{\overline{\Sigma}} \frac{T(B,v,\lambda)}{\Gamma_e(B,v,\lambda)}\, dv \quad . \tag{III-11}$$

Thus, where $\Lambda(\lambda,B) \neq 0$, we find

$$f(\lambda,B) = \frac{S(\lambda,B)}{\Lambda(\lambda,B)} \quad . \tag{III-12}$$

We can use these results to construct the solutions for $\tilde{\varphi}(B,v,\mu,\lambda)$ and $\tilde{\psi}(B,v,\lambda)$. They are

$$\tilde{\varphi}(B,v,\mu,\lambda) = \frac{1}{(\lambda + v\Sigma_T(v) + iBv\mu)} \left\{ \frac{v\Sigma_i(v)M(v)}{2\overline{\Sigma}} \frac{S(\lambda,B)}{\Lambda(\lambda,B)} + \frac{v\Sigma_{el}(v)S(B,v,\lambda)}{2\Gamma_e(B,v,\lambda)} + Q(B,v,\mu) \right\} \tag{III-13}$$

and

$$\tilde{\psi}(B,v,\lambda) = \frac{1}{\Gamma_e(B,v,\lambda)} \left\{ \frac{v\Sigma_i(v)M(v)}{\Sigma} \frac{S(\lambda,B)}{\Lambda(\lambda,B)} T(B,v,\lambda) + S(B,v,\lambda) \right\} . \tag{III-14}$$

When the source is isotropic, i.e.,

$$Q(B,v,\mu) = \frac{Q(B,v)}{2} \tag{III-15}$$

the expressions III-13 and III-14 become

$$\tilde{\varphi}(B,v,\mu,\lambda) = \frac{1}{2(\lambda + v\Sigma_T(v) + iBv\mu)\Gamma_e(B,v,\lambda)} \left\{ \frac{v\Sigma_i(v)M(v)}{\Sigma} \frac{S(\lambda,B)}{\Lambda(\lambda,B)} + Q(B,v) \right\} \tag{III-16}$$

and

$$\tilde{\psi}(B,v,\lambda) = \frac{T(B,v,\lambda)}{\Gamma_e(B,v,\lambda)} \left\{ \frac{v\Sigma_i(v)M(v)}{\Sigma} \frac{S(\lambda,B)}{\Lambda(\lambda,B)} + Q(B,v) \right\} . \tag{III-17}$$

The solution, $\varphi(B,v,\mu,t)$, is given by the transform inversion of $\tilde{\varphi}(B,v,\mu,\lambda)$, namely,

$$\varphi(B,v,\mu,t) = \lim_{\gamma \to \infty} \frac{1}{2\pi i} \int_{a-i\gamma}^{a+i\gamma} e^{\lambda t} \tilde{\varphi}(B,v,\mu,\lambda)\, d\lambda \tag{III-18}$$

where "a" lies to the right of all singularities of $\tilde{\varphi}$. To interpret this solution, we would like to use contour deformation. This requires that we know the features of the analytic continuation of $\tilde{\varphi}(B,v,\mu,\lambda)$ in the left half plane.

C. STRUCTURE OF THE TRANSFORM PLANE

An examination of the analyticity of $\tilde{\varphi}$ or $\tilde{\psi}$ in λ yields the same results as those obtained in chapter II. That is, $\tilde{\varphi}(B,v,\mu,\lambda)$ is analytic in the entire λ-plane with the exception of the sets defined by

$$\lambda + v\Sigma_T(v) + iBv\mu = 0 \qquad v \in [0,\infty);\ \mu \in [-1,1] \tag{III-19}$$

and

$$\Gamma_e(B,v,\lambda) = 0 \qquad v \in [v_B^+,\infty) \ . \tag{III-20}$$

These, as expected, yield the same continuum regions as equations II-31 and II-32. In addition, $\tilde{\varphi}$ and $\tilde{\psi}$ are not analytic at those values of λ for which

$$\Lambda(\lambda,B) = 0 \ . \tag{III-21}$$

The function $\Lambda(\lambda,B)$ is called the dispersion function and equation III-21 the dispersion law. The roots of the dispersion law are the discrete eigenvalues of the problem, and the dependence of the fundamental eigenvalue, λ_o, on B^2 is the dispersion curve.

Thus, the λ-plane structure is that of figure 7 except, possibly, for the number and location of the discrete eigenvalues.

D. PROPERTIES OF THE DISPERSION LAW

The arguments in appendix A demonstrate that the dispersion law has only real roots. Furthermore, the number of roots and their sign can be determined by examining the derivative of $\Lambda(\lambda,B)$ with

respect to real λ, i.e.,

$$\frac{\partial \Lambda(\lambda,B)}{\partial \lambda} = \int_o^\infty \frac{v^2 \Sigma_i^2(v) M(v)\, dv}{\overline{\Sigma}(\Gamma_e(B,v,\lambda))^2\{(\lambda+v\Sigma_T(v))^2+(Bv)^2\}} > 0. \quad \text{(III-22)}$$

For fixed B^2, $\Lambda(\lambda,B)$ has, at most, one root on either side of Γ_{SB}. More detailed calculations[21,43,44] of eigenvalues below λ^* in both graphite and beryllium indicate there is only one such eigenvalue.

The sign of the root, or discrete eigenvalue, is determined by noting that at $B^2 = 0$, the only solution of III-21 is $\lambda = 0$ (neglecting absorption). Since $T(B,v,\lambda)$ is non-increasing in B (denoted $T(B,v,\lambda) \in \downarrow$ in B), we have

$$\Lambda(0,B>0) > \Lambda(0,0) = 0 \quad . \quad \text{(III-23)}$$

This combined with III-22 implies that any eigenvalue of III-21, for $B^2 > 0$, lies to the left of the origin, i.e., is negative. One would expect this conclusion on physical grounds.

The dispersion curve will exhibit the same general behavior as predicted for the more general inelastic kernel in chapter II. Thus, consider the behavior of $\Lambda(\lambda,B)$ when λ is near Γ_{SB}. As before, define

$$\Lambda_1(\lambda,B) = \int_o^{v_B}\int_{-1}^{1} \frac{v^2 \Sigma_i^2(v) M(v)\, dv\, d\mu}{2\overline{\Sigma}(\lambda+\lambda^*+iBv\mu)} \quad \text{(III-24)}$$

and

$$\Lambda_2(\lambda,B) = \int_{v_B}^{\infty}\int_{-1}^{1} \frac{v^2\Sigma_i^2(v)M(v)\,dv\,d\mu}{2\overline{\Sigma}\Gamma_e(B,v,\lambda)(\lambda+v\Sigma_T(v)+iBv\mu)} \quad \text{(III-25)}$$

In the integrand of III-24, $(v\Sigma_i(v))^2 = \{v\Sigma_T(v) - v_T\Sigma_a(v_T)\}^2 \equiv \beta^{*2}$ because $v\Sigma_T(v) = \lambda^*$ and $\Sigma_a(v)$ is proportional to $1/v$ for all v. A more transparent form of $\Lambda_1(\lambda,B)$ is obtained by converting to cylindrical coordinates. Thus,

$$\Lambda_1(\lambda,B) = \frac{\beta^{*2}}{2iB\overline{\Sigma}v_T^2}\int_{-v_B}^{v_B} \frac{(e^{-z^2/v_T^2} - e^{-v_B^2/v_T^2})}{z - i\left(\frac{\lambda+\lambda^*}{B}\right)}\,dz \quad \text{(III-26)}$$

where v_T is the thermal speed, 2200 m/s. In this form, the integral is of the Cauchy type and the Plemelj formulas[37] can be applied to evaluate $\Lambda_1(\lambda,B)$ as λ approaches Γ_{SB} from the right (+) or the left (-). For $\lambda = \zeta$, $\zeta \in \Gamma_{SB}$, we have

$$\Lambda_1^{\pm}(\zeta,B) = \frac{\beta^*}{2iB\overline{\Sigma}v_T^2}\left\{\int_{-v_B}^{v_B} \frac{e^{-z^2/v_T^2} - e^{-v_B^2/v_T^2}}{z - i\left(\frac{\zeta+\lambda^*}{B}\right)}\,dz \right.$$

$$\left. \pm \pi i\left(e^{[(\zeta+\lambda^*)/Bv_T]^2} - e^{-(v_B/v_T)^2}\right)\right\} \quad \text{(III-27)}$$

and when $\zeta = -\lambda^*$,

$$\Lambda_1^{\pm}(-\lambda^*,B) = \pm\frac{\pi\beta^{*2}}{2B\overline{\Sigma}v_T^2}\left(1 - e^{-(v_B/v_T)^2}\right). \quad \text{(III-28)}$$

Define, as before, B^{*2} to be that buckling such that

$$\Lambda^{+}(-\lambda^{*},B^{*}) = 0 \ . \qquad \text{(III-29)}$$

Then $\Lambda^{-}(-\lambda^{*},B^{*}) \neq 0$ implying the dispersion curve does not extend continuously past λ^{*}. Since $\Lambda_2(-\lambda^{*},B^{*}) < 1$ and $\frac{T(B,v,-\lambda^{*})}{\Gamma_e(B,v,-\lambda^{*})} \in \downarrow$ in B, we can obtain a zero of

$$\Lambda^{-}(-\lambda^{*},B) = 0 \qquad \text{(III-30)}$$

only by decreasing B. Hence, that B satisfying III-30, denoted B_{+}, is less than B^{*}, i.e., $B_{+} - B^{*} < 0$. This agrees with the result in chapter II.

We can again estimate $B_{+} - B^{*}$ by subtracting III-29 from III-30 and expanding $\frac{T(B_{+},v,-\lambda^{*})}{\Gamma_e(B_{+},v,-\lambda^{*})}$ about B^{*2}. This yields

$$B_{+} - B^{*} = \frac{\frac{\pi\beta^{*2}}{\overline{\Sigma} v_T^2}\left(1 - e^{-(v_B/v_T)^2}\right)}{\int_{v_B}^{\infty} \frac{v^2\Sigma_i^2(v)M(v)}{\overline{\Sigma}} \frac{\partial}{\partial B^2}\left(\frac{T(B,v,-\lambda^{*})}{\Gamma_e(B,v,-\lambda^{*})}\right)_{B=B^{*}} dv} + O(B_{+} - B^{*})^2 \qquad \text{(III-31)}$$

As before, the derivative with respect to B^2 in III-31 is negative confirming $B_{+} - B^{*} < 0$.

The dispersion curve is also expected to have the same large B^2 behavior as before. The role of λ_{el}, the edge of the elastic continuum, is, quite naturally, unaffected by approximations of the inelastic kernel. An examination of $\Lambda_2(\lambda,B)$ in III-25 shows that,

indeed, λ_o tends to λ_{el} with increasing buckling.[1]

E. NUMERICAL EVALUATION OF THE DISPERSION CURVE

With this information as a guide to the nature of the dispersion curve, numerical calculations of $\lambda_o(B^2)$ were performed for graphite and beryllium. A Newton-Raphson technique was programmed for use on the IBM-7090-7094 computer. The cross sections used are shown in figures 12 and 13 while figure 14 presents the resulting dispersion curve for graphite. As indicated, the total cross section is assumed constant above the Bragg cutoff while the elastic cross section tends to zero at high energies. The inelastic cross section is obtained by subtraction and $\Sigma_a(v)$ is proportional to $1/v$. No discontinuities other than that at v_B were included. We did perform a calculation in which the structure of the first Bragg peak was modeled and found the dispersion curve to be somewhat cooler.[2] This results from enhancing

---

[1] By performing estimates valid for large B^2 (beyond the range of current experimental interest), we find

$$\lambda_o = \lambda_{el}\left\{1 - \exp\left(-\frac{\overline{\Sigma}\left(\frac{\Sigma_{el}(v_B)}{B}\right)^2 \sin^2\left(\frac{B}{\Sigma_T(v_B)}\right)\left[\Sigma_T(v_B) - B\cot\left(\frac{B}{\Sigma_{el}(v_B)}\right)\right]}{\lambda^{*2}M(v_B)}\right)\right\}$$

The diffusion theory counterpart of this result[25] can be derived by expanding the exponential in powers of B^2 and retaining only terms of order B^2.

[2] The maximum error made in computing $\lambda_o(B^2)$ with cross sections that are constant above v_B is 2% when compared with $\lambda_o(B^2)$ calculated with the cross sections in figure 13. The error is less than 1% in the range $\lambda_o < \lambda^*$. The maximum error made in computing $\lambda_o(B^2)$ with a cross section model that includes the first Bragg peak is $3\frac{1}{2}$% when compared with the $\lambda_o(B^2)$ values that result with the cross sections in figure 13. Again, the error is less than 1% in the range $\lambda_o < \lambda^*$.

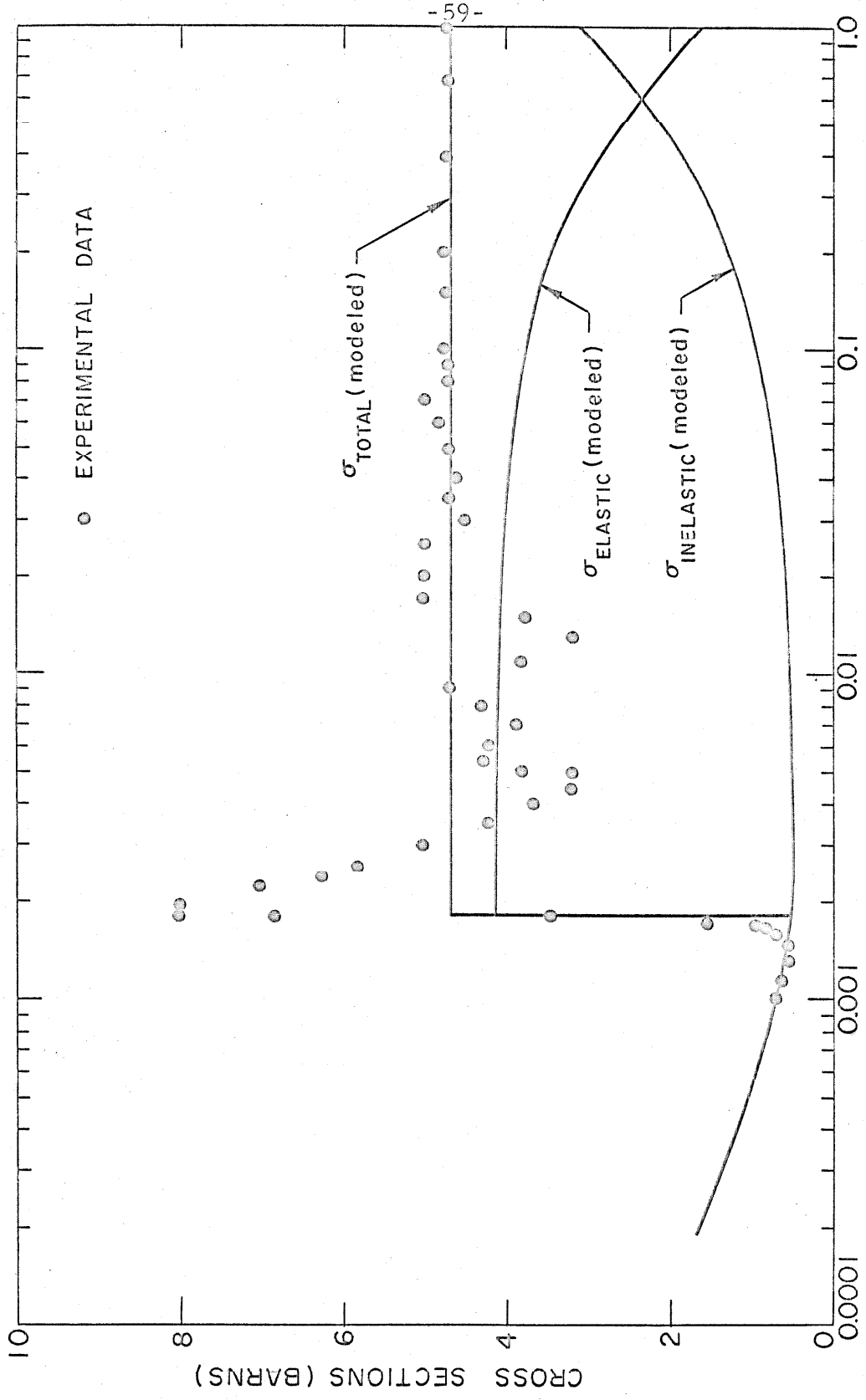

FIG. 12. Cross section models for graphite.

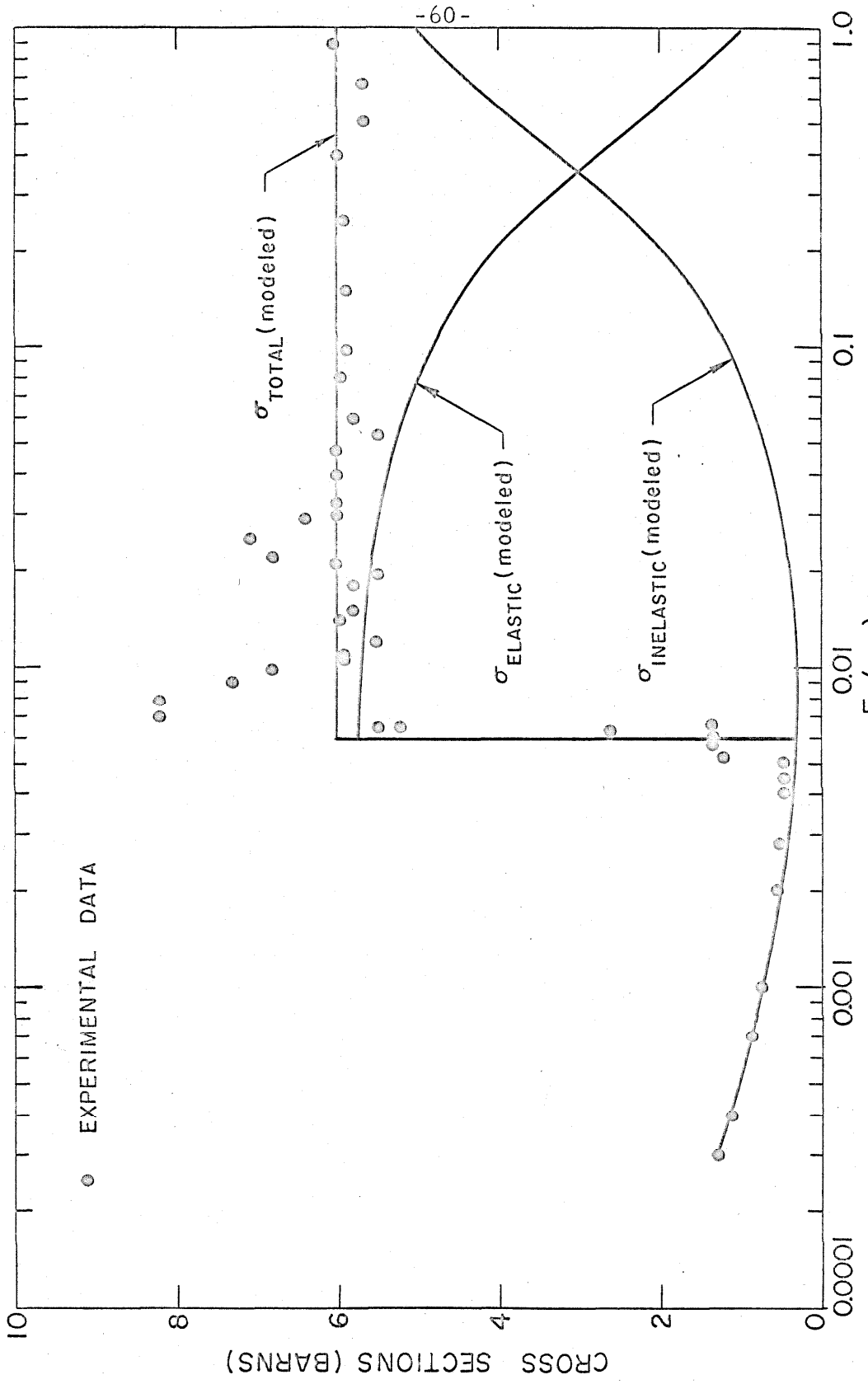

FIG. 13. Cross section models for beryllium.

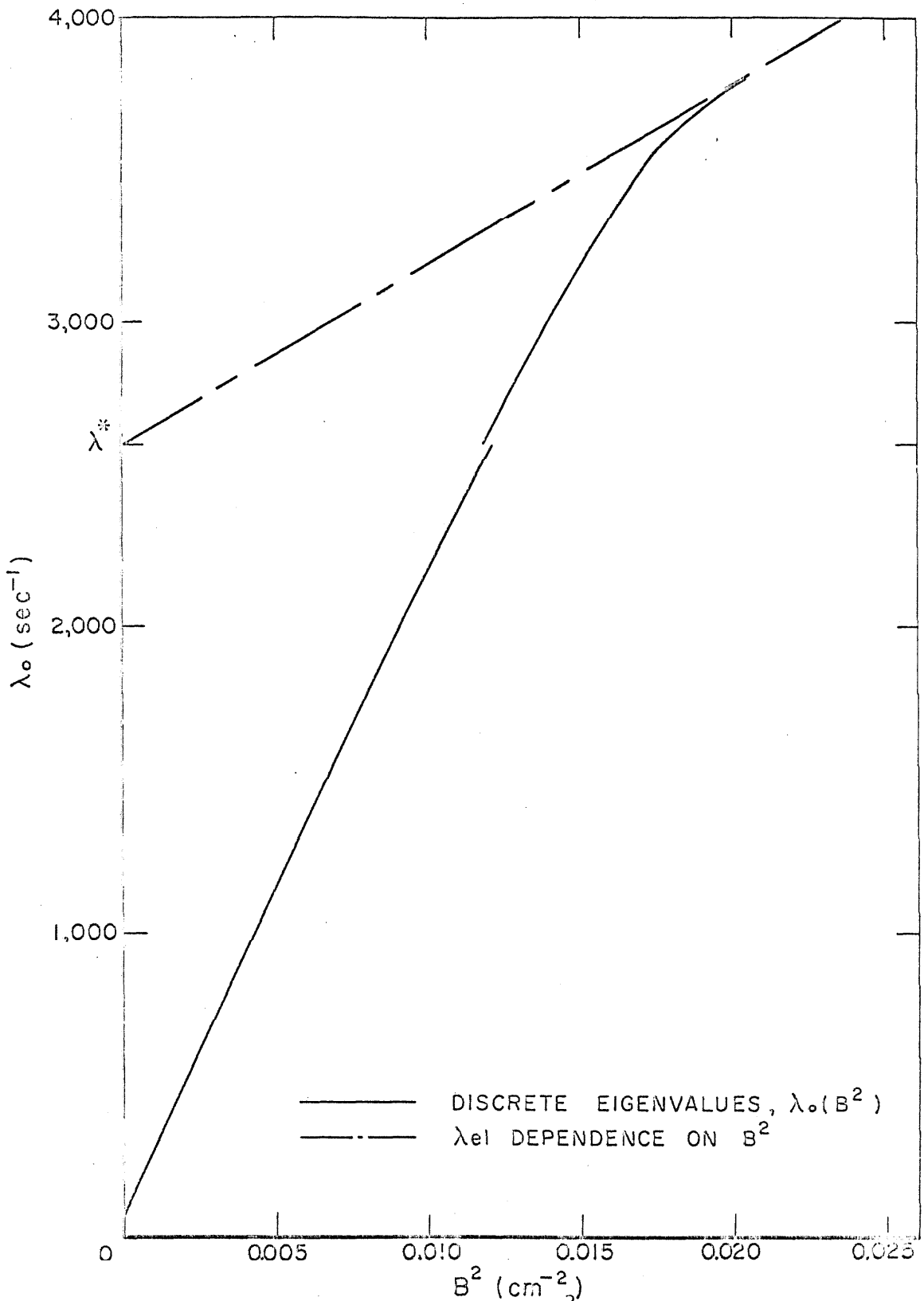

FIG. 14. The dispersion curve, $\lambda_o(B^2)$, for graphite.

de Saussure's trapping effect[45]. However, the dispersion c· ·s which result with the modified synthetic kernel are alway· ·re heated than results obtained with more detailed kernels ecause of the thermalizing power of the modeled inelastic k· ·. Thus, while small quantitative differences exist in dispersion curves with various cross section models, they are relatively minor. Since our modeled kernel is not expected to yield excellent quantitative agreement with experiment, the cross section model of figure 13 is employed in all further calculations. Of course, all qualitative effects remain.

The discontinuity in B shown in figure 12 is well described by the expansion III-31. As expected, the discontinuity is small reflecting its dependence on the relative sizes of the sub-Bragg and post-Bragg neutron populations.

It again remains true, as it was in chapter II, that the conventional expansion[6] of $\lambda_o(B^2)$ about $B^2 = 0$ is not valid when λ_o is greater than λ^*. As for the interpretation of the expansion coefficient, the first two, α_o and D_o in

$$\lambda_o(B^2) = \alpha_o + D_o B^2 - CB^4 \quad \ldots \qquad \text{(III-32)}$$

involve only $\Sigma_a(v)$ and $\Sigma_T(v)$, respectively. Thus, they are unaffected by the scattering kernel employed and depend solely on the cross section modeling. On the other hand, C, the diffusion cooling coefficient, depends critically on the thermalizing power of the kernel. So again, because the synthetic part of the kernel is a perfect thermalizer, we

expect C to differ considerably from other theoretical, and experimental, predictions. This is, again, graphically illustrated by the fact that dispersion curves with a modified synthetic kernel are less diffusion cooled than results obtained with more detailed kernels. The cooling that is present is a result of the effect of $\Gamma_e(B,v,\lambda)$. Including a discontinuous cross section but neglecting elastic scattering (set $\Sigma_{el}(v) \equiv 0$) predicts $C \sim 0$.

F. DEVELOPMENT OF THE TOTAL SOLUTION

The solution for the transformed density is given by equation III-16 and can be divided into two parts,

$$\tilde{\varphi}(B,v,\mu,\lambda) = \tilde{\varphi}_c(B,v,\mu,\lambda) + \tilde{\varphi}_s(B,v,\mu,\lambda) \tag{III-33}$$

where

$$\tilde{\varphi}_c(B,v,\mu,\lambda) = \frac{1}{2} \frac{v\Sigma_i(v)M(v)}{\Sigma \Gamma_e(B,v,\lambda)} \frac{S(\lambda,B)}{\Lambda(\lambda,B)} \frac{1}{(\lambda + v\Sigma_T(v) + iBv\mu)} \tag{III-34}$$

and

$$\tilde{\varphi}_s(B,v,\mu,\lambda) = \frac{v\Sigma_{el}(v)S(B,v,\lambda) + \Gamma_e(B,v,\lambda)Q(B,v,\mu)}{\Gamma_e(B,v,\lambda)(\lambda + v\Sigma_T(v) + iBv\mu)} \tag{III-35}$$

The original Bromwich inversion contour can be deformed using Cauchy's Theorem[38] to form the contours shown in figure 15. From this, we write $\varphi(B,v,\mu,t)$ as

$$\varphi(B,v,\mu,t) = \underset{\text{(Residue)}}{\varphi_R} + \underset{\text{(Sub-Bragg)}}{\varphi_{SB}} + \underset{\text{(Elastic)}}{\varphi_{el}} + \underset{\text{(Area)}}{\varphi_A} + \underset{\text{(Source)}}{\varphi_s} \tag{III-36}$$

The first four terms on the right are the inversion of $\tilde{\varphi}_c(B,v,\mu,\lambda)$ while the last term is the inversion of $\tilde{\varphi}_s$. $\varphi_c(B,v,\mu,\lambda)$ has poles where

$$1)\quad \lambda + v\Sigma_T(v) + iBv\mu = 0 \tag{III-37a}$$

$$2)\quad \Gamma_e(B,v,\lambda) = 0 \tag{III-37b}$$

$$3)\quad \Lambda(\lambda,B) = 0 \tag{III-37c}$$

On the other hand, $\tilde{\varphi}_s(B,v,\mu,\lambda)$ has poles only where conditions 1) and 2) are satisfied. This is a consequence of the fact that condition 3) involves the multi-velocity collective mode while $\tilde{\varphi}_s$ describes only neutrons which maintain their initial source speed.

We can readily interpret $\varphi_s(B,v,\mu,t)$ by considering each of its two parts separately. $\varphi_{s1}(B,v,\mu,t)$ results from inverting $Q(B,v,\mu)/(\lambda + v\Sigma_T(v) + iBv\mu)$ and equals

$$\varphi_{s1}(B,v,\mu,t) = Q(B,v,\mu)e^{-(v\Sigma_T(v) + iBv\mu)t} \tag{III-38}$$

This, however, is just a solution of the first-flight Boltzmann equation

$$\left(\frac{\partial}{\partial t} + v\Sigma_T(v) + iBv\mu\right)\varphi(B,v,\mu,t) = Q(B,v,\mu)\delta(t) \tag{III-39}$$

Therefore, φ_{s1} represents those neutrons that have not made a collision following emission by the source.

The second part of φ_s, $\varphi_{s2}(B,v,\mu,t)$, is obtained by inverting

$v\Sigma_{el}(v)S(B,v,\lambda)/[\Gamma_e(B,v,\lambda)(\lambda+v\Sigma_T(v)+iBv\mu)]$ and equals

$$\varphi_{s2}(B,v,\mu,t) = \frac{v\Sigma_{el}(v)S(B,v,-\lambda_e(v))\,e^{-\lambda_e(v)t}}{(-\lambda_e(v)+v\Sigma_T(v)+iBv\mu)\dfrac{\partial\Gamma_e(B,v,\lambda)}{\partial\lambda}}\Bigg|_{\lambda=-\lambda_e(v)}$$

$$+\frac{v\Sigma_{el}(v)}{2}\left\{\frac{S^+(B,v,\lambda)}{\Gamma_e^+(B,v,\lambda)}+\frac{S^-(B,v,\lambda)}{\Gamma_e^-(B,v,\lambda)}\right\}e^{-(v\Sigma_T(v)+iBv\mu)t}$$

$$+\frac{1}{2\pi i}\int_{-v\Sigma_T-iBv}^{-v\Sigma_T(v)+iBv} e^{\lambda t}\frac{v\Sigma_{el}(v)}{(\lambda+v\Sigma_T(v)+iBv\mu)}\left\{\frac{S^+}{\Gamma_e^+}-\frac{S^-}{\Gamma_e^-}\right\}d\lambda \qquad \text{(III-40)}$$

We can understand this by considering the figure at the right. The first and second terms result from conditions III-37a and III-37b. The third term is the integral about the cut.

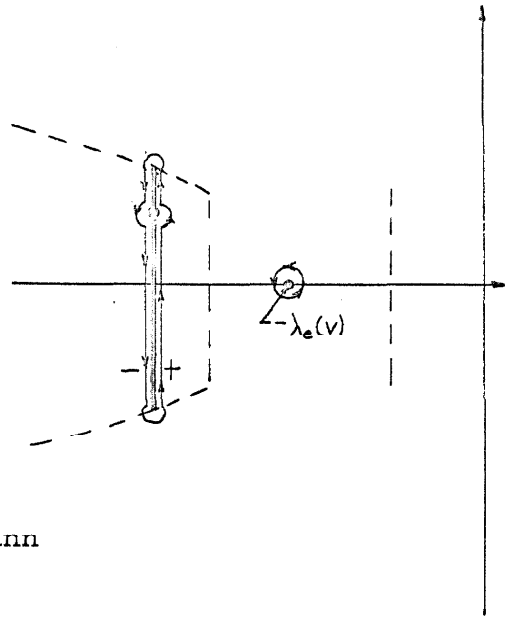

We can interpret $\varphi_{s2}(B,v,\mu,t)$ by recognizing that III-40 is the solution of the "one-velocity" Boltzmann equation

$$\left(\frac{\partial}{\partial t}+v\Sigma_T(v)+iBv\mu\right)\varphi(B,v,\mu,t) = \frac{v\Sigma_{el}(v)}{2}\int_{-1}^{1}\varphi(B,v,\mu',t)\,d\mu'$$

$$+Q(B,v,\mu)\delta(t) \qquad \text{(III-41)}$$

The variable, v, is a free parameter in this equation. Thus $\varphi_{s2}(B,v,\mu,t)$ describes those neutrons which, prior to detection, have made only elastic collisions.

The remaining four terms in equation III-36 result from inverting $\tilde{\varphi}_c(B,v,\mu,\lambda)$. Referring to figure 15, $\varphi_R(B,v,\mu,t)$ represents the contribution from the isolated pole caused by III-37c and corresponds to the collective or discrete mode. For a discrete eigenvalue, $\lambda_o < \lambda^*$, the discrete mode dominates the solution asymptotically in time and for all λ_o is given by

$$\varphi_R(B,v,\mu,t) = \frac{v\Sigma_i(v)M(v)S(-\lambda_o,B)}{2\overline{\Sigma}(-\lambda_o+v\Sigma_T(v)+iBv\mu)} \frac{e^{-\lambda_o t}}{\Gamma_e(B,v,-\lambda_o)} \frac{1}{\frac{\partial\Lambda}{\partial\lambda}}\Bigg|_{\lambda=-\lambda_o} \tag{III-42}$$

The contours in figure 15 indicate, however, that when $\lambda_o > \lambda^*$, the discrete mode will not dominate at long times because the sub-Bragg continuum is less damped. The interplay of these two contributions will be considered shortly.

The energy spectrum associated with the discrete mode is proportional to

$$\chi_R(B,v,\lambda) = \frac{v\Sigma_i(v)M(v)T(B,v,-\lambda_o)}{\Gamma_e(B,v,-\lambda_o)} \tag{III-43}$$

and becomes cooler with increasing buckling. This is caused by the preferential leakage of fast neutrons. Note that de Saussure's trapping effect[45] results from the presence of $\Gamma_e(B,v,-\lambda_o)$ in the denominator.

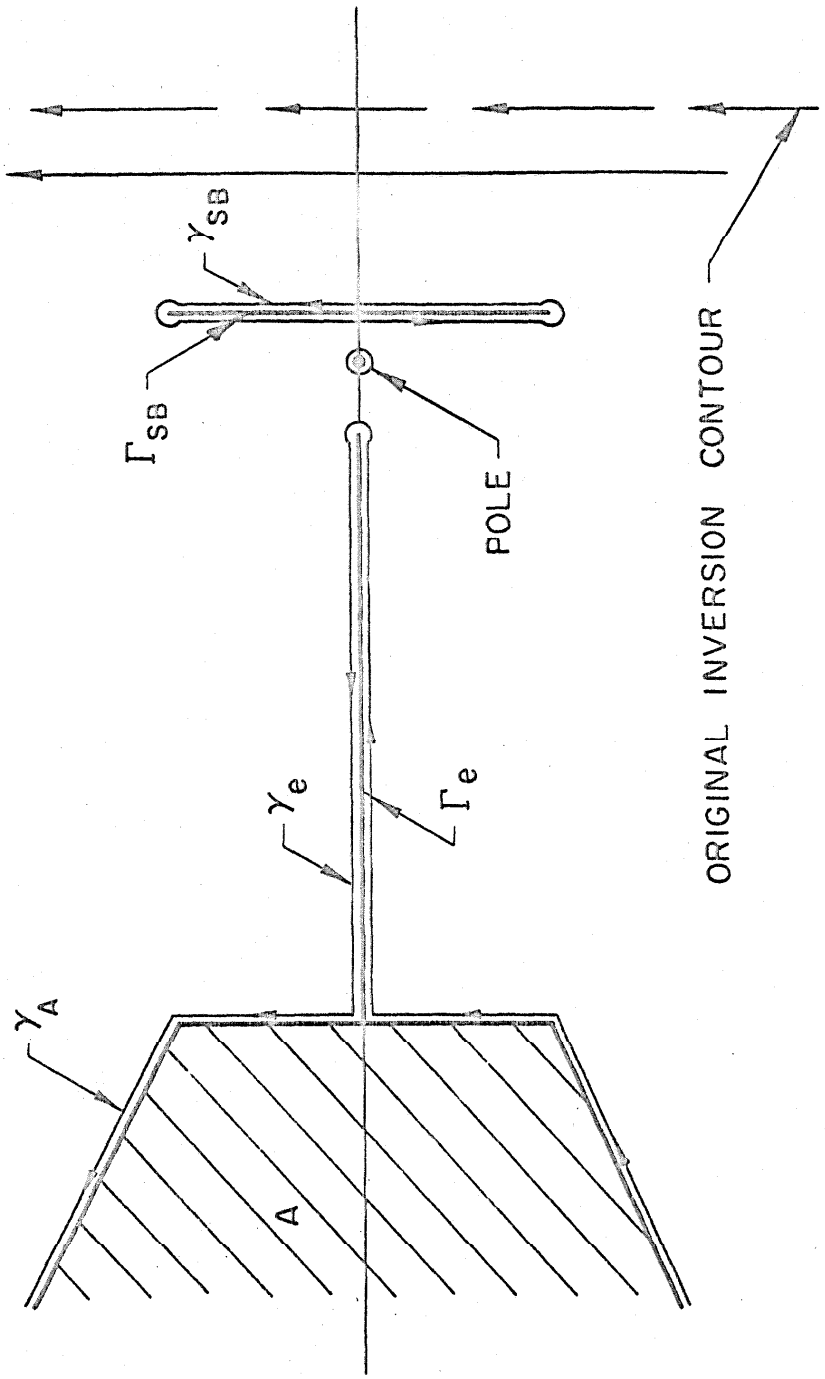

FIG. 15. The deformed contour in the primary λ-plane

As $|\lambda_o - \lambda_{el}|$ decreases, so does $\Gamma_e(B,v_B,-\lambda_o)$ causing the spectrum to rise most sharply at v_B. This effect is enhanced when $\Sigma_T(v)$ is peaked near v_B but occurs dramatically even when $\Sigma_T(v)$ is constant for $v > v_B$. Figure 16a illustrates this behavior for graphite where the cross sections are those in figure 12 and $\lambda_o < \lambda^*$. When $v < v_B$ and $\lambda_o > \lambda^*$, $\chi_R(B,v,\lambda)$ is negative as in figure 16b. Since the total solution must be positive at all times, the sub-Bragg continuum must counterbalance this effect in the sub-Bragg regime.

A closer examination of $\varphi_R(B,v,\mu,t)$ will help us interpret the large buckling behavior of the total solution. If we multiply φ_R by $v\Sigma_i(v)$ and integrate over μ and v, we obtain

$$N_R(t) = \int_o^\infty \int_{-1}^1 d\mu\, dv\, \varphi_R(B,v,\mu,t) = \frac{S(-\lambda_o,B)}{\left.\frac{\partial \Lambda}{\partial \lambda}\right|_{\lambda=-\lambda_o}} e^{-\lambda_o t} \qquad \text{(III-44)}$$

For simplicity, assume the source spectrum is a δ-function in energy at some high $v_s > v_B$. Then $S(-\lambda_o,B)$ exhibits no singular behavior for λ_o near λ^* or λ_{el}. On the other hand, the derivative of the dispersion law is

$$\frac{\partial \Lambda}{\partial \lambda} = \int_o^\infty \frac{(v\Sigma_i(v))^2 M(v)\, dv}{\bar{\Sigma}\Gamma_e(B,v,\lambda)^2\{(\lambda + v\Sigma_T(v))^2 + (Bv)^2\}} \qquad \text{(III-45)}$$

and its integrand has a pole of order two for $\lambda_o = \lambda_{el}$. Thus, for λ_o close to λ_{el}, $\partial\Lambda/\partial\lambda$ behaves like $1/(\lambda_{el}-\lambda_o)$, i.e. the amplitude of the discrete mode tends to zero as λ_o approaches λ_{el}. Since

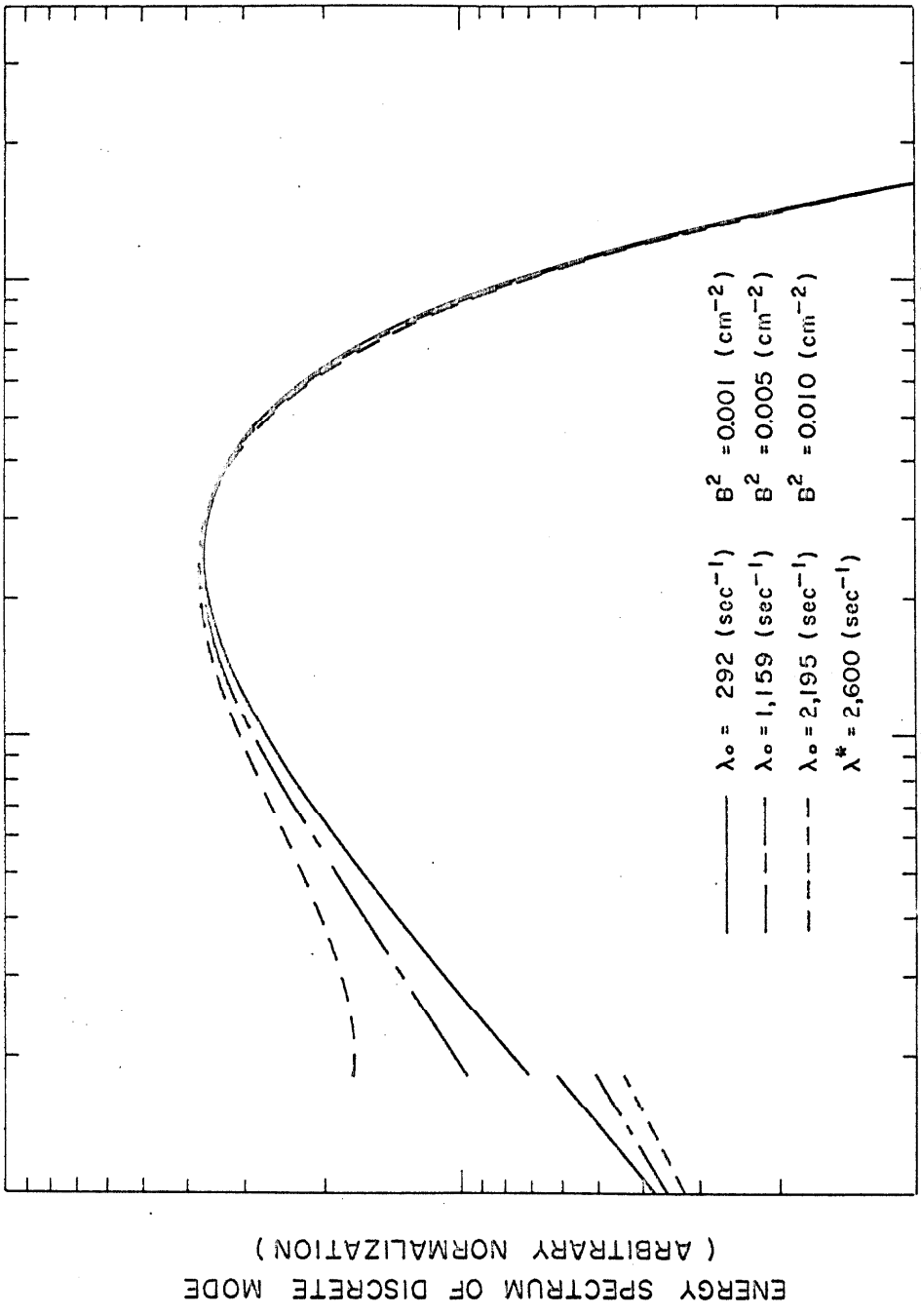

FIG. 16a. Energy dependence of the discrete mode in graphite when $B^2 < B^{*2}$.

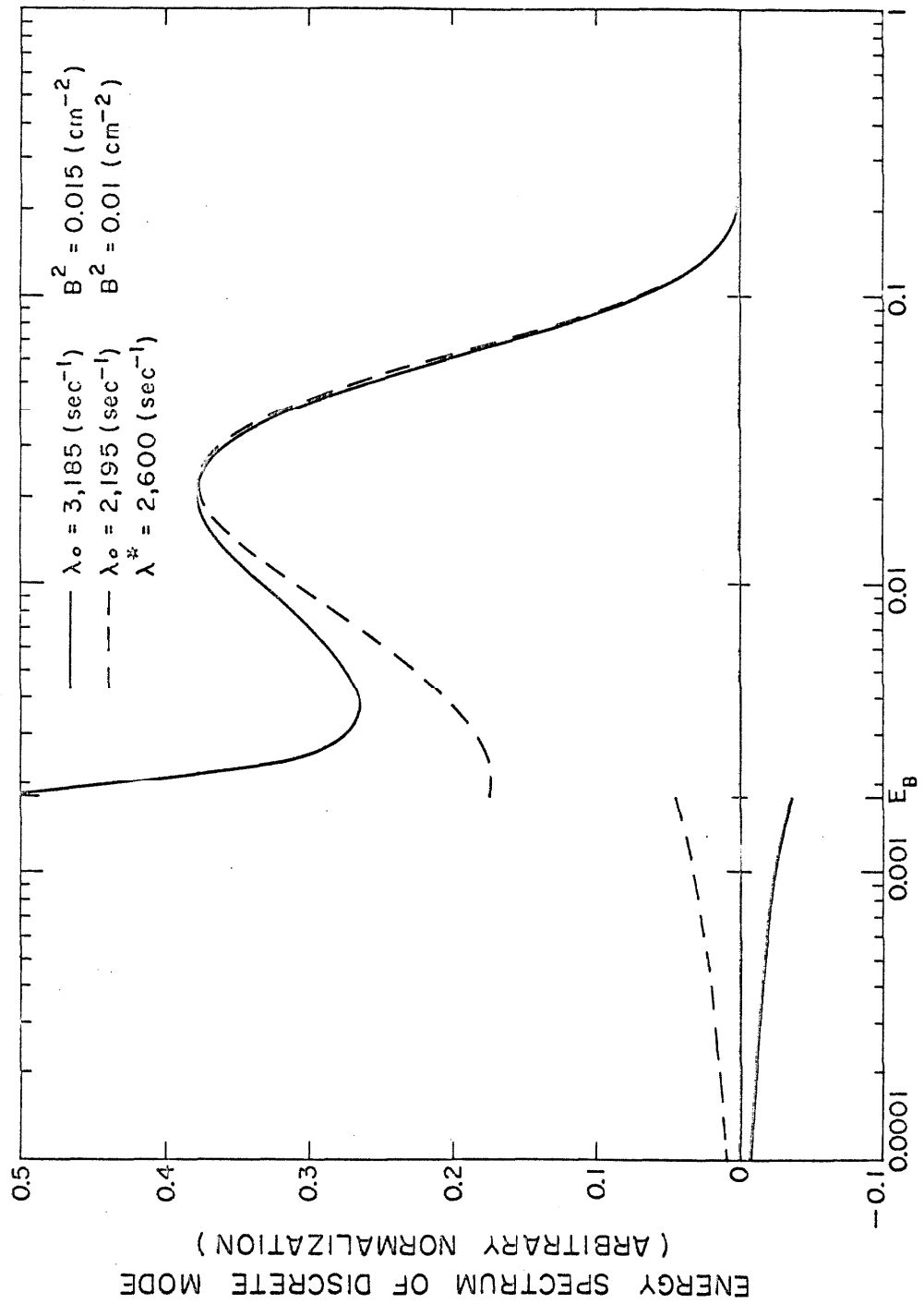

FIG. 16b. Energy dependence of the discrete mode in graphite. $(B^*)^2 = .011$ cm^{-2}.

$\lambda_{el} - \lambda_o$ decreases with increasing B^2 (see footnote, page 58), the discrete mode should play a decreasingly important role compared with the continuum contributions. When this happens, the solution is primarily the sum of the sub-Bragg and elastic continuum contributions. By examining the expression for $S(-\lambda_o, B)$, one can readily see that this conclusion is independent of the initial source distribution.

The remaining three terms in $\varphi_c(B,v,\mu,t)$ are integrals about Γ_{SB}, Γ_e, and the area in figure 14 and can be written as:

1) for the sub-Bragg continuum contribution

$$\varphi_{c_{SB}}(B,v,\mu,t) = \frac{v\Sigma_i(v)M(v)}{2\pi i(2\overline{\Sigma})} \int_{-\lambda^*-iBv_B}^{-\lambda^*+iBv_B} \frac{d\lambda e^{\lambda t}}{\Gamma_e(B,v,\lambda)} \left\{ \frac{S^+(\lambda,B)}{\Lambda^+(\lambda,B)} - \frac{S^-(\lambda,B)}{\Lambda^-(\lambda,B)} \right\}$$

$$\times \frac{1}{(\lambda+v\Sigma_T(v)+iBv\mu)} + \frac{H(v_B-v)}{2(2\overline{\Sigma})} \frac{v\Sigma_i(v)M(v)e^{-\lambda^* t_e - iBv\mu t}}{\Gamma_e(B,v,-\lambda^*-iBv\mu)}$$

$$\times \left\{ \frac{S^+}{\Lambda^+} + \frac{S^-}{\Lambda^-} \right\} \Bigg|_{\lambda=-\lambda^*-iBv\mu} \qquad \text{(III-46)}$$

Here $S^+(S^-)$ and $\Lambda^+(\Lambda^-)$ are the limits of these functions as λ approaches Γ_{SB} from the right (left).

2) for the elastic continuum contribution

$$\varphi_{c_e}(B,v,\mu,t) = \frac{v\Sigma_i(v)M(v)}{(2\overline{\Sigma})\,2\pi i} \int_{-\lambda_{el}}^{-\lambda_A} \frac{d\lambda e^{\lambda t} \left\{ \frac{S_e^+}{\Lambda_e^+} - \frac{S_e^-}{\Lambda_e} \right\}}{(\lambda+v\Sigma_T(v)+iBv\mu)\Gamma_e(B,v,\lambda)}$$

(relation continued)

$$+\frac{H(v-v_B)}{2(2\bar{\Sigma})}\frac{v\Sigma_i(v)M(v)\left\{\frac{S_e^+}{\Lambda_e^+}-\frac{S_e^-}{\Lambda_e}\right\}\Big|_{\lambda=-\lambda_e(v)} e^{-\lambda_e(v)t}}{(-\lambda_e(v)+v\Sigma_T(v)+iBv\mu)\frac{\partial\Gamma_e(B,v,\lambda)}{\partial\lambda}\Big|_{\lambda=-\lambda_e(v)}} \qquad \text{(III-47)}$$

where S_e^+ (S_e^-) and Λ_e^+ ($-\Lambda_e^-$) are the limits of S and Λ as λ approaches Γ_e from above (below).

3) from the area,

$$\varphi_{c_A}(B,v,\mu,t)=\frac{v\Sigma_i(v)M(v)}{(2\bar{\Sigma})(2\pi i)}\int_{\partial A}d\lambda\, e^{\lambda t}\left\{\frac{S(\lambda,B)}{(\lambda+v\Sigma_T(v)+iBv\mu)\Gamma_e(B,v,\lambda)\Lambda(\lambda,B)}\right\} \qquad \text{(III-48)}$$

The fact that each of these three terms is proportional to $v\Sigma_i(v)M(v)$ implies each is describing neutrons that have suffered inelastic collisions. $\varphi_{c_{SB}}$ and φ_{c_A} arise because of condition III-19. As such, the integrands have the form $e^{-v\Sigma_T(v)t}e^{-iBv\mu t}$ indicating free streaming modes. These modes are connected by inelastic collisions implying the coefficients of the exponential in the integrand act as mode coupling coefficients. A neutron, on making an inelastic collision, is shifted from one free streaming mode to another.

On the other hand $\varphi_{c_e}(B,v,\mu,t)$ is proportional to $e^{-\lambda_e(v)t}$ and an integral over this exponential. As such, φ_{c_e} apparently describes neutrons behaving in a one-velocity manner but with many "characteristic" speeds. That is, a neutron in such a mode can suffer an inelastic collision and be shifted to another "one-velocity mode" with a different characteristic speed. Notice that all three terms

involve "modes" from which neutrons are removed after a single collision. This contrasts with the discrete or collective mode in which neutrons are expected to suffer many collisions without being removed.

Before continuing, it is worthwhile to develop a simplified formula for a response function depending only on time. The response to a detector with cross section $\Sigma_d(v)$ is obtained by multiplying III-7 by $v\Sigma_d(v)$ and integrating over v, namely

$$\tilde{N}_d(\lambda,B) = \frac{S(\lambda,B)}{\Lambda(\lambda,B)}\,\chi(\lambda,B) + s(\lambda,B) \qquad \text{(III-49)}$$

where we have defined

$$\chi(\lambda,B) = \int_o^\infty \frac{v\Sigma_d(v)v\Sigma_i(v)M(v)T(B,v,\lambda)\,dv}{\overline{\Sigma}\,\Gamma_e(B,v,\lambda)} \quad , \qquad \text{(III-50)}$$

$$\tilde{N}_d(\lambda,B) = \int_o^\infty v\Sigma_d(v)\,\tilde{\Psi}(B,v,\lambda)dv \quad , \qquad \text{(III-51)}$$

and

$$s(\lambda,B) = \int_o^\infty \frac{v\Sigma_d(v)S(B,v,\lambda)\,dv}{\Gamma_e(B,v,\lambda)} \quad . \qquad \text{(III-52)}$$

By choosing $\Sigma_d(v) = \Sigma_i(v)$, the macroscopic inelastic cross section of the system of interest, we obtain the further simplified expression,

$$\tilde{N}(\lambda,B) = \frac{S(\lambda,B)}{\Lambda(\lambda,B)} \quad . \qquad \text{(III-53)}$$

We will later numerically invert III-53 to obtain a response function.

III-53 contains all the pertinent physics and is somewhat easier to use than III-49.

G. ANALYTIC CONTINUATION OF THE DISPERSION LAW

In chapter II, we posed the question of whether the total solution is a continuous function of B^2, particularly as B^2 passes through B^{*2}. For both the general and modeled kernels, the dispersion curve is discontinuous at λ^*. The eigenvalues which comprise this curve exist in the "physical plane" or primary Riemann sheet. On the other hand, we found that analytically continuing the total solution past Γ_{SB} allows an alternate representation in which the continuity of $\varphi(B,\nu,\mu,t)$ in B^2 is manifest. That is, with the deformed contour in the diagram, there is no cut at $-\lambda^*$ passing through the real axis to cause a discontinuity in the total solution, or, for that matter, in the dispersion curve. In such a representation, one would not even ask whether $\varphi(B,\nu,\mu,t)$ is continuous in B^2.

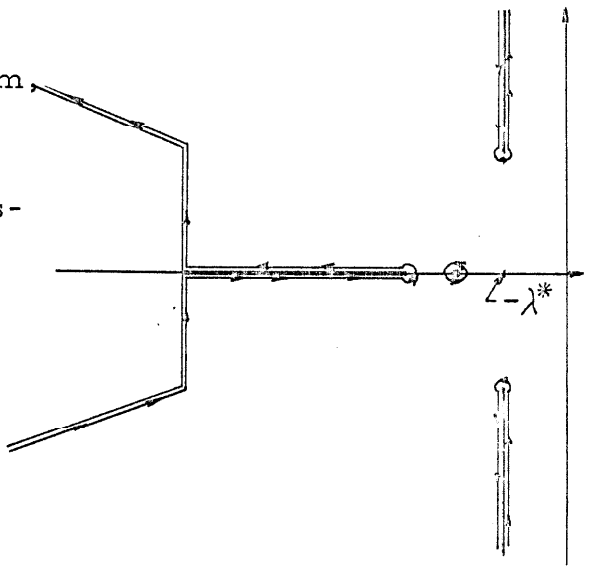

It remains to be demonstrated that such a continuation exists. This is equivalent to proving, in the physical plane, that the solution is continuous in B^2. The latter approach can be performed by employing the theory of boundary values of Cauchy type integrals[37]. The former approach is presented here because it provides a method of

smoothly extending the dispersion curve beyond λ^*.

The dispersion function $\Lambda(\lambda,B)$ can be written as $1 - \Lambda_1(\lambda,B) - \Lambda_2(\lambda,B)$. In section III-D, we found, for $\zeta \in \Gamma_{SB}$, that

$$\Lambda_1^{\pm}(\zeta,B) = \frac{\beta^*}{2iB\bar{\Sigma}v_T^2}\left\{\int_{-v_B}^{v_B} \frac{e^{-\left(\frac{z}{v_T}\right)^2} - e^{-\left(\frac{v_B}{v_T}\right)^2}}{z - i\left(\frac{\zeta+\lambda^*}{B}\right)}\,dz \right.$$

$$\left. \pm \pi i\left(e^{\left(\frac{\zeta+\lambda^*}{Bv_T}\right)} - e^{-\left(\frac{v_B}{v_T}\right)}\right)\right\} \qquad \text{(III-54)}$$

Knowing this, the analytic continuation of $\Lambda(\lambda,B)$ from the right to the left of Γ_{SB} is

$$\Lambda_c(\lambda,B) = \Lambda(\lambda,B) - \frac{\pi}{B\bar{\Sigma}}\left(\frac{\beta^*}{v_T}\right)^2\left(e^{\left(\frac{\lambda+\lambda^*}{Bv_T}\right)^2} - e^{-\left(\frac{v_B}{v_T}\right)^2}\right) \qquad \text{(III-55)}$$

for the following reasons:

Referring to the figure at the right, $\Lambda(\lambda,B)$ is analytic in D_1, $\Lambda_c(\lambda,B)$ is analytic in D_2, the intersection, $D_1 \cap D_2$, is the empty set, ϕ, and $\bar{D}_1 \cap \bar{D}_2 = \Gamma_{SB}$. $\Lambda(\lambda,B)$ is continuous in $D_1 \cup \Gamma_{SB}$ and $\Lambda_c(\lambda,B)$ is continuous in $D_2 \cup \Gamma_{SB}$. Furthermore, $\Lambda_c^-(\zeta,B) = \Lambda^+(\zeta,B)$

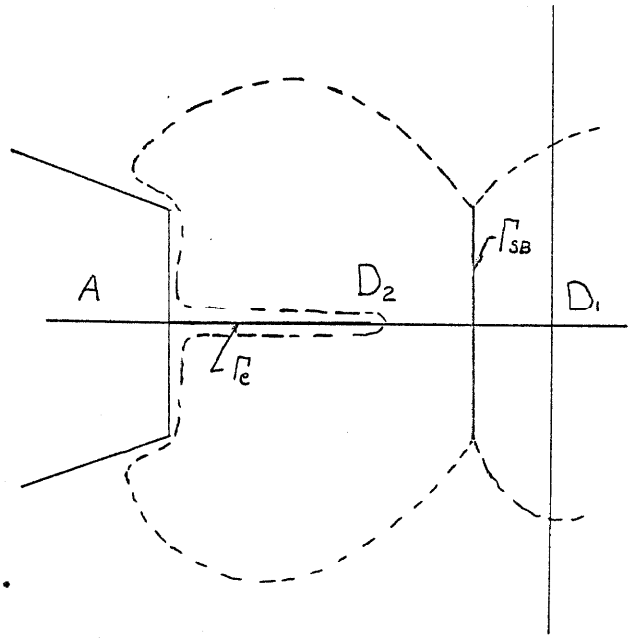

for $\zeta \in \Gamma_{SB}$. Hence, we conclude[38] that $\Lambda_c(\lambda,B)$ is the analytic continuation of $\Lambda(\lambda,B)$ from D_1 to D_2 and vice versa.

The same arguments allow the construction of the analytic continuation of $S(\lambda,B)$ and $T(B,v,\lambda)$. The function $\Gamma_e(B,v,\lambda)$ is analytic for λ on Γ_{SB} because $\Sigma_{el}(v) = 0$ for $v < v_B$. Note that in constructing the continuation of $T(B,v,\lambda)$, the speed v is a parameter and $T(B,v,\lambda)$ is analytic on Γ_{SB} if $v > v_B$. For $v < v_B$, it must be continued through a cut extending from $-\lambda^* - iBv$ to $-\lambda^* + iBv$.

In pulsed neutron experiments, the source energy distribution contains no neutrons with speed less than v_B. In such a case, $S(\lambda,B)$ is analytic for $\lambda \in \Gamma_{SB}$.

These results allow the construction of the analytic continuation of $\tilde{\varphi}(B,v,\mu,\lambda)$, $\tilde{\Psi}(B,v,\lambda)$, and $\tilde{N}(\lambda,B)$ through Γ_{SB}. Thus, it is possible to deform the Bromwich inversion contour as in figure 11 of chapter II and obtain an alternate representation of the total solution. As well, this demonstration makes the continuity of the total solution in B^2 manifest.

H. PROPERTIES OF THE ANALYTICALLY CONTINUED DISPERSION LAW

An examination of $\partial\Lambda_c/\partial\lambda$ for real λ as in equation III-22 shows that $\Lambda_c(\lambda,B)$ has, at most, one real root. However, it may have additional complex roots occurring in conjugate pairs.

The real roots are contained in (λ^*,λ_{el}) and, as before, λ_{el} bounds any real eigenvalue from above. When $[(-\lambda_o+\lambda^*)/Bv_T]^2 << 1$,

we can simplify $\Lambda_c(\lambda,B)$ by expanding the exponential, namely

$$\Lambda_c(\lambda,B) = \Lambda(\lambda,B) - \frac{\pi}{B\bar{\Sigma}}\left(\frac{\beta^*}{v_T}\right)^2\left(1 - e^{-\left(\frac{v_B}{v_T}\right)^2}\right) - O\left(\left(\frac{-\lambda_o+\lambda^*}{Bv_T}\right)^2\right) \qquad \text{(III-56)}$$

This expression, neglecting higher order terms, can be obtained by simply replacing the arctangent function in $\Lambda_1(\lambda,B)$ by its next determination, i.e., by $\mathrm{Tan}^{-1}\left(\frac{Bv}{\lambda+\lambda^*}\right)+\pi$, where Tan^{-1} denotes the principal determination of the function. We have found that neglecting higher order terms in III-56 yields a dispersion curve that differs by less than one part in six thousand from the exact one for B^2 as large as twice B^{*2}. Thus, this method of handling the arctangent function should be useful in a multi-group $e^{i\underline{B}\cdot\underline{r}}$ theory computer code in which a more detailed inelastic scattering kernel is used.

The fact that complex roots must occur in conjugate pairs can be used to bound the real part of such roots when $B^2 > B^{*2}$. Thus, $\Lambda_c(\lambda_i,B) = 0$ implies $\Lambda_c(\bar{\lambda}_i,B) = 0$. Subtracting gives

$$\Lambda_c(\bar{\lambda}_i,B) - \Lambda_c(\lambda_i,B) = \frac{C_1}{B}\left\{e^{\left(\frac{\bar{\lambda}_i+\lambda^*}{Bv_T}\right)^2} - e^{\left(\frac{\lambda_i+\lambda^*}{Bv_T}\right)^2}\right\} \qquad \text{(III-57)}$$

where $C_1 = \left(\frac{\pi}{2\bar{\Sigma}}\right)\left(\frac{\beta^*}{v_T}\right)^2$. Letting $\lambda_i = x + iy$ allows us to rewrite III-57 as

$$\int_o^\infty \frac{(v\Sigma_i(v))^2 M(v)}{v\bar{\Sigma}\,|\Gamma_e(B,v,\lambda_i)|^2}\left(\log\frac{(x+v\Sigma_T(v))^2+(Bv+y)^2}{(x+v\Sigma_T(v))^2+(Bv-y)^2}\right)dv$$

$$= 4C_1 e^{\frac{(x+\lambda^*)^2-y^2}{(Bv_T)^2}} \sin\left\{\frac{2(x+\lambda^*)y}{(Bv_T)^2}\right\} \qquad \text{(III-58)}$$

For $y > 0$, the L.H.S. is greater than zero implying the R.H.S. must be positive for λ_i to be a root. But $x + \lambda^* < 0$ so the R.H.S. is positive only when

$$n\pi \leq \frac{2|x+\lambda^*|y}{(Bv_T)^2} \leq 2n\pi \; ; \quad n = 1,3,5,\ldots \tag{III-59}$$

Thus, the minimum value of y for which III-58 can possibly hold is

$$y_{min} = \frac{(Bv_T)^2}{|x+\lambda^*|} \; \frac{\pi}{2} \tag{III-60}$$

For polycrystals like graphite, taking $x = -\lambda_{el}$ and $B = B^*$ implies $y_{min} = O(10^6)$. This means asymptotically large y for the integrand on the L.H.S. of III-58. The Maxwellian, $M(v)$, destroys any large v contribution to the integral.

For large y, the L.H.S. behaves like

$$\frac{1}{y}\left\{ 4B \int_o^\infty \frac{(v\Sigma_i(v))^2 M(v)\, dv}{\Sigma} \right\}$$

while the R.H.S. is $O\left(e^{-\left(\frac{v_B}{v_T}\right)^2 y^2}\right)$. Thus, III-58 cannot be satisfied by any $|x| < \lambda_{el}$. Indeed, we can infer from the numbers involved that any such roots lie by a factor of two or more to the left of $-\lambda_{el}$. Therefore, any such zeros of $\Lambda_c(\lambda, B)$ should not affect the total response function in the alternate representation for times of experimental importance.

The energy spectrum associated with the analytically continued discrete mode is presented in figure 17 for graphite. As before, when

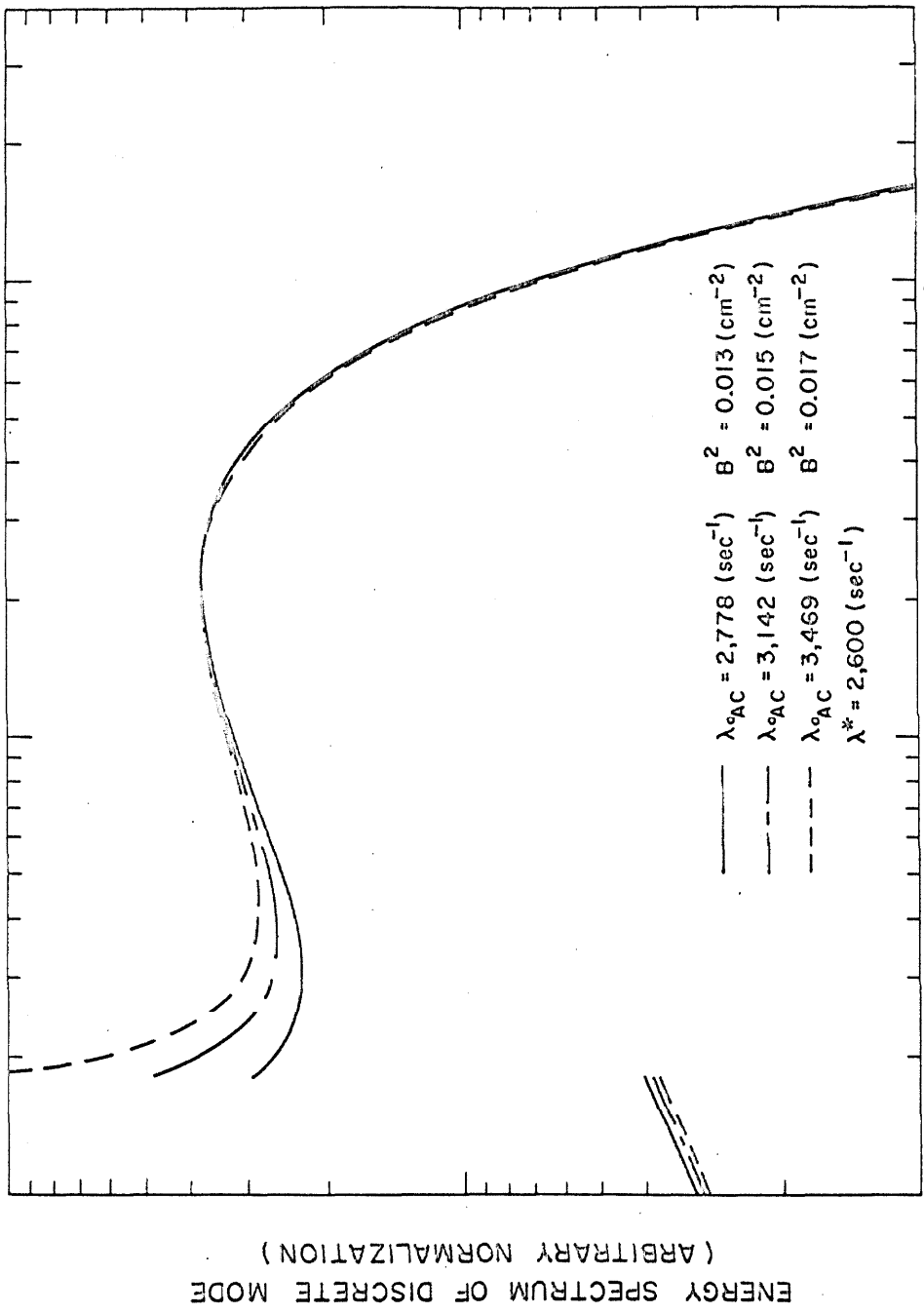

FIG. 17. Energy dependence of the analytic continuation of the discrete mode in graphite when $B^2 > B^{*2}$

$\lambda_{o_{AC}}$ approaches λ_{el}, the spectrum peaks considerably at v_B. This again reflects the role of $\Gamma_e(B,v,-\lambda_{o_{AC}})$ in the denominator of the residue, III-42. For the cross section model in figure 12, all post-Bragg neutrons have the same mean free path. The trapping at v_B results from these neutrons having the smallest collision frequency and leakage rate of all neutrons with speeds greater than v_B.

Multi-group calculations have found a sharp increase in the sub-Bragg population with increasing time. In our theory, this effect is connected with the energy dependence of the sub-Bragg continuum and is nowhere reflected in the discrete mode.

I. INTERPRETATION--COMPARISON OF THEORY AND EXPERIMENT

1) The Analytically Continued Dispersion Law

The numerical results for the analytically continued dispersion law in beryllium are presented in figure 18 along with experimental data and results of multi-group calculations. The results of Lee and Daitch[43] beyond λ^* represents a "pseudo-fundamental" decay constant. This concept was introduced because no discrete decay constants can exist beyond λ^* in diffusion theory. Both Lee and Daitch and Wood[46] employed rather sophisticated isotropic scattering kernels. Lee and Daitch, for instance, used the Summit code[47] which employs the incoherent approximation and the frequency spectrum of Young and Koppel[34].

Figure 19 is a similar plot for graphite on which the multi-group diffusion theory results of Ghatak and Honeck[21] are included.

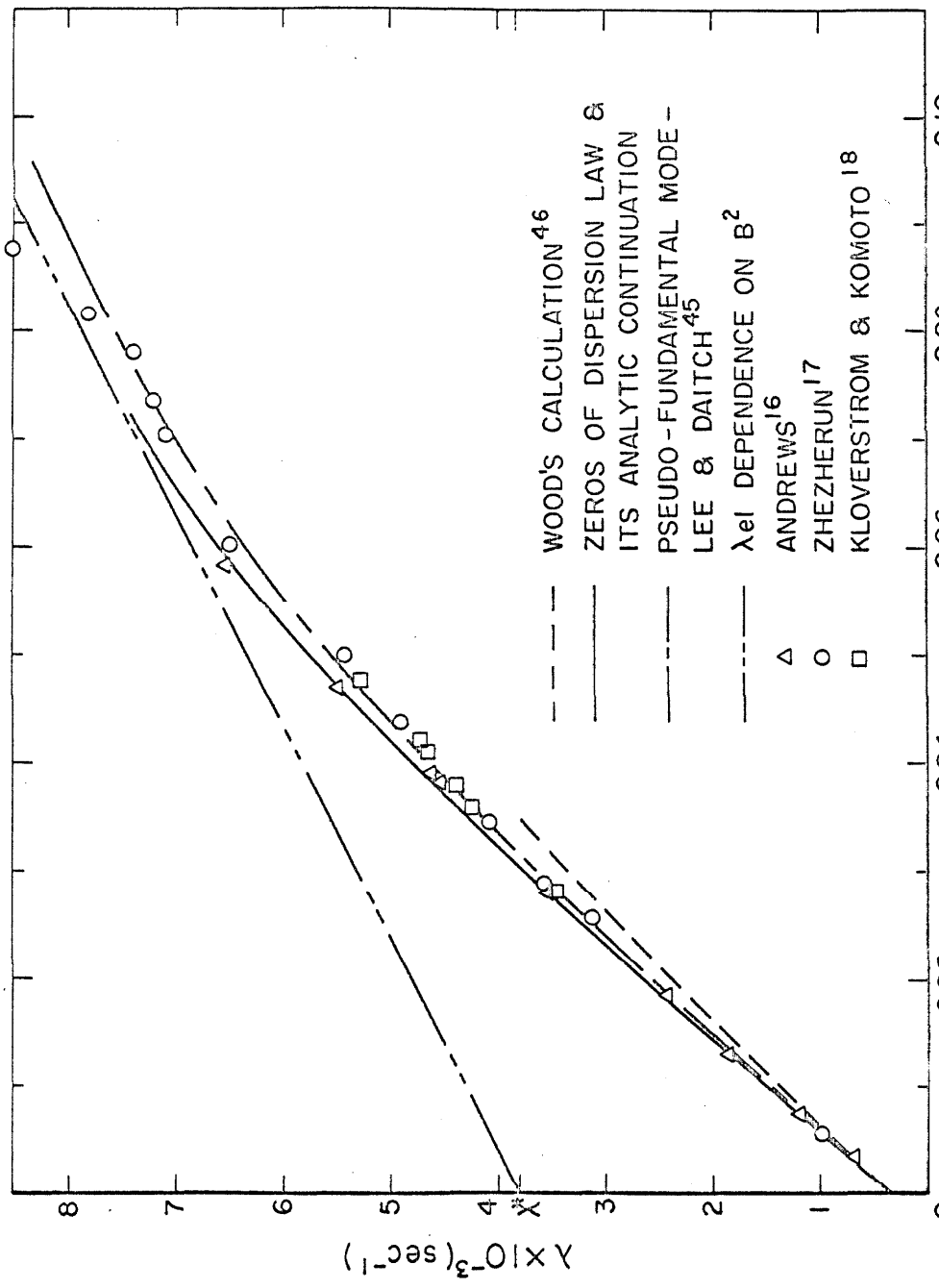

FIG. 18. $\lambda_o(B^2)$ for beryllium, using $\lambda_{oA.C.}(B^2)$ when $B^2 > B^{*2}$. $\lambda^* = 3800\ sec^{-1}$

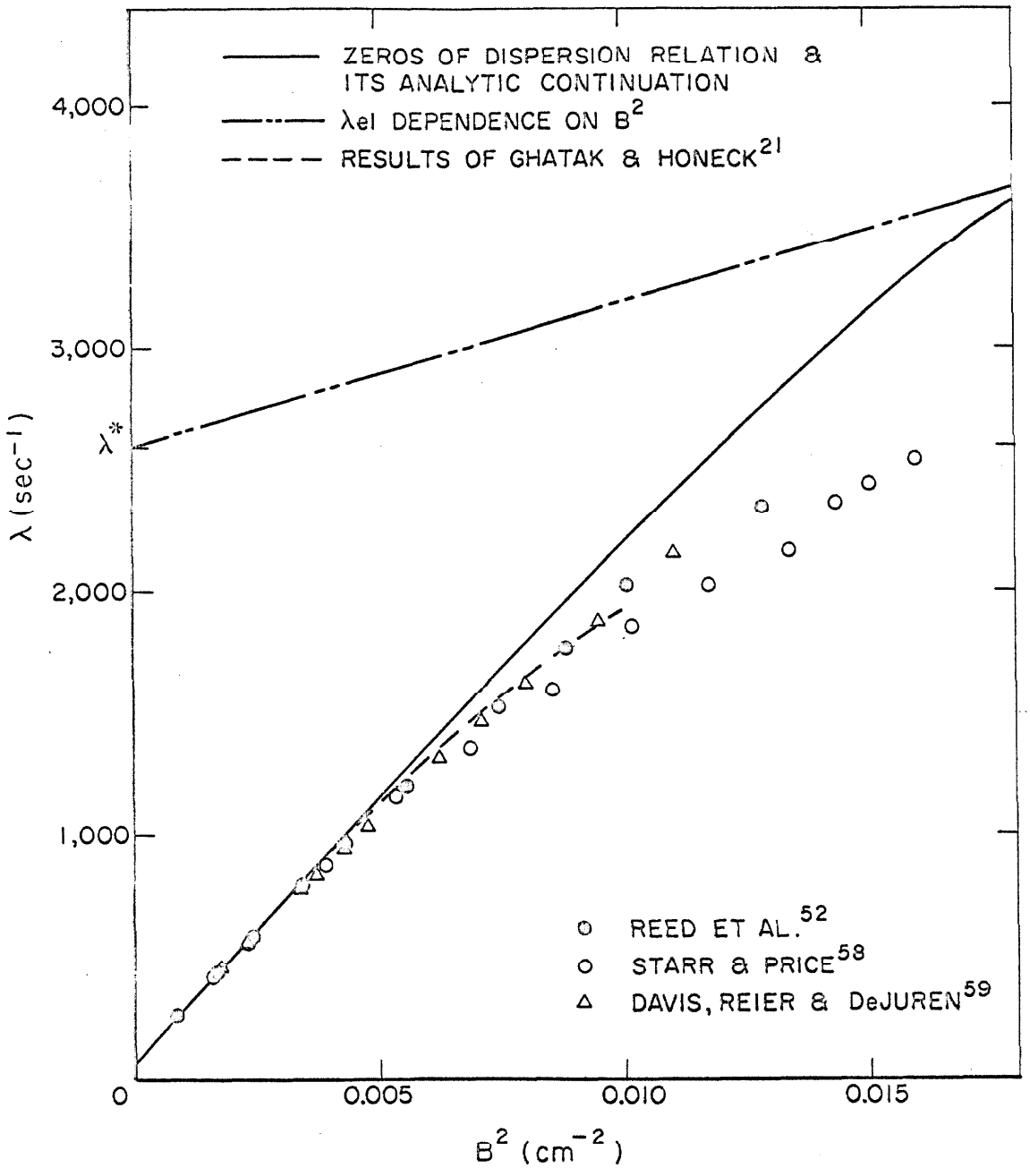

FIG. 19. $\lambda_o(B^2)$ for graphite, using $\lambda_{o\,A.C.}(B^2)$ when $B^2 > B^{*2}$. $\lambda^* = 2600\ \text{sec}^{-1}$.

They also use the Summit code together with the Parks' model[48] for scattering in graphite. Agreement between theories in graphite is not as good as in beryllium and we shall elaborate on this point shortly. Note, however, that for both materials, calculations with the modified synthetic kernel are not as "diffusion cooled" as other results.

In both figures 18 and 19, the edge of the elastic continuum, λ_{el}, has been plotted as a function of B^2. For fixed B^2, the value of λ_{el} bounds the discrete eigenvalue. In beryllium, for example, we see that it bounds the "pseudo-fundamental" eigenvalue of Lee and Daitch.

We must now investigate the total solution and the relation of the analytically continued eigenvalues to it.

2) The Total Solution and Analytically Continued Eigenvalues

In section III-F, we developed expressions for the total angle, energy, time dependent neutron distribution function together with a simplified expression, III-53, for a transformed response function. Basically, three contributions are important: 1) the residue from the discrete pole, 2) the sub-Bragg continuum contribution, and 3) the elastic continuum contribution. The area continuum contribution is neglected because it decays much too rapidly to be of importance. To illustrate this, note that for beryllium, $\lambda^* = 3800\ \text{sec}^{-1}$ whereas λ_A is approximately $80{,}000\ \text{sec}^{-1}$.

We will be concerned with the inversion of $\tilde{N}(\lambda, B)$ as given in equation III-53. In performing this calculation, the source is taken to be a δ-function in energy at $\frac{1}{2}$ ev. This is based on the work of Wood[44]

who found that the decay in time is insensitive to the source energy spectrum. Also, in calculating the contribution from integrals along Γ_e, we choose $\Sigma_{el}(v)$ to be constant above the Bragg cutoff. This greatly simplified the numerical work because it meant that with a simple variable transformation, we could explicitly represent the integrals along Γ_e as Cauchy integrals. Such an approximation introduces only a small error, for example, in the eigenvalues of the problem. Eigenvalues with fixed $\Sigma_{el}(v)$ were found to differ by, at most, 2% from those calculated with $\Sigma_{el}(v)$ going to zero at high speeds.

When the buckling is such that the discrete eigenvalue is further than 50 to 100 sec^{-1} from λ_{el}, but greater than λ^*, we find that the contribution from Γ_e can be safely neglected over measuring times compared with the discrete mode and contribution from Γ_{SB}. In this regime of the dispersion curve ($\lambda^* < \lambda_o << \lambda_{el}$), the sub-Bragg continuum decays more slowly than the discrete mode. Its amplitude, however, is only about 2% of the amplitude of the discrete mode in beryllium and $\frac{1}{2}$ % in graphite. This is reasonable because the contribution from Γ_{SB} is initially excited by the low energy tail of the distribution of first collision neutrons. The percentage is higher in beryllium because its Bragg cutoff is higher.

The result is to produce a decay which appears exponential for a period of time with an effective decay constant somewhat lower than the discrete eigenvalue. Just enough lower, in fact, that this effective decay constant appears to extend the portion of the dispersion curve below λ^* smoothly past this critical limit. Figures 20 through 23

illustrate this behavior in beryllium and graphite.

In addition to this, we find that over times where the decay appears exponential, the effective decay constant is well described by the eigenvalue of the analytically continued dispersion law. Hence, to evaluate the decay constant observed over experimental measuring times, one need only compute the zero of the analytically continued dispersion law.

This last result is not coincidence. The additional term in $\Lambda_c(\lambda, B)$ is integrally connected with the sub-Bragg regime. It "corrects" the eigenvalue in roughly the same manner as the sub-Bragg continuum contribution "corrects" the ordinary discrete eigenvalue. This, as well, ties in with the fact that the total solution is continuous in B^2 through B^{*2}.

We can conclude, then, that the "pseudo-fundamental" mode of diffusion theory plays the same role as the discrete analytically continued eigenvalue of this thesis. However, the role of the sub-Bragg regime in determining decay rates is now more explicit.

As buckling increases, the curvature in the decay curve caused by the sub-Bragg continuum sets in at earlier times. Figure 24 illustrates the various contributions to the total solution at $B^2 = 0.016$ cm^{-2} for graphite. The sub-Bragg contribution is approximately 10% at $t = 2.6$ msec.

The attenuation of the sub-Bragg continuum is roughly exponential over measuring times with an effective decay constant close to λ^*. For large times, $t \gtrsim 10$ msec, the sub-Bragg continuum behaves asymptotically as $e^{-\lambda^* t}/(\lambda^* t)^2$ (see appendix B).

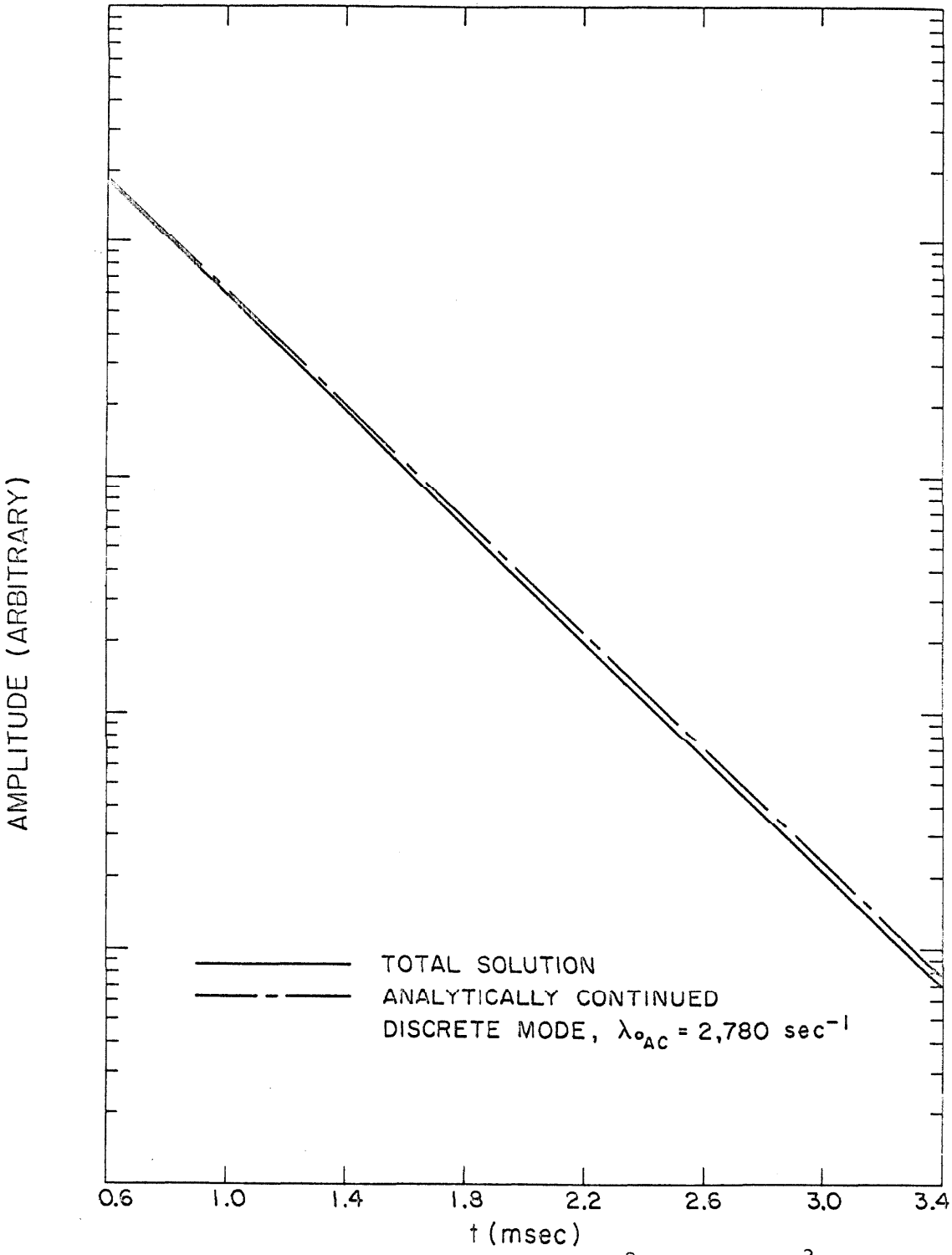

FIG. 20. Response function in graphite at $B^2 = .013$ cm^{-2} illustrating $\lambda_{eff} \sim \lambda_{o_{A.C.}}$ $\lambda^* = 2600$ sec^{-1}, $(B^*)^2 = .011$ cm^{-2}.

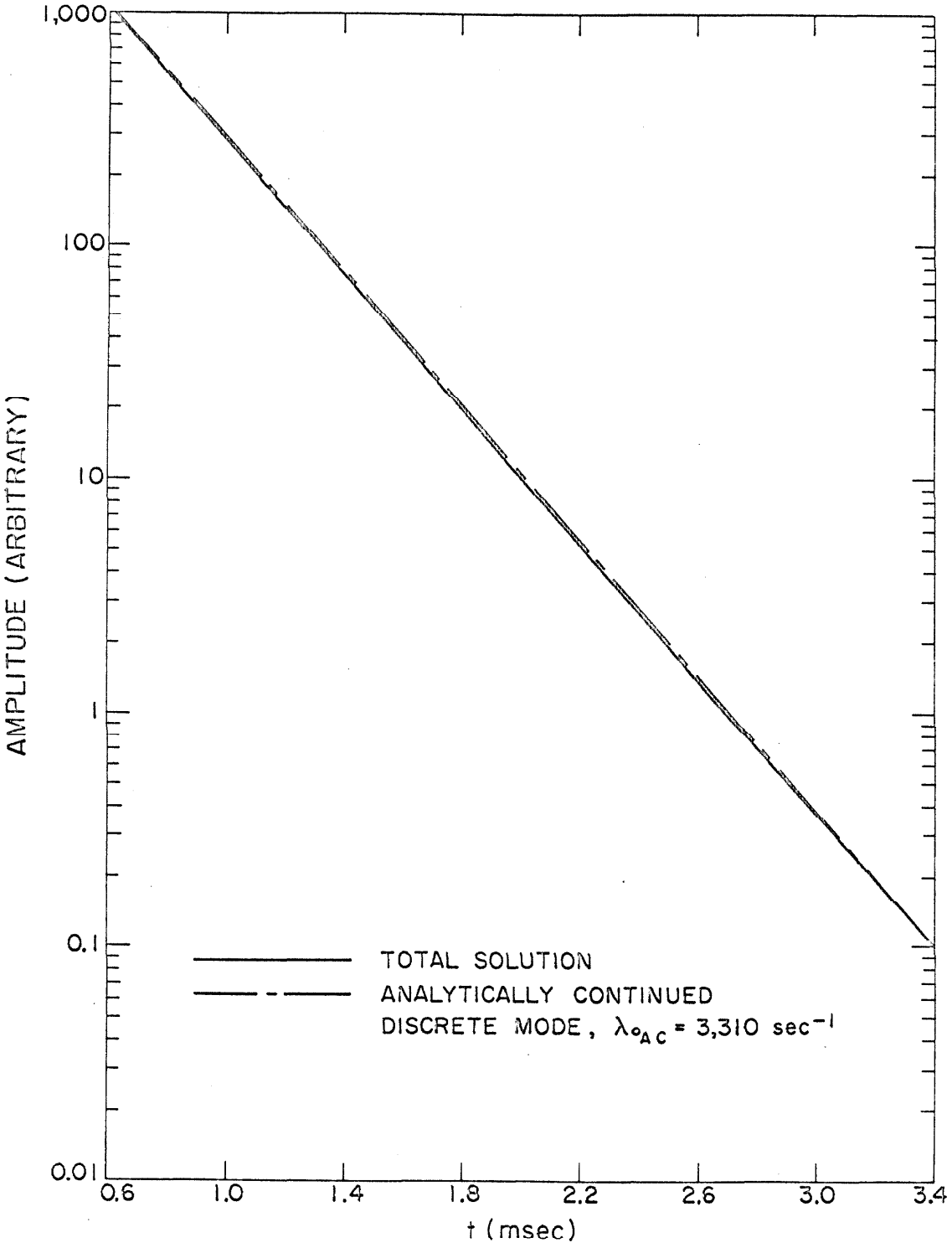

FIG. 21. Response function in graphite at $B^2 = .016\ cm^{-2}$ illustrating $\lambda_{eff} \sim \lambda_{o_{A.C.}}$ $\lambda^* = 2600\ sec^{-1}$, $(B^*)^2 = .011\ cm^{-2}$.

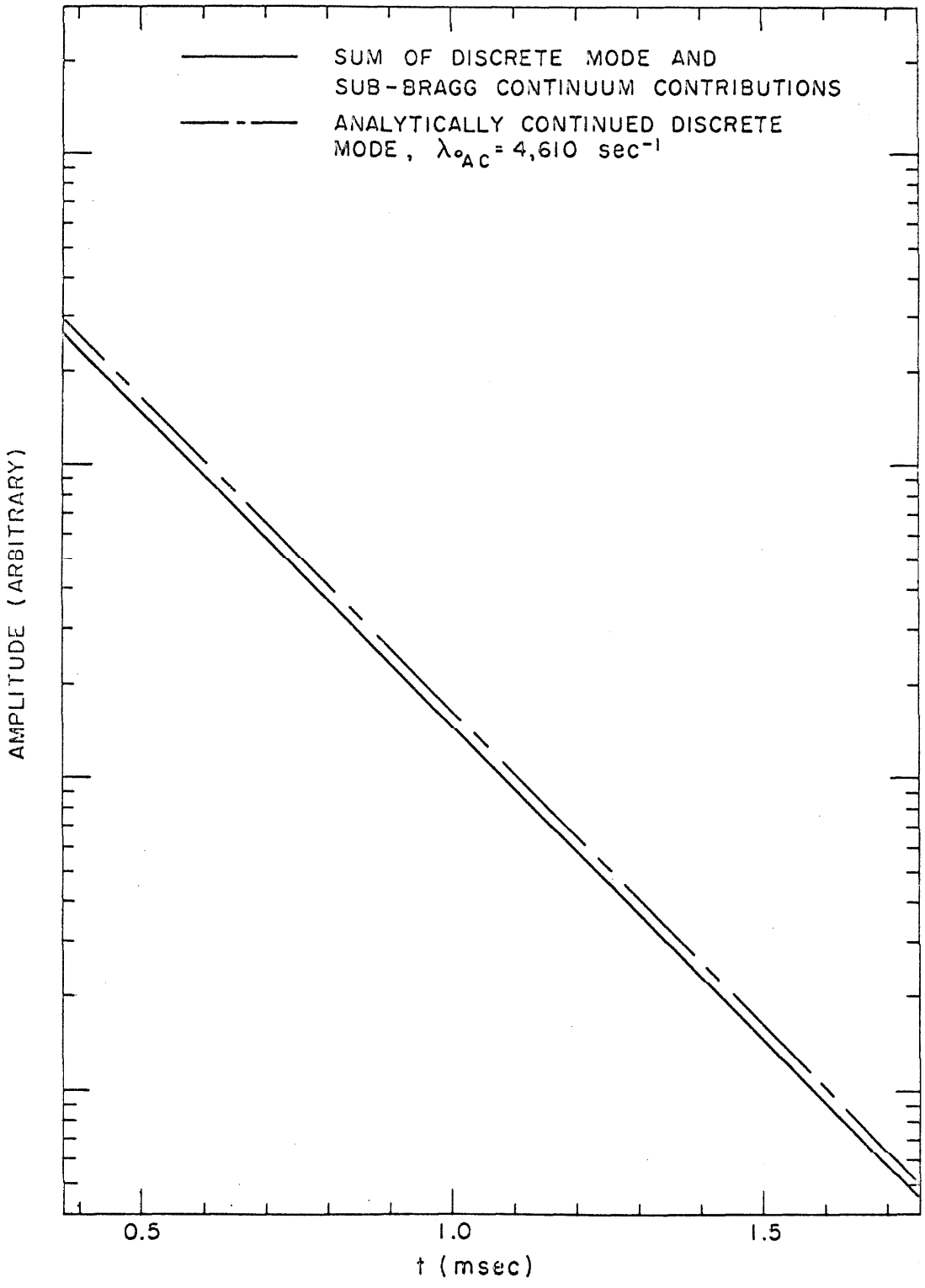

FIG. 22. Response function in beryllium at $B^2 = .038$ cm^{-2} illustrating $\lambda_{eff} \sim \lambda_{o_{A.C.}}$. $\lambda^* = 3800$ sec^{-1}, $(B^*)^2 = .03$ cm^{-2}.

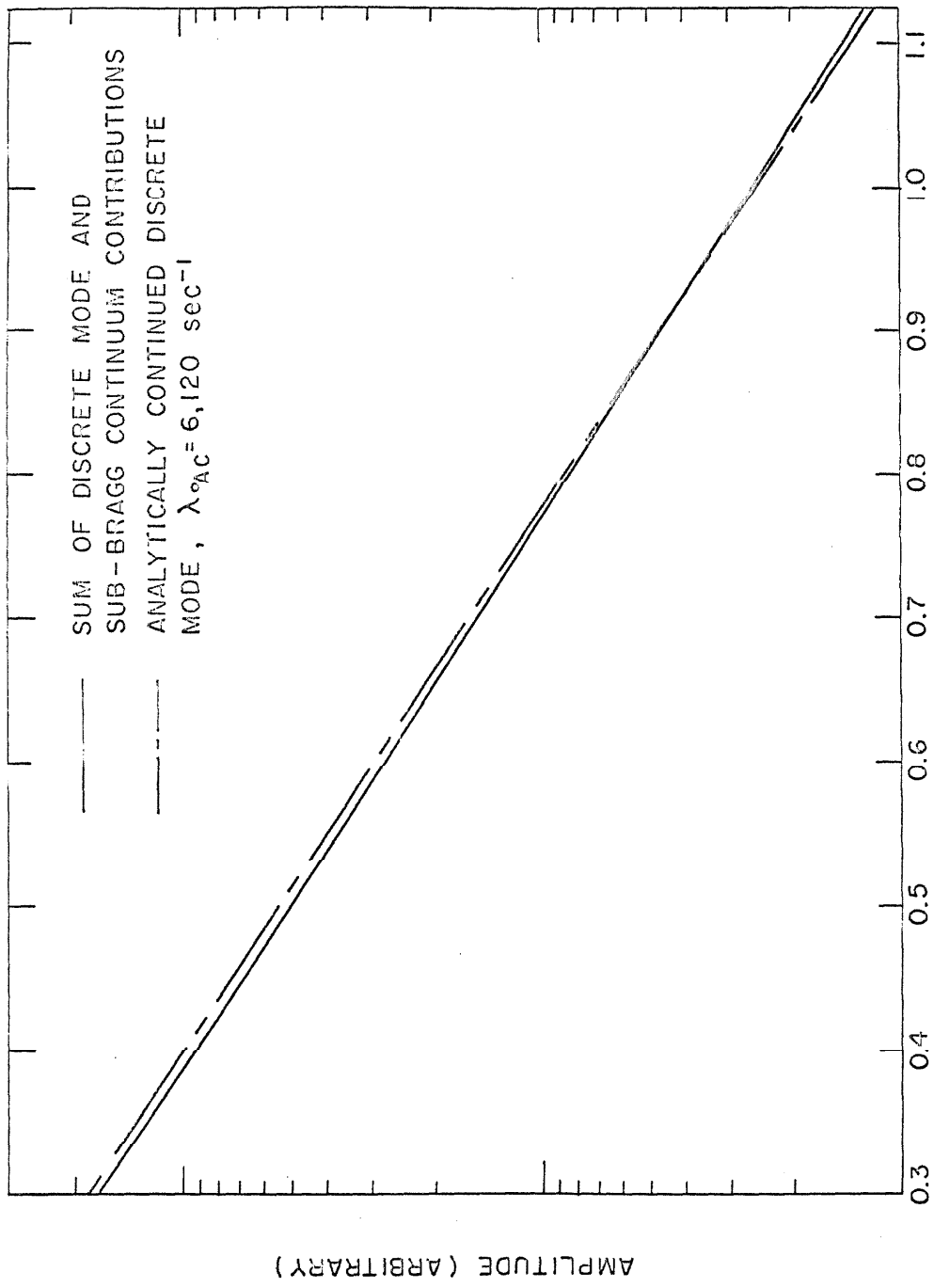

FIG. 23. Response function in beryllium at $B^2 = .054\ cm^{-2}$ illustrating $\lambda_{eff} \sim \lambda_{o_{A.C.}}$ $\lambda^* = 3800\ sec^{-1}$, $(B^*)^2 = .03\ cm^{-2}$.

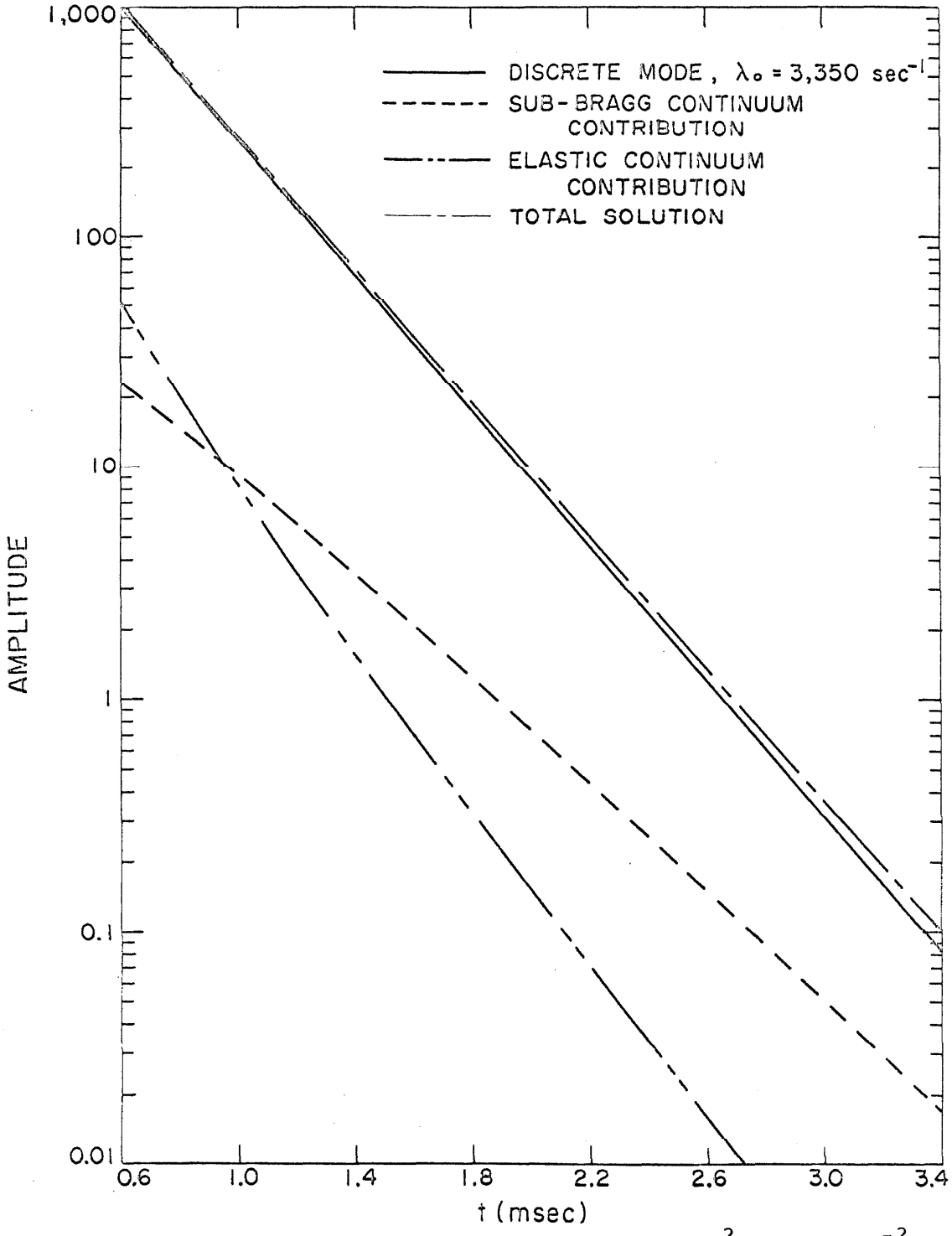

FIG. 24. The response function in graphite at $B^2 = .016$ cm^{-2} including the various contributions. $\lambda^* = 2600$ sec^{-1}, $(B^*)^2 \simeq .011$ cm^{-2}.

At still higher bucklings, when λ_o is close to λ_{el}, the relationship

$$\left\{\begin{array}{l}\text{effective decay constant} \\ \text{(physical plane)}\end{array}\right\}_{\Gamma_{SB}} + \text{discrete pole} \sim \left\{\begin{array}{l}\text{eigenvalue of analytically} \\ \text{continued dispersion law}\end{array}\right\} \qquad \text{(III-61)}$$

found to work earlier begins to break down. This is caused by the increasing importance of the elastic continuum. We noted previously that when λ_o is close to λ_{el}, the amplitude of the discrete mode decreases while that associated with Γ_e increases. As well, for these large B^2, the dispersion law relies more and more heavily on the proximity of λ_o to λ_{el} to maintain itself. The result is to diminish the importance of the sub-Bragg terms in $\Lambda(\lambda,B)$ and $\Lambda_c(\lambda,B)$ causing $\lambda_{o_{A.C.}}$ to approach λ_o.

Thus, in beryllium, the relation III-61 is useful for B^2 less than about .054 to .056 cm^{-2}. In graphite, III-61 is valid for B^2 less than .018 cm^{-2}, i.e., the relation is useful for B^2 about as large as twice $(B^*)^2$. Beyond this, any deduced effective decay constant will be lower than $\lambda_{o_{A.C.}}$. This agrees with the result of Ghatak and Honeck[21] which indicate a "pseudo-fundamental" eigenvalue is well defined to about twice B^{*2}.

3) Comparisons with Other Theoretical Calculations and Experiments

The high buckling effects just discussed are illustrated in figure 25 for beryllium. The results of this thesis are presented along

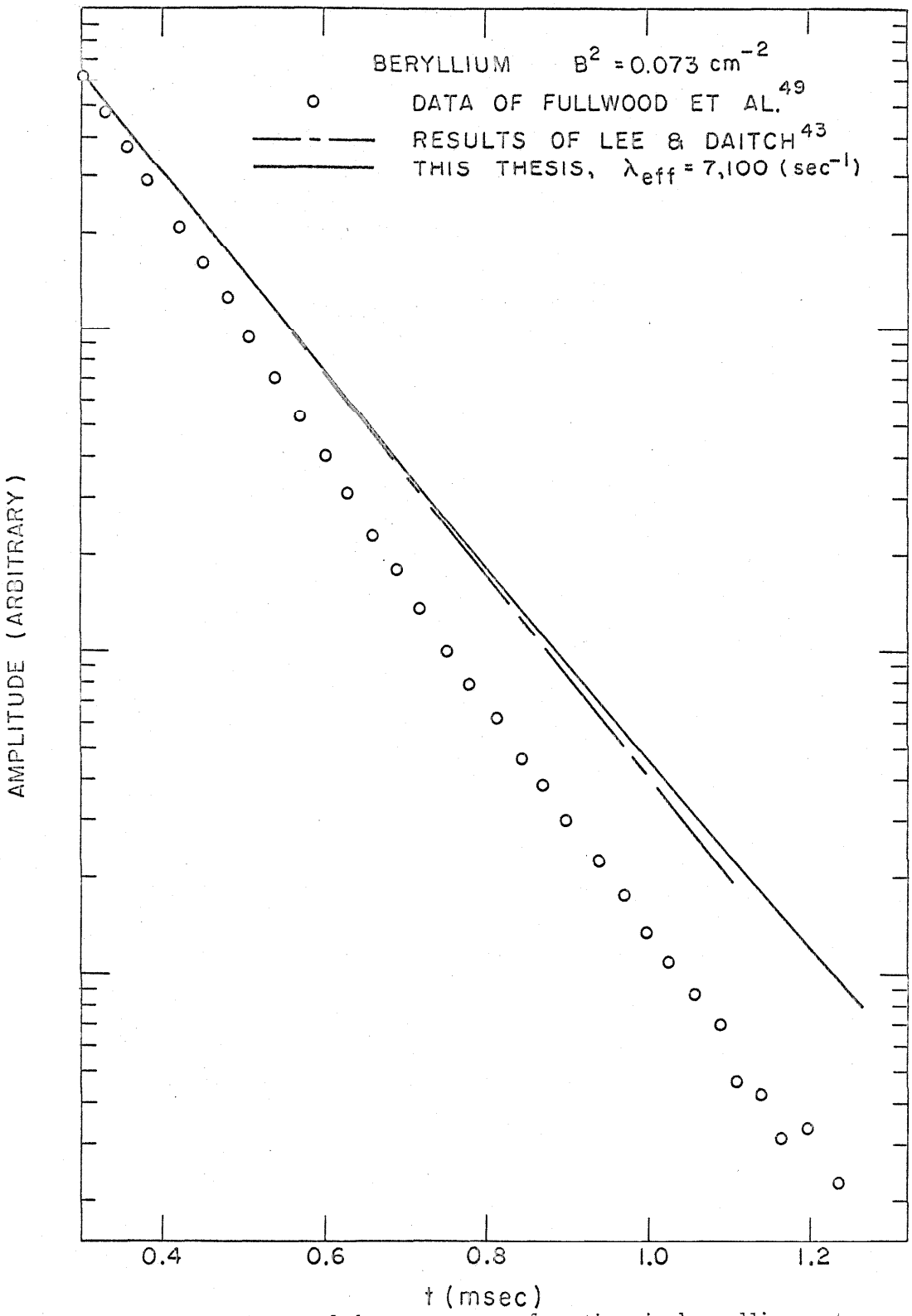

FIG. 25. A comparison of the response function in beryllium at $B^2 = .073\ cm^{-2}$ with the calculation of Lee and Daitch[43] and the data of Fullwood et al.[49]

with the experimental data of Fullwood et al.[49] and the multi-group diffusion theory calculation of Lee and Daitch[43]. Notice that while an effective decay constant is close to 7100 sec^{-1}, $\lambda_{o_{A.C.}}$ is 7400 sec^{-1}. Lee and Daitch attribute the disagreement between theory and experiment to inadequacies in the scattering kernel[47]. While we also suffer from such inadequacies, we see the differences also depend sensitively on the location of λ_{el}. And this is intimately related to $\Sigma_i(v_B)$ and $\Sigma_{el}(v_B)$. Thus, results in this range of B^2 are quite sensitive to the elastic cross section modeling near v_B and the validity of the λ-law at that speed.

At very high bucklings, the discrete mode contribution becomes unimportant and the total solution is composed of the contributions from Γ_e and Γ_{SB}. For example, in beryllium at $B^2 = 0.12$, we find both theoretical decay curves illustrated in figure 26 do not exibit quasi-exponential behavior. Both Lee and Daitch[43] and Ghatak and Honeck[21] have noted that far into the diffusion theory continuum (as at B^2=0.12 cm^{-2} for Be), no well-defined "pseudo-fundamental" eigenvalue exists. We suggest this is caused by the loss of amplitude associated with their "p-f" mode, much like the behavior of the discrete mode in this thesis. This would leave only various continuum contributions or, in the approach of Corngold and Durgun[25], would imply wide peaks in the diffusion theory continuum integrands.

The loss of amplitude of the discrete mode when compared with the amplitude of the contribution from Γ_e is illustrated in figure 27 for graphite. These calculations were performed using

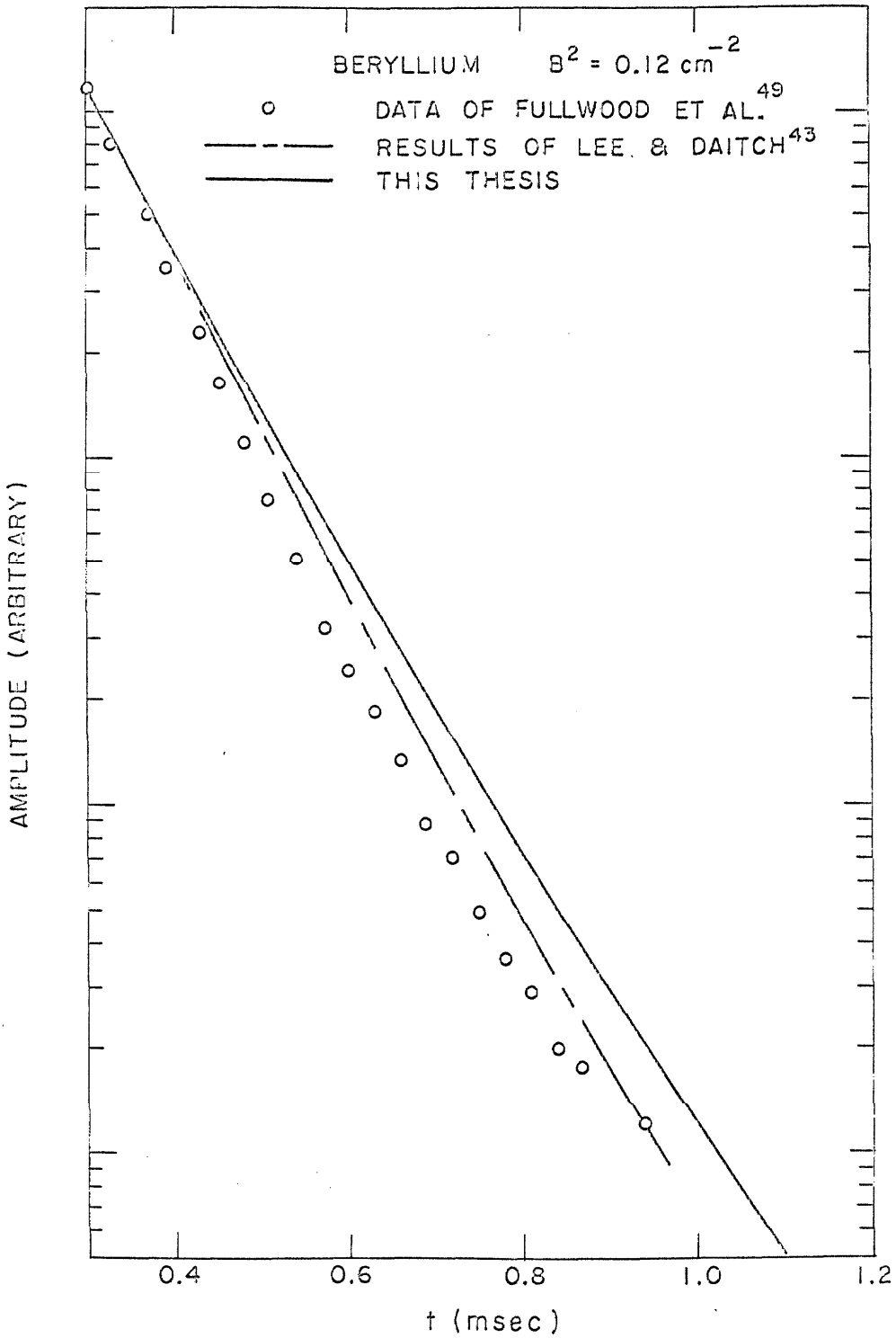

FIG. 26. A comparison of the response function in beryllium at $B^2 = 0.12\ cm^{-2}$ with the calculation of Lee and Daitch[43] and the data of Fullwood et al.[49]

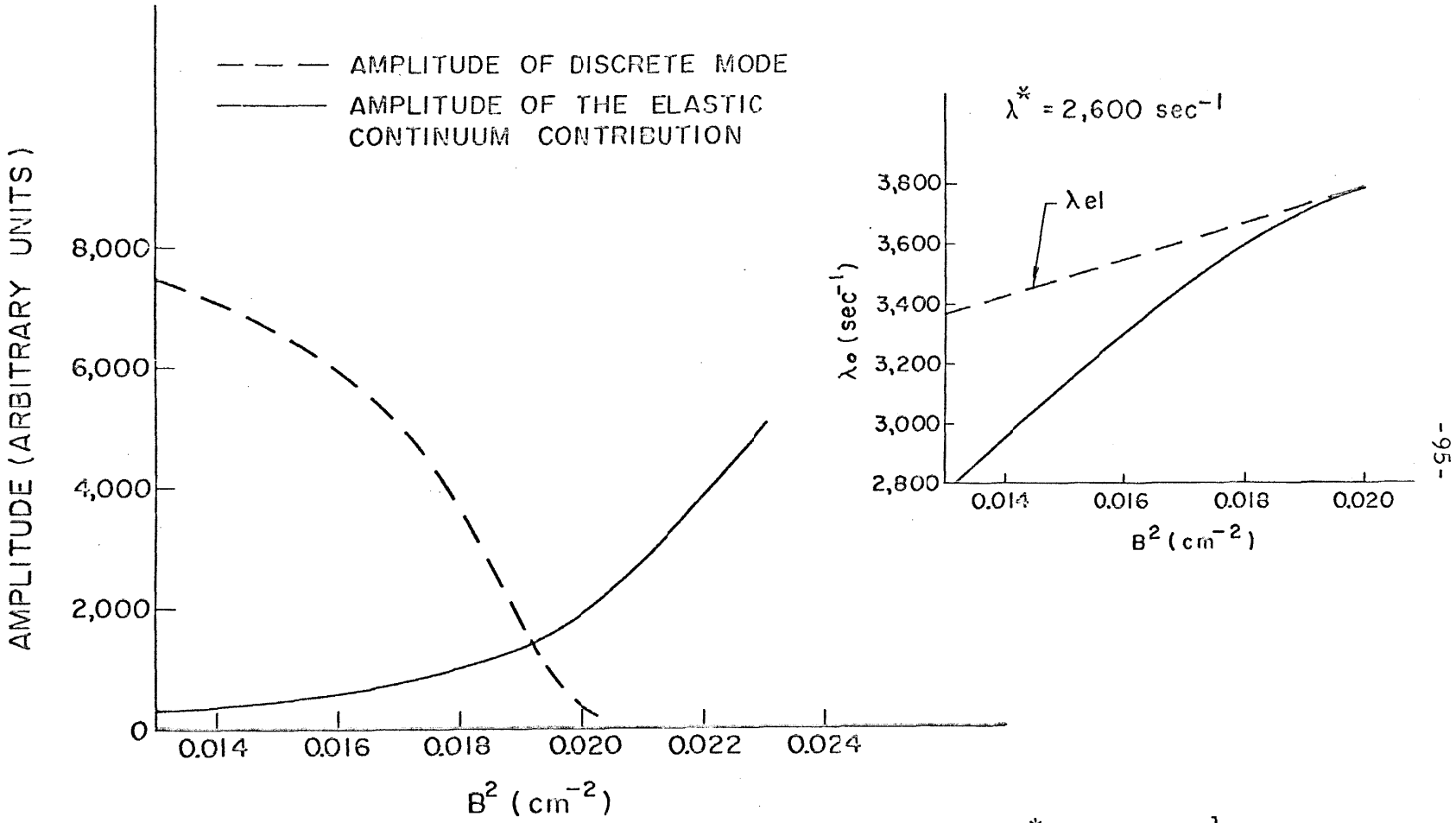

Fig. 27 A demonstration of "mode switching" in graphite. $\lambda^* = 2600\,\mathrm{sec}^{-1}$, $(B^*)^2 = .011\ \mathrm{cm}^{-2}$. The evaluation of the amplitude of the elastic continuum contribution is described in the text.

$\lambda^* = 2600\ \text{sec}^{-1}$. The calculated value of B^{*2} was $0.011\ \text{cm}^{-2}$. The corresponding dispersion curve is given in figure 19, from which one can determine the proximity of λ_o to λ_{el}. The amplitude of Γ_e plotted in figure 27 was obtained by extrapolating, to $t = 0.0$, an effective exponential fit of the actual decay from Γ_e over the time range 0.6 to 3.4 msec.

During the "mode switching" process just described, the decay constants deduced depend critically on the time range over which measurements are made. However, when the discrete mode is no longer important, reported decay constants will be higher than we would expect if we had smoothly extrapolated the low B^2 portion of the dispersion curve. This effect results because the contribution from Γ_e (which is now dominant over measuring times) decays faster than any combination of discrete mode and sub-Bragg continuum contributions. Thus, the reported dispersion curve should include decay constants at large bucklings that are too high to be fitted smoothly to the low B^2 data with a concave curve (see figure at right). An examination of the data of Andrews and Zhezherun in figure 1 illustrate this effect. In general, reported decay constants in graphite and beryllium are too large for $B^2 > 2B^{*2}$ when compared with the lower buckling data.

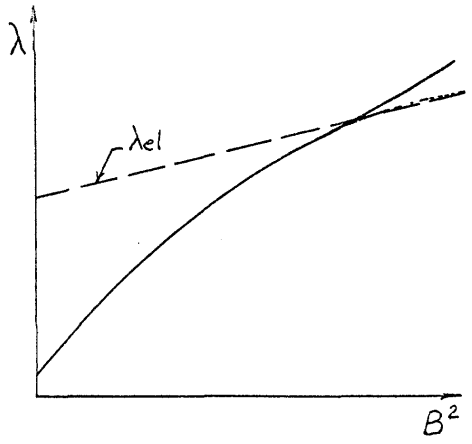

In previous discussions, we have demonstrated the important

role of λ_{cl}. Since, as a function of B^2, λ_{el} emanates from $v_B\Sigma_i(v_B) = \lambda^*$ (λ-law), we must use the proper λ^* if we are to make any headway at all. Thus, comparisons with the work of Lee and Daitch are to their calculations with a BNL-325 kernel normalization. In fact, their results with a bound-atom kernel normalization must involve a $\lambda^* > 3800$ sec^{-1} for Be because, at every B^2, the eigenvalue with this kernel is too high. This is just the effect of raising λ_{el}.

We noted previously that the agreement between the results of this thesis and Ghatak and Honeck[21] for graphite is poorer than agreement in beryllium. (see figure 19). We must realize, however, that Ghatak and Honeck employ a scattering kernel which predicts a λ^* approximately half the generally accepted value[30] of 2600 sec^{-1} for graphite. Moreover, though they have four energy groups below the Bragg cutoff where the λ-law appears to be obeyed[61], the values of $v\Sigma_i(v)$ are not identical in each of these groups (see figure 28a or 28b). An examination of their 50-group eigenvalue structure in figure 28a shows that at $B^2 = 0$, the values of λ_1 through λ_5 vary from 1000 to 1400 sec^{-1}. λ_5 represents the decay constant of the first group above the Bragg cutoff. This means that the bounding line analogous to λ_{el} and, in diffusion theory, given by $\lambda^* + v_B D(v_B) B^2$, actually emanates from $\lambda_5(B^2 = 0) = 1400$ sec^{-1}.

By using a value of $\lambda^* = 1400$ sec^{-1}, we can generate a bounding line equivalent to that which exists for Ghatak and Honeck. The dispersion curve which results with $\lambda^* = 1400$ sec^{-1} and the modified synthetic kernel is shown in figure 29. We now find much improved

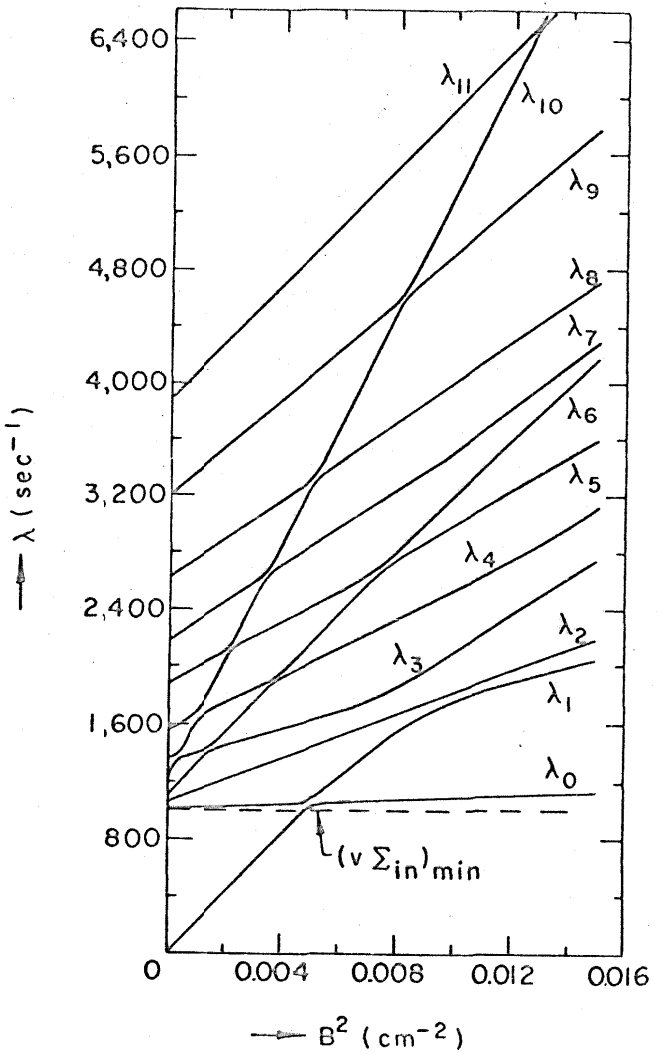

Fig. 28a. Buckling dependence of the first few eigenvalues in the 50-group calculation by Ghatak and Honeck[21] for graphite.

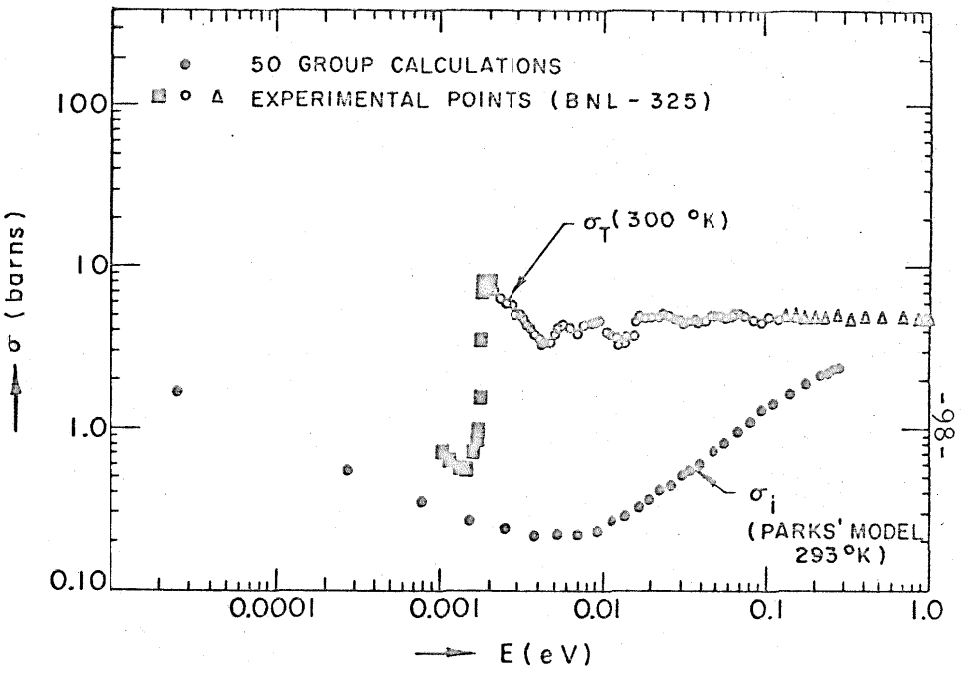

FIG. 28b. A comparison of the inelastic scattering cross section employed by Ghatak and Honeck[21] with the total cross section for graphite.

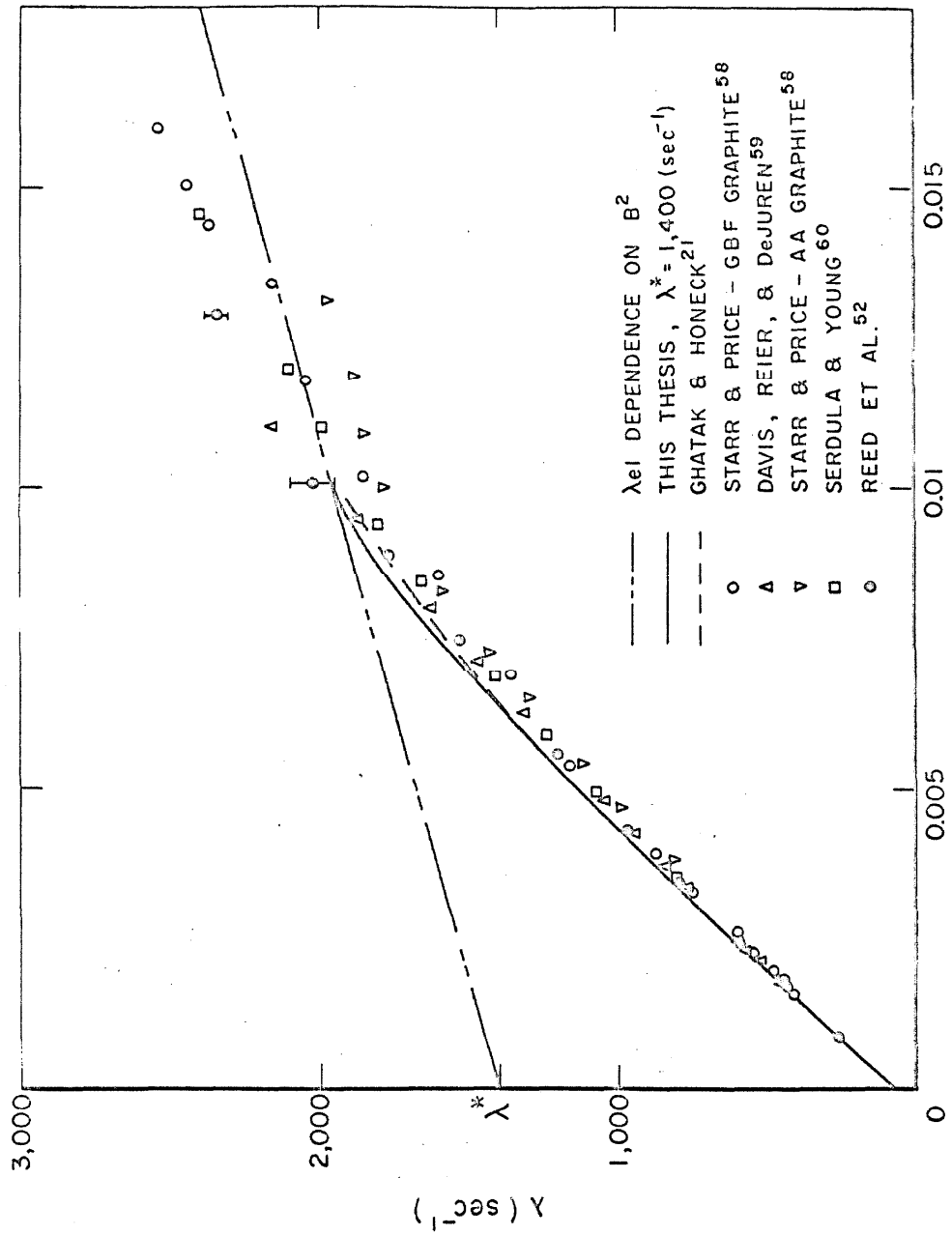

FIG. 29. $\lambda_o(B^2)$ for graphite using $\lambda^* = 1400\ sec^{-1}$.

agreement between theoretical results. Furthermore, the dispersion curve of this thesis curves under λ_{el} at the largest value of B^2 for which Ghatak and Honeck report a "pseudo-fundamental" eigenvalue. Referring to earlier arguments, we expect this because the discrete mode now begins to decrease in importance. Beyond this buckling, the integrals about Γ_{SB} and Γ_e are the main contributions to the total solution.

Additionally, had Ghatak and Honeck's kernel yielded $\lambda^* = 2600\ sec^{-1}$, their agreement with data in the range $B^2 = .006$ to $.009\ cm^{-2}$ would be somewhat poorer because their eigenvalues would be higher.

Very recently, Ardente and Rossi[50] examined pulsed neutron experiments in both graphite and beryllium using a phenomenological description of the decay process based on an energy dependent mean neutron life and diffusion theory. They achieve qualitatively the same results as Lee and Daitch[43] for beryllium and Ghatak and Honeck[21] for graphite. Ardente and Rossi used $\lambda^* = 4060\ sec^{-1}$ for beryllium and $\lambda^* = 741\ sec^{-1}$ for graphite.

Since general agreement between theory and experiment in graphite seems to require a value of λ^* about half $2600\ sec^{-1}$, one might ask how well established this value is. And indeed, on surveying the literature, one finds $\lambda^* = 2600\ sec^{-1}$ not to be well founded either experimentally or theoretically. Both Hughes[61] and Bacon[62] indicate $\sigma_i = 0.9$ barns at $\lambda = 8$ Å and Hughes indicates σ_i is proportional to λ (the neutron wavelength) from 7 Å to 11 Å. The value $\sigma_i = 0.9$ barns

at 8 Å implies $\lambda^* = 3600\ \text{sec}^{-1}$ for graphite. On the other hand, Egelstaff[63] reports $\sigma_i = 0.6$ barns at 8 Å which implies $\lambda^* = 2400\ \text{sec}^{-1}$ (this is apparently the Harwell data reported in BNL-325). In addition, Kothari and Singwi[33] report data due to Palevsky which indicates $\sigma_i = 0.28$ barns at 8 Å implying $\lambda^* = 1200\ \text{sec}^{-1}$. Also, Palevsky's data does not yield σ_i proportional to the neutron wavelength. It has been suggested[63] that the high cross section measurements (greater than 0.6 barns at 8 Å) may be due to small-angle scattering. This, however, does not account for the difference between the data of Egelstaff, who accounted for small-angle scattering, and Palevsky. A theoretical calculation has been performed by Khubchandani, Kothari, and Singwi[64] of the coherent, one-phonon absorption cross section which indicates σ_i is proportional to the neutron wavelength and gives λ^* approximately equal to $1100\ \text{sec}^{-1}$. However, their "λ-law" does not extrapolate to the origin, as it should, but to a negative value on the σ axis.

We see therefore that $\lambda^* = 2600\ \text{sec}^{-1}$ for graphite is not well established. Combining this with the results of this theoretical analyses of pulsed neutron experiments in graphite shows that a careful re-measurement of $\sigma_i(v)$ below the Bragg cutoff is required.

Another polycrystalline material to which the results of the thesis apply is beryllium oxide (BeO). Although we have not carried out specific calculations, the recent results of Ritchie and Rainbow[20] can be readily interpreted. Their results are presented in figure 30. Below the bounding line λ_{el}, they find well defined decay constants.

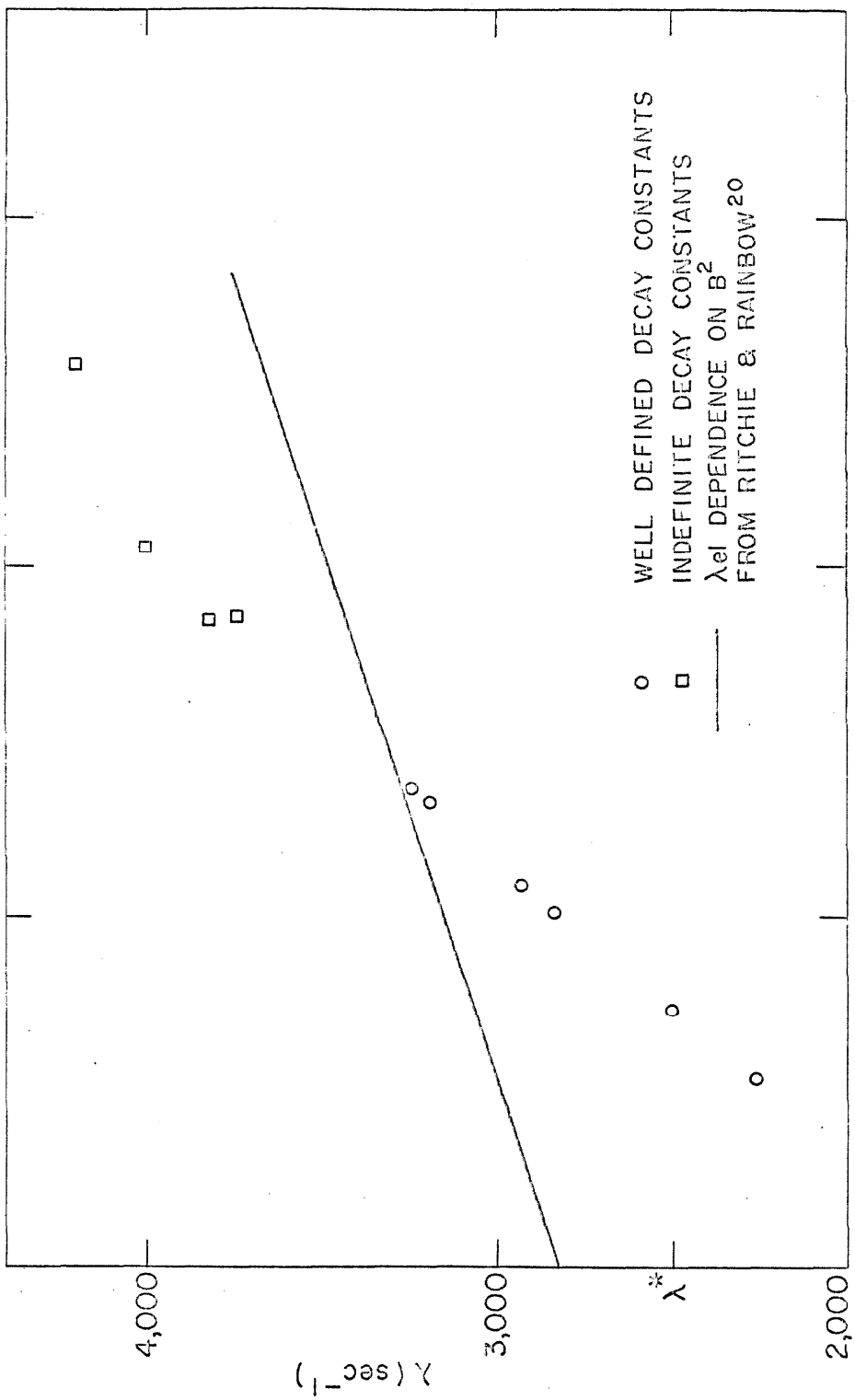

FIG. 30. Experimental data for beryllium oxide from Ritchie and Rainbow[20].

This agrees with the result that in this region, the discrete mode amplitude is dominant and $\lambda_{o_{A.C.}}$ should predict the correct decay constant. Furthermore, decay constants higher than λ_{el} are not well defined indicating that the discrete mode is no longer dominant. $\lambda_{o_{A.C.}}$ no longer represents the decay constant and the solution is composed mainly of contributions from Γ_{SB} and Γ_e. In fact, this interpretation emphasizes the value of the philosophy employed by Ritchie and Rainbow. By finding the buckling beyond which a discrete decay mode has lost amplitude and an effective decay constant is not well defined, an experimenter should be able to locate λ_{el}. Knowledge of $\Sigma_{el}(v_B)$ would allow one to estimate λ^* or $v_B\Sigma_i(v_B)$. This requires, however, that experimenters overcome other difficulties so that they agree among themselves about the behavior of neutron pulses. This is not the situation in either graphite or beryllium oxide.

J. HIGHER MODES AND THE ROLE OF Γ_e

Not long ago, the thermalization time, τ_{th}, defined as $1/\lambda_1$ where λ_1 is the first eigenvalue above the fundamental, was thought to be a well defined quantity in polycrystals. Küchle and Schweikert[51] obtained values of λ_1 as a function of B^2 in graphite (see figure 31) by effectively subtracting the fundamental mode from the total decay. However, numerical calculations now indicate that no discrete eigenvalue other than the fundamental exists in graphite or beryllium. Thus, subtracting the fundamental mode must leave only continuum contributions.

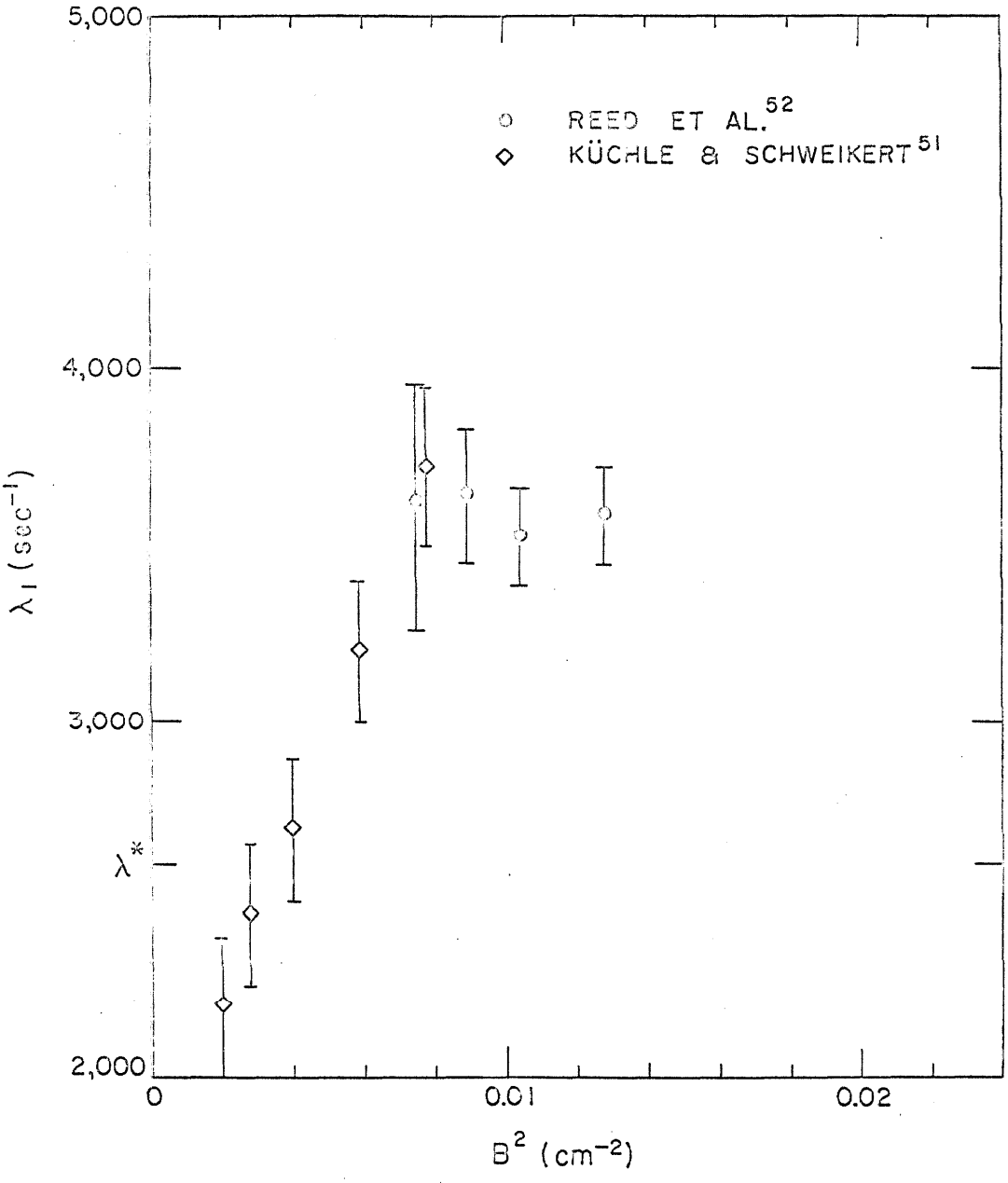

FIG. 31. Experimental results for $\lambda_1(B^2)$ in graphite.

This thesis has shown that the sub-Bragg continuum and discrete mode can be treated as one with an effective decay constant given by the eigenvalue of the analytically continued dispersion law. Alternatively, the representation indicated by figure 11 implies the decay following the pulse is primarily a discrete mode decay with eigenvalue $\lambda_{o_{A.C.}}$. Thus, by subtracting the "fundamental" mode, one is primarily left with the contribution from the elastic continuum.

In figure 32, the results of a calculation of the contribution from Γ_e as a function of B^2 for graphite with $\lambda^* = 2600\ \text{sec}^{-1}$ are presented. The smaller buckling curves show significant curvature, and, while these contributions are dependent on the source, we do not expect their character to alter. In addition, the amplitude increases with buckling as λ_o approaches λ_{el} as previously discussed. Basically, the presence of the pole excites the elastic continuum. Thus, experimental results for λ_1 should vary depending on where the spectrum is assumed asymptotic. Indeed, this was found by Ghatak and Honeck. Notice that Küchle and Schweikert's results contain two values of λ_1 below $\lambda^* = 2600\ \text{sec}^{-1}$. The nominal agreement obtained by Ghatak and Honeck with this experiment is due to their low value of λ^*.

Recently, Reed et al.[52] reported values of λ_1 at large buckling that agree with Küchle and Schweikert's highest point but disagree in character (see figure 31). We should note that the method of obtaining λ_1 is quite difficult and hopefully further experimental work will clarify the picture. Suffice it to say that the contribution from Γ_e should be the result of subtracting the effective fundamental or analytically

continued mode from the total solution when only one discrete mode exists.

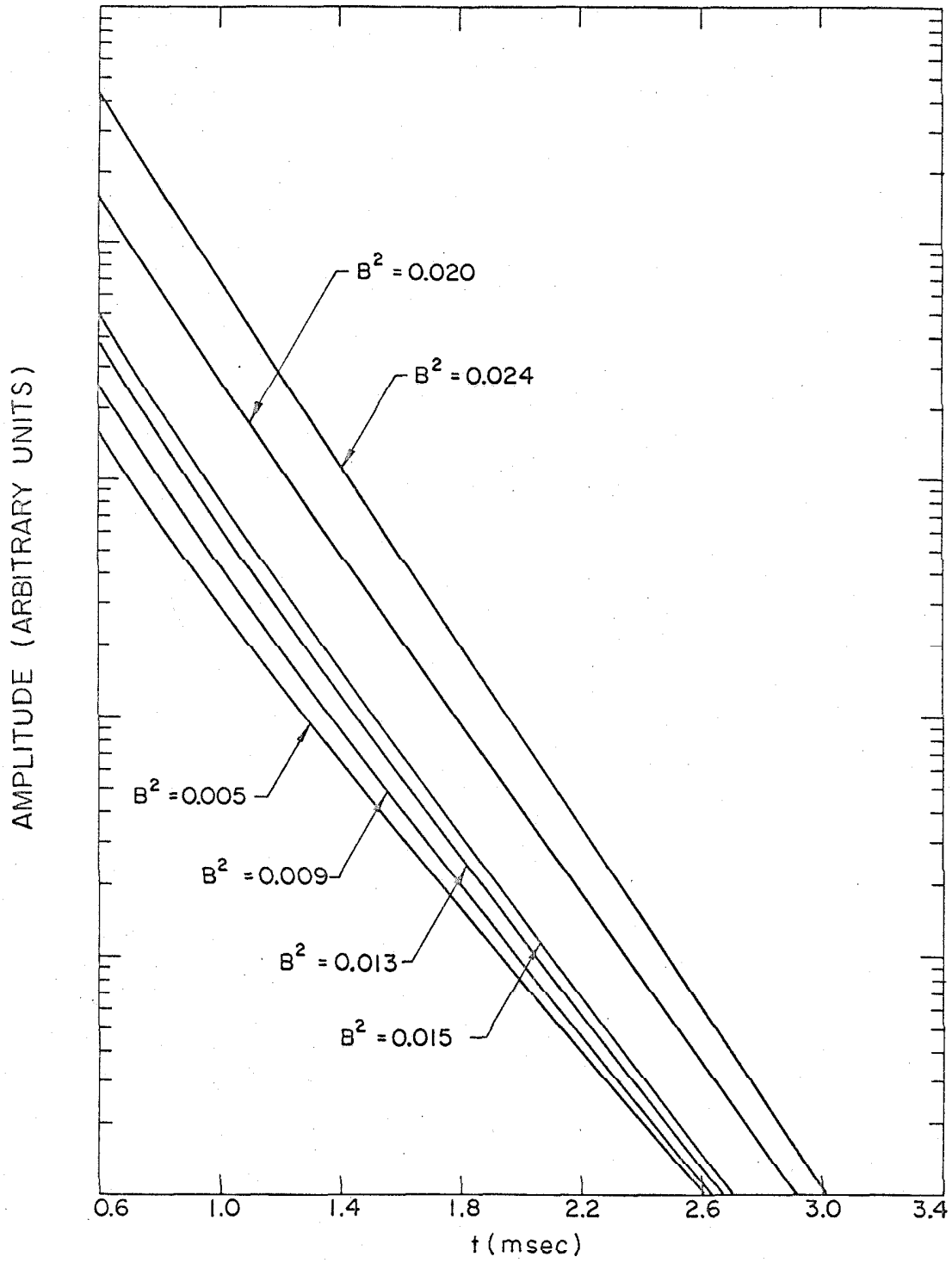

FIG. 32. The contribution from Γ_e at various bucklings for graphite with $\lambda^* = 2600\ \text{sec}^{-1}$.

IV. CONCLUSIONS AND DISCUSSION

A. SUMMARY OF RESULTS

This thesis has been an attempt to understand the decay of a thermalized pulse of neutrons in a homogeneous, polycrystalline medium. Towards this end, we have included several features of slow neutron scattering in polycrystals such as elastic scattering and non-monotonic (actually, discontinuous) cross sections. These features have produced a number of interesting and unexpected results.

One of the most striking differences from previous theoretical efforts is the structure of the transform plane. By including a non-square-integrable kernel to describe elastic scattering, a new continuum, Γ_e, is produced which has a crucial effect on the behavior of the dispersion curve. Furthermore, using discontinuous cross sections results in the existence of discrete eigenvalues with magnitude <u>greater than</u> λ^*.

The dispersion curve itself exhibits interesting and unusual behavior. For example, we found that on the "physical plane" or primary Riemann sheet, the eigenvalue variation with buckling is discontinuous at λ^* and consists of two disjoint segments. On the other hand, by searching for an alternate representation of the total solution, we discovered that the dispersion curve could be smoothly extended past λ^*. This required eigenvalues from a dispersion law that had been analytically continued past Γ_{SB}. However, the line cut at Γ_{SB} appears to invalidate the standard interpretation of the Nelkin expansion coefficients when data beyond λ^* is included.

An examination of the total solution revealed that the contributions from the discrete pole and sub-Bragg continuum in the "physical" plane has an effective decay constant over measuring times that is represented by an analytically continued eigenvalue. Such a relationship appears to hold for B^2 as large as twice $(B^*)^2$.

However, an alternative "maximum B^2" theorem has been proven which implies that discrete eigenvalues fail to exist for polycrystals of roughly a mean free path in size. This is the same order of magnitude as the critical size for a substance like water. The critical nature of λ^* and $(B^*)^2$ is caused by sub-Bragg neutrons having exceptionally long mean free paths. This makes normally "large" systems appear small to neutrons in this energy range.

We were able to show that the amplitude of the discrete mode drops when λ_o is close to λ_{el} while that of the contribution from Γ_e increases. This mode switching may provide a technique for locating λ_{el}. Thus, while a discrete mode exists at very large buckling, it plays no role in determining the response function.

In either of the two representations developed for the solution, we found that when $\lambda_o > \lambda^*$, the sub-Bragg continuum contribution dominates the decay at long times. In fact, Fullwood et al.[49] appear to have seen the effects of Γ_{SB} in their work on beryllium. However, current measurement techniques are not capable of waiting long enough to see the uncontaminated contribution from Γ_{SB}.

B. IMPLICATIONS FOR EXPERIMENT

We can conclude from this work that nothing drastic happens to the experimentally observed response function as B^2 passes $(B^*)^2$. Additionally, a good exponential decay (with decay constant equal to the analytically continued eigenvalue) is observable over early measuring times.

As $\lambda_{o_{A.C.}}$ approaches λ_{el}, it should be possible to observe the mode switching between the contributions from the pole and Γ_e. In fact, a worthwhile procedure is to plot, beforehand, λ_{el} using the best available values of $\Sigma_i(v_B)$ and $\Sigma_e(v_B)$. By knowing the shape of the dispersion curve for $\lambda_o < \lambda_{el}$, it is possible to decide on roughly the range of B^2 over which mode switching occurs.

For polycrystals like beryllium oxide, where λ^* is not experimentally known, an interesting combination of experiments is to employ standard transmission techniques to measure $\sigma_i(v)$ for $v < v_B$ thus obtaining λ^* and $\Sigma_i(v_B)$ and then to perform a pulsed neutron experiment to investigate several of the results of this theoretical effort.

The same combination of experiments on graphite would, as well, be valuable since, as we have seen, the value $\lambda^* = 2600\ \text{sec}^{-1}$ is not well established either experimentally or theoretically. In fact, for pulsed neutron experiments in graphite, agreement is significantly improved between theory and experiment when λ^* is taken to be approximately $1400\ \text{sec}^{-1}$. Certainly if this is true, it goes a long way towards explaining the disagreement among experimenters for B^2 greater than approximately $0.009\ \text{cm}^{-2}$ for it implies decay constants

deduced in this range will depend, for one, on the time over which the decay was assumed exponential (see figure 29). At this time, there exists no theoretical argument which can explain the disagreement among experimenters indicated by figure 29 using $\lambda^* = 2600\ \text{sec}^{-1}$.

In any of these polycrystalline solids, by waiting long enough (e.g. $t > 0.8$ to 1.0 msec in beryllium at $B^2 \simeq 0.07\ \text{cm}^{-2}$) one should observe curvature in the decay caused by the contribution from the sub-Bragg continuum when $B^2 > B^{*2}$. As mentioned previously, this appears to have been observed in beryllium[49] and beryllium oxide[20]. This effect can be magnified by performing the pulsed experiments at low temperatures[53].

C. IMPLICATIONS FOR MULTI-GROUP COMPUTER CALCULATIONS

From the results herein, one expects a multi-group B_o code which includes elastic scattering and discontinuous cross sections (see Wood[46]) to yield eigenvalues independent of group structure with magnitude greater than λ^*. In such a calculation, the response function should exhibit the characteristic high B^2 behavior we have described. One might also attempt multi-group calculations of $\lambda_{o_{A.C.}}$ by extending the definition of the arctangent function when $B^2 > B^{*2}$ and $v < v_B$. We have demonstrated with a modified synthetic kernel that such an approximation causes negligible errors because neglected terms are of order $\left(\frac{-\lambda_{o_{A.C.}} + \lambda^*}{Bv_T}\right)^2$.

Characteristic singular lines analogous to λ_{el} will exist and are given by

$$\lambda_e(v_j) = v_j\left(\Sigma_T(v_j) - \frac{B}{\tan\left(\frac{B}{\Sigma_{el}(v_j)}\right)}\right) ; \quad v_j > v_B$$

or

$$\lambda_e(v_j) = v_j\Sigma_i(v_j) + \frac{v_j B^2}{3\Sigma_{el}(v_j)} + O(B^4) ; \quad v_j > v_B .$$

Here, v_j is the speed corresponding to the jth energy group. For multi-group calculations in which several Bragg peaks are included, these lines can cross causing the multi-group eigenvalue structure to appear similar to its diffusion theory counterpart (see figure 3).

D. SUGGESTIONS FOR FURTHER RESEARCH

The work in this thesis indicates several interesting areas for further research. For example, we have indicated that certain physical parameters, namely, λ^*, $\sigma_i(v_B)$, and $\sigma_e(v_B)$, play an important role in understanding pulsed neutron experiments. Furthermore, the importance of the sub-Bragg neutrons described by the contribution from Γ_{SB} demonstrates the necessity of treating this energy range carefully. The sub-Bragg parameters like λ^* are incorrectly predicted[31,35] by computer-oriented scattering kernels for polycrystals, e.g. the Summit code[47], because they use the incoherent approximation to describe inelastic scattering for $v < v_B$. We might note here that while the Summit code underestimates λ^* for graphite, it overestimates it for beryllium. Since the scattering below the Bragg cutoff is inelastic, coherent scattering, further work is required to correctly describe very slow neutron scattering.

Considerable work remains on the exact spatially dependent transport theory analysis of pulsed neutron experiments in polycrystals. Recently, Cercignani[54] has developed a method for solving boundary value problems of the Boltzmann equation when a synthetic kernel is used. Furthermore, full-range problems can be handled by this method when a general square-integrable kernel is included[55]. Thus, the problem of pulsed experiments in infinite slabs of water with a source at the center is amenable to exact solution. However, full and half-range boundary value problems with a non-square-integrable, non-degenerate kernel remain unsolvable. Since the modified synthetic kernel utilized in this thesis is non-degenerate and non-square-integrable, a general method for solving the pulsed neutron problem in polycrystals with correct boundary conditions does not exist at this time.

If we could solve such problems exactly, we could then investigate the range of validity of asymptotic reactor theory. Recently, Williams[56] examined the pulse neutron problem in slabs using a synthetic kernel and the end-point method. Thus, his results are not directly applicable to polycrystals. However, he found that the buckling concept is valid as long as a discrete time eigenvalue exists. As well, he conjectured that when a "pseudo-fundamental" time eigenvalue exists (as in diffusion theory), a "pseudo-fundamental" buckling will exist as well. We have found that in place of "pseudo" eigenvalues, real eigenvalues exist with magnitude greater than λ^*. If we extend Williams' conjecture, it implies that the buckling concept has validity where he

suggests "pseudo" bucklings. However, the buckling concept might break down at long times. Of course, all this is a subject for further work.

Of somewhat more mathematical interest is the problem of evaluating the total solution when only area continuum exists (or discrete eigenvalues embedded in the area). Cercignani utilized the theory of generalized analytic functions[57] on problems of this kind. Additionally, one can examine in a general way the dispersion law of neutron transport as a function of two complex variables.

APPENDIX A

PROOF THAT THE DISCRETE EIGENVALUES ARE REAL

Begin by considering the eigenvalue problem analogous to equation II-32 in chapter II

$$\tilde{\psi}_H(B,v,\lambda) = \frac{T(B,v,\lambda)}{\Gamma_e(B,v,\lambda)}\int_o^\infty v'\Sigma_i(v',v)\Psi_H(B,v',\lambda)\,dv'. \qquad (A-1)$$

Since $\Sigma_i(v',v)$ obeys detailed balance, we can rewrite A-1 as

$$\chi(B,v,\lambda) = \alpha(B,v,\lambda)\int_o^\infty K(v',v)\chi(B,v',\lambda)\,dv' \qquad (A-2)$$

where

$$\chi(B,v,\lambda) = \frac{\tilde{\psi}_H(B,v,\lambda)}{\sqrt{M(v)}}\quad , \qquad (A-3)$$

$$K(v',v) = v'\Sigma_i(v',v)\left(\frac{M(v')}{M(v)}\right)^{\frac{1}{2}} = K(v,v')\ , \qquad (A-4)$$

and

$$\alpha(B,v,\lambda) = \frac{T(B,v,\lambda)}{\Gamma_e(B,v,\lambda)}\ . \qquad (A-5)$$

If we complex conjugate A-2, we find

$$\bar{\chi}(B,v,\lambda) = \bar{\alpha}(B,v,\lambda)\int_o^\infty K(v',v)\bar{\chi}(B,v',\lambda)\,dv'. \qquad (A-6)$$

Multiply A-2 by $\bar{\chi}(B,v,\lambda)/\alpha(B,v,\lambda)$, A-6 by $\chi(B,v,\lambda)/\bar{\alpha}(B,v,\lambda)$, subtract and integrate over v to obtain

$$\int_o^\infty \bar{\chi}(B,v,\lambda)\chi(B,v,\lambda)\left[\frac{1}{\alpha(B,v,\lambda)} - \frac{1}{\bar{\alpha}(B,v,\lambda)}\right] dv = 0 \qquad (A-7)$$

By letting $\lambda = x + iy$, we can rewrite the bracket term in A-7 as

$$\frac{\bar{\alpha} - \alpha}{|\alpha|^2} = \frac{1}{|\alpha|^2 |\Gamma_e(B,v,\lambda)|^2} \frac{1}{2iBv} \log\left\{\frac{(x + v\Sigma_T(v))^2 + (Bv - y)^2}{(x + v\Sigma_T(v))^2 + (Bv + y)^2}\right\} \qquad (A-8)$$

Thus, A-7 can be written as

$$\int_o^\infty \frac{|\chi(B,v,\lambda)|^2}{|\Gamma_e(B,v,\lambda)|^2 |\alpha(B,v,\lambda)|^2 v} \log\left\{\frac{(x + v\Sigma_T(v))^2 + (Bv - y)^2}{(x + v\Sigma_T(v))^2 + (Bv + y)^2}\right\} dv = 0 \qquad (A-9)$$

However, the function

$$\frac{|\chi(B,v,\lambda)|^2}{|\Gamma_e(B,v,\lambda)|^2 |\alpha(B,v,\lambda)|^2 v} > 0$$

for all $v \in [0,\infty)$. As well, the log term is sign definite, i.e., for $y > 0$, the log is < 0, or for $y < 0$, the log is > 0. Either way, the integrand of A-9 is sign definite. Therefore A-9 can hold only if

$$\log\left\{\frac{(x \mp v\Sigma_T(v))^2 + (Bv - y)^2}{(x \mp v\Sigma_T(v))^2 + (Bv \mp y)^2}\right\} = 0$$

for all v. But this is true for all v only if $y \equiv 0$ implying only real eigenvalues can exist.

APPENDIX B

ASYMPTOTIC EXPANSION OF THE SUB-BRAGG CONTINUUM CONTRIBUTION

The expression

$$\tilde{N}(\lambda,B) = \frac{S(\lambda,B)}{\Lambda(\lambda,B)} \tag{B-1}$$

defined by equation III-53 is the Laplace transform of a time response function. Consider the case when $B^2 > B^{*2}$ so that the only zero of $\Lambda(\lambda,B) = 0$ occurs for $\lambda_o > \lambda^*$. Then at long times, the solution will be governed by the contribution from the integrals about Γ_{SB}. This contribution is given by

$$N_{SB}(t,B) = \frac{1}{2\pi i}\int_{-\lambda^*-iBv_B}^{-\lambda^*+iBv_B} d\lambda\, e^{\lambda t} S(\lambda,B)\left\{\frac{1}{\Lambda^+(\lambda,B)} - \frac{1}{\Lambda^-(\lambda,B)}\right\} \tag{B-2}$$

where we have assumed the source contains no sub-Bragg neutrons. Setting $\lambda = -\lambda^* - iBv_B\alpha$ yields

$$N_{SB}(t,B) = ae^{-\lambda^* t}\int_{-1}^{1} d\alpha\, e^{-i\alpha\tau} S(\lambda(\alpha),B)\left\{\frac{1}{\Lambda^+} - \frac{1}{\Lambda^-}\right\} \tag{B-3}$$

where "a" is a constant and $\tau = Bv_B t$. We will use integration by parts to obtain an asymptotic expansion. Define

$$z(\alpha,B) = \frac{\Lambda^-(\lambda(\alpha),B) - \Lambda^+(\lambda(\alpha),B)}{\Lambda^+\Lambda^-} = \frac{\delta(\alpha,B)}{\Lambda^+\Lambda^-}$$

and

$$\delta(\alpha,B)=\frac{\pi\lambda^*}{B\overline{\Sigma}v_T^2}\left(e^{-\alpha^2}-e^{-(v_B/v_T)^2}\right)$$

Integrating B-3 by parts once yields

$$N_{SB}(t,B)=ae^{-\lambda^* t}S(\lambda(\alpha),B)\frac{\delta(\alpha,B)}{\Lambda^+\Lambda^-}\Bigg|_{-1}^{1}$$

$$+\frac{1}{i\tau}\int_{-1}^{1}e^{-i\tau\alpha}\frac{\partial}{\partial\alpha}\left\{\frac{S\delta}{\Lambda^+\Lambda^-}\right\}d\alpha \qquad \text{(B-4)}$$

However, since $\delta(\pm\alpha,B)=0$, we integrate by parts again and obtain

$$N_{SB}(t,B)=\frac{ae^{-\lambda^* t}S(\lambda(\alpha),B)e^{-i\tau\alpha}}{\tau^2\Lambda^+\Lambda^-}\frac{\partial\delta(\alpha)}{\partial\alpha}\Bigg|_{-1}^{1}$$

$$-\frac{1}{\tau^2}\int_{-1}^{1}e^{-i\tau\alpha}\frac{\partial^2}{\partial\alpha^2}\left\{\frac{S\delta}{\Lambda^+\Lambda^-}\right\}d\alpha \qquad \text{(B-5)}$$

If we can integrate by parts one more time, we will have that $N_{SB}(t,B)=\frac{e^{-\lambda^* t}}{t^2}a(t)+O\left(\frac{e^{-\lambda^* t}}{t^3}\right)$ where $a(t)$ is $O(1)$. The only term that may not be integrable is the principle value integral in both $\Lambda^+(\lambda(\alpha),B)$ and $\Lambda^-(\lambda(\alpha),B)$. That integral is contained in equation III-27 and $\Lambda^{\pm}(\lambda(\alpha),B)$ may be written as

$$\Lambda^{\pm}(\lambda(\alpha),B)=\alpha^{\pm}(\alpha,B)+f(\alpha,B)\log\left(\frac{1+\alpha}{1-\alpha}\right) \qquad \text{(B-6)}$$

where $f(\alpha,B) = b(e^{-(v_B/v_T)^2(\alpha^2-1)} - 1)$ and b is a constant. By examining the second derivative in equation B-5, we find that, when written out, all the individual terms but two can be integrated by parts again. The derivative of the remaining two terms contains a single pole. Thus, we find

$$N_{SB}(t,B) = \frac{ae^{-\lambda^* t}S(\lambda(\alpha),B)e^{-i\tau\alpha}}{\tau^2\Lambda^+\Lambda^-}\frac{\partial\delta(\alpha)}{\partial\alpha}\Bigg|_{-1}^{1}$$

$$- \frac{ae^{-\lambda^* t}}{\tau^2}\int_{-1}^{1} d\alpha\, e^{-i\tau\alpha}\left\{2S\frac{\partial\delta}{\partial\alpha}\frac{\partial\left(\frac{1}{\Lambda^+\Lambda^-}\right)}{\partial\alpha} + S\delta\frac{\partial^2\left(\frac{1}{\Lambda^+\Lambda^-}\right)}{\partial\alpha^2}\right\}$$

$$+ O\left(\frac{e^{-\lambda^* t}}{t^3}\right) \qquad (B-7)$$

We can readily show that $\int_{-1}^{1} d\alpha e^{-i\tau\alpha} S\delta\frac{\partial^2\left(\frac{1}{\Lambda^+\Lambda^-}\right)}{\partial\alpha^2}$ exists and can be bounded independent of τ. On the other hand, $2S\frac{\partial\delta}{\partial\alpha}\frac{\partial\left(\frac{1}{\Lambda^+\Lambda^-}\right)}{\partial\alpha}$ contains a term proportional to $2S\frac{\partial\delta}{\partial\alpha}\frac{\partial f}{\partial\alpha}\log\left(\frac{1+\alpha}{1-\alpha}\right)$. The derivative of such a term has a simple pole at $\alpha = \pm 1$. However, since $\log\frac{1+\alpha}{1-\alpha}$ is an integrable function over $\alpha \in [-1,1]$, we have that $\int_{-1}^{1} d\alpha\, e^{-i\tau\alpha} 2S\frac{\partial\delta}{\partial\alpha}\frac{\partial\left(\frac{1}{\Lambda^+\Lambda^-}\right)}{\partial\alpha}$ is $O(1)$ in τ. Hence, the asymptotic form of $N_{SB}(t,B)$ is

$$N_{SB}(t,B) = \frac{e^{-\lambda^* t}}{(\lambda^* t)^2}\left\{a_1 + a_2 g(t)\right\} + O\left(\frac{e^{-\lambda^* t}}{(\lambda^* t)^3}\right) \qquad (B-8)$$

where $g(t)$ is bounded in t. Estimates indicate such an expansion should hold for t greater than about 10 msec.

APPENDIX C

OTHER THEORIES OF PULSED NEUTRON EXPERIMENTS

I. ONE-VELOCITY DIFFUSION THEORY

The one-velocity diffusion equation is

$$-D\nabla^2\phi(\underline{r},t) + \Sigma_a\phi(\underline{r},t) = -\frac{1}{v}\frac{\partial\phi(\underline{r},t)}{\partial t} \qquad (C\text{-}1)$$

where the solution must satisfy the conditions

$$\phi(\underline{R},t) = 0, \quad t > 0 ; \quad \phi(\underline{r},0) = q_o(\underline{r})$$

and $\underline{R}$ represents the extrapolated size of the system. Solving by separation of variables yields the long time behavior $\phi(\underline{R},t) \sim a_o e^{-\lambda_o t}$, where the decay constant, λ_o, is given by

$$\lambda_o = v\Sigma_a + vDB^2 \qquad (C\text{-}2)$$

The quantity B^2 is the eigenvalue corresponding to the fundamental spatial mode and, thus, is the buckling.

II. ONE-VELOCITY, ISOTROPIC, ASYMPTOTIC REACTOR THEORY

The one-velocity Boltzmann equation with isotropic scattering and asymptotic reactor theory is

$$\left(\frac{\partial}{\partial t} + v\Sigma_T + iBv\mu\right)\varphi(B,\mu,t) = \frac{v\Sigma_s}{2}\int_{-1}^{1}\varphi(B,\mu',t)\,d\mu' + \frac{q_o}{2}\delta(t) \qquad (C\text{-}3)$$

The Laplace transform of C-3 is

$$(\lambda + v\Sigma_T + iBv\mu)\tilde{\varphi}(B,\mu,\lambda) = \frac{v\Sigma_s}{2}\int_{-1}^{1} \tilde{\varphi}(B,\mu',\lambda)\, d\mu' + \frac{q_o}{2} \qquad (C\text{-}4)$$

and the solution for $\tilde{\varphi}$ is

$$\tilde{\varphi}(B,\mu,\lambda) = \frac{q_o}{2}\left(\frac{1}{\Lambda(\lambda,B)}\right)\left(\frac{1}{\lambda + v\Sigma_T + iBv\mu}\right) \qquad (C\text{-}5)$$

where

$$\Lambda(\lambda,B) = 1 - \frac{\Sigma_s}{B}\tan^{-1}\frac{Bv}{\lambda + v\Sigma_T}\,. \qquad (C\text{-}6)$$

Note that this function is the same as $\Gamma_e(B,v,\lambda)$ defined by equation II-26. The solution $\tilde{\varphi}$ is analytic in the λ-plane except for

i) the set Γ_c: $\lambda + v\Sigma_T + iBv\mu = 0 \quad \mu \in [-1,1]$ (C-7)

ii) the set Γ_d: $\Lambda(\lambda,B) = 0$ (C-8)

where Γ_c and Γ_d correspond to the continuous and discrete spectrum of the Boltzmann transport operator. The function $\Lambda(\lambda,B)$ is the one-velocity dispersion function and its zeros generate the λ_o-vs-B^2 curve.

The sets Γ_c and Γ_d imply the λ-plane structure at the right. By deforming contours, the total solution can be written as

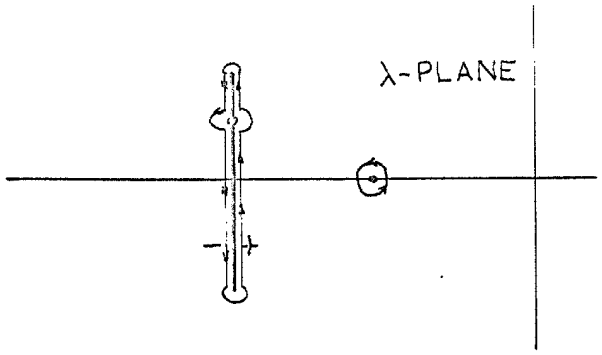

$$\varphi(B,\mu,t) = \sum_i \varphi_{-\lambda_i}(B,\mu)e^{-\lambda_i t} + \frac{q_o}{4} e^{-(v\Sigma_T + iBv\mu)t}\left\{\frac{1}{\Lambda^+(\lambda,B)} + \frac{1}{\Lambda^-(\lambda,B)}\right\}$$

$$+ \frac{1}{4\pi i}\int_{-v\Sigma_T - iBv}^{-v\Sigma_T + iBv} d\lambda e^{\lambda t} \frac{q_o/2}{\lambda + v\Sigma_T + iBv\mu}\left\{\frac{1}{\Lambda^+(\lambda,B)} - \frac{1}{\Lambda^-(\lambda,B)}\right\} \qquad (C-9)$$

In a manner analogous to that used in chapters II and III, one can deform the contour in an alternative form by using the analytic continuation of $\tilde{\varphi}(B,\mu,\lambda)$ past Γ_c. The analytic continuation of $\Lambda(\lambda,B)$ is given by

$$\Lambda_c(\lambda,B) = 1 - \frac{\Sigma_s}{B}\left(\mathrm{Tan}^{-1}\left(\frac{Bv}{\lambda + v\Sigma_T}\right) + \pi\right)$$

i.e., one obtains $\Lambda_c(\lambda,B)$ by extending the definition of the arctangent. The symbol Tan^{-1} stands for the principle determination of the arctangent.

The dispersion curve obtained by solving C-8 is

$$\lambda_o = v\Sigma_T - Bv\cot\left(\frac{B}{\Sigma_s}\right)$$

or, expanding in powers of B^2,

$$\lambda_o = v\Sigma_a + \frac{v}{3\Sigma_s}B^2 + \frac{v}{45\,\Sigma_s^3}B^4 + O(B^6)\ ; \quad \left(\frac{B}{\Sigma_s}\right)^2 < \pi^2 \qquad (C-10)$$

Notice that the expansion is valid for $B^2 < B_c^2 \equiv \Sigma_s^2\pi^2$. On the other hand, B^{*2} (that value of B^2 for which $\lambda_o = v\Sigma_T$ is a solution of

C-8) is $B^{*2} = \frac{1}{4} B_c^2$. Thus, when $B^2 < B^{*2}$, C-10 converges to a zero of $\Lambda(\lambda,B)$. However, when $B^{*2} < B^2 < B_c^2$, C-10 converges to a zero of $\Lambda_c(\lambda,B)$.

Since the coefficients of B^4 and higher order terms are positive, the λ_o-vs-B^2 curve is convex.

III. SHIFTED TEMPERATURE MODEL

Beckurts[51] has developed a simple model that is applicable to pulse neutron experiments. In the framework of diffusion theory, the flux is given by

$$\frac{1}{v}\frac{\partial\varphi(\underline{r},E,t)}{\partial t} + \Sigma_T(E)\varphi = D(E)\nabla^2\varphi + \int_o^\infty \Sigma_s(E'\rightarrow E)\varphi(\underline{r},E',t)\,dE' \quad \text{(C-11)}$$

Assuming $\varphi(\underline{r},E,t) = \phi(E)\chi(\underline{r},t)$ and integrating C-11 over all E gives

$$\frac{1}{\overline{v}}\frac{\partial\chi(\underline{r},t)}{\partial t} = -\overline{\Sigma}_a\chi(\underline{r},t) + \overline{D}\nabla^2\chi(\underline{r},t) \quad \text{(C-12)}$$

where $\overline{\Sigma}_a$ and $\overline{D}$ are the normal spectrum average quantities. An equation for the energy density $\overline{E}\cdot n(\underline{r},t) = \int_o^\infty \frac{E}{v}\phi(\underline{r},E,t)\,dE$ is

$$\frac{\overline{E}}{\overline{v}}\frac{\partial\chi(\underline{r},t)}{\partial t} = -\overline{\Sigma}_a\overline{E}\chi(\underline{r},t) + \overline{D}E_D\nabla^2\chi(\underline{r},t)$$

$$+ \chi(\underline{r},t)\int_o^\infty E\left\{\int_o^\infty \Sigma_s(E'\rightarrow E)\phi(E')\,dE' - \Sigma_s(E)\phi(E)\right\}dE \quad \text{(C-13)}$$

where

$$E_D = \frac{\int_0^\infty ED(E)\phi(E)\,dE}{\int_0^\infty D(E)\phi(E)\,dE} \qquad (C-14)$$

Multiplying C-12 by $\overline{E}$ and subtracting from C-13 yields

$$D(E)\frac{\nabla^2\chi}{\chi}(E_D - \overline{E}) = \int_0^\infty\int_0^\infty (E'-E)\Sigma_s(E'-E)\phi(E')\,dE'\,dE\,. \quad (C-14)$$

When $\frac{\nabla^2\phi}{\phi} = 0$ implying no diffusion (infinite medium), the flux is

$$\phi(E) = M(E;T_o) = \frac{E}{(kT)^2}\,e^{-E/kT_o} \qquad (C-16)$$

i.e., the Maxwellian.

We now assume that the spectrum in a finite medium can be represented by a Maxwellian at a shifted temperature, namely, M(E;T). Since we assume $|T-T_o|/T_o << 1$, expand $\phi(E) = M(E;T)$ about $T = T_o$ to obtain

$$\phi(E) = M(E;T_o) + \frac{T-T_o}{T_o}\left(\frac{E}{kT_o} - 2\right)M(E;T_o) + O\left(\frac{T-T_o}{T_o}\right)^2 \qquad (C-17)$$

From this, we have that

$$\int_0^\infty\int_0^\infty (E'-E)\Sigma_s(E'\to E)\phi(E')\,dE'\,dE = \frac{1}{2}k(T-T_o)M_2N \qquad (C-18)$$

where N is the number of atoms per cm^3 and M_2 is the second energy moment of the microscopic scattering kernel, i.e.,

$$M_2 = \frac{1}{(kT_o)^2}\int_0^\infty\int_0^\infty (E'-E)^2M(E';T_o)\sigma_s(E'\to E)\,dE'\,dE \qquad (C-19)$$

Using these results in C-15 yields

$$\frac{T - T_o}{T_o} = \overline{D}\,\frac{\nabla^2\chi}{\chi}\;\;\frac{1 + 2\,\frac{d\ln\overline{D}}{d\ln T}}{NM_2} \tag{C-20}$$

For the pulsed neutron experiment, we assume $\chi(\underline{r},t) = R(\underline{r})e^{-\lambda t}$, where $R(\underline{r})$ is the lowest eigenfunction of $\nabla^2 R + B^2 R(\underline{r}) = 0$ subject to $R(\underline{r})$ vanishing at the extrapolated boundary of the system. This means C-20 becomes

$$\frac{T - T_o}{T_o} = -\overline{D}B^2\;\;\frac{1 + 2\,\frac{d\ln\overline{D}}{d\ln T}}{NM_2} \tag{C-21}$$

which implies $T < T_o$. This effect is called diffusion cooling and results from the preferential leakage of fast neutrons from the system during the decay of the pulse. From C-12, the decay constant is given by

$$\lambda = v_o\Sigma_a(v_o) + \overline{v}\,\overline{D}\,B^2 \tag{C-22}$$

Expanding $\overline{v}\,\overline{D}$ about T_o

$$\overline{v}\,\overline{D} = (\overline{v}\,\overline{D})(T_o) + (T - T_o)\,\frac{d(\overline{v}\,\overline{D})}{dT}\bigg|_{T=T_o} \tag{C-23}$$

means that with $D_o = (\overline{v}\,\overline{D})(T_o)$ and

$$C = T_o\overline{D}\,\frac{d(\overline{v}\,\overline{D})}{dT}\bigg|_{T=T_o}\left(\frac{1 + 2\,\frac{d\ln\overline{D}}{d\ln T}}{NM_2}\right)$$

we obtain

$$\lambda_o = v_o \Sigma_a(v_o) + D_o B^2 - CB^4 \qquad \text{(C-24)}$$

Since C is positive, equation C-24 implies a concave λ_o-vs-B^2 curve in contrast to the one-velocity transport result of appendix C-II. However, the transport effect is generally less than 10% of the spectral or energy effect and diffusion cooling is experimentally observed.

IV. COMPUTATIONAL APPROACHES

Much of the analysis of pulsed neutron experiments is performed with multi-group or discrete ordinate (in energy) diffusion theory computer codes which allow for a rather detailed description of the scattering kernel. Both approaches begin with energy dependent diffusion equation

$$\frac{1}{v}\frac{\partial \varphi(E,B^2,t)}{\partial t} = -[\Sigma_T(E) + D(E)B^2]\phi(E,B^2,t) + \int_o^\infty \Sigma_s(E' \rightarrow E)\phi(E',B^2,t)\, dE' + S(E)\delta(t) \qquad \text{(C-25)}$$

where the spatial dependence is described by a single buckling, B^2. The associated eigenvalue problem is

$$P\varphi = \lambda\varphi \qquad \text{(C-26)}$$

where the operator P is defined by

$$P = (v\Sigma_T(E) + vD(E)B^2) - \int_o^\infty v\Sigma_s(E' \rightarrow E)\, dE' \qquad \text{(C-27)}$$

If we define $\psi(E,B^2,t) = \sqrt{\frac{v}{M(E)}}\,\phi(E,B^2,t)$

$$K(E',E) = \sqrt{vv'\frac{M(E')}{M(E)}}\,\Sigma_s(E'\rightarrow E) = K(E,E') \qquad (C\text{-}28)$$

we obtain the eigenvalue problem $S\psi = \lambda\psi$, where S is given by

$$S = (v\Sigma_T(E) + vD(E)B^2) - \int_o^\infty K(E',E)\,dE' \,. \qquad (C\text{-}29)$$

The corresponding multi-group or discrete ordinate eigenvalue problem is

$$(v_i\Sigma_T(E_i) + v_iD(E_i)B^2)\psi_i - \sum_{j=1}^{N} dE_jK(E_j,E_i)\psi_j = \lambda\psi_j \qquad (C\text{-}30)$$

This symmetrized matrix eigenvalue problem is then solved by diagonalization to obtain the eigenvalues $\lambda_j(B^2)$ and the total solution,

$$\varphi(E,B^2,t) = \sum_j A_j\,\phi_j(E,B^2)e^{-\lambda_j t} \qquad (C\text{-}31)$$

In the discrete ordinates approach, the cross sections of interest are evaluated at certain discrete energy points and are assumed constant in the energy intervals between the points. In contrast, the usual multi-group approach uses group averaged cross sections and the number and spacing of the energy points is chosen to give an adequate representation in the energy ranges where cross sections are rapidly changing.

A multi-group transport theory approach based on asymptotic

reactor theory has been used by Wood to calculate λ_o-vs-B^2 curves for beryllium. We begin with the Boltzmann equation II-5 and consider solutions of the form $\phi(B,E,\mu,t) = \phi(B,E,\mu)e^{-\lambda t}e^{i\underline{B}\cdot\underline{r}}$. Substituting into II-5 and assuming isotropic scattering yields

$$\left(-\frac{\lambda}{v}+\Sigma_T(E)+iB\mu\right)\phi(B,E,\mu,\lambda) = \int_{-1}^{1} d\mu' \int_{o}^{\infty} \Sigma_s(E'\rightarrow E)\phi(B,E',\mu',\lambda)\, dE' . \qquad \text{(C-32)}$$

Divide by $\left(-\frac{\lambda}{v}+\Sigma_T(E)+iB\mu\right)$, integrate over μ, and use $\phi_o(B,E) = \int_{-1}^{1} \phi(B,E,\mu)\, d\mu$ to obtain

$$\phi_o(B,E) = T(B,E,\lambda)\int_{o}^{\infty} \Sigma_s(E' \quad E)\phi_o(B,E')\, dE' \qquad \text{(C-33)}$$

where $T(B,E,\lambda) = \frac{1}{B}\tan^{-1}\frac{Bv}{-\lambda+v\Sigma_T(E)}$. It is equation C-33 which is normally converted to a multi-group form and it is the equation considered by Wood. Notice that with a kernel of the form II-8 for polycrystals, it is convenient to rewrite C-33 as

$$\phi_o(B,E) = \frac{T(B,E,\lambda)}{1-\Sigma_{el}(E)T(B,E,\lambda)}\int_{o}^{\infty} \Sigma_{inel}(E'\rightarrow E)\phi_o(E,E')\, dE' \qquad \text{(C-34)}$$

We can obtain a symmetrized kernel for C-34 by defining

$$\chi_o(B,E) = \phi_o(B,E)\left\{\frac{1-\Sigma_{el}(E)T(B,E,\lambda)}{T(B,E,\lambda)\ M(E)}\right\}^{\frac{1}{2}} \qquad \text{(C-35)}$$

The kernel is

$$K(E',E) = \left\{ \frac{T(B,E,\lambda)T(B,E',\lambda)}{[1-\Sigma_{el}(E)T(B,E,\lambda)][1-\Sigma_{el}(E')T(B,E',\lambda)]} \frac{M(E')}{M(E)} \right\}^{\frac{1}{2}} \Sigma_{inel}(E' \rightarrow E)$$

$$= K(E,E'). \qquad \text{(C-36)}$$

For polycrystals, $\lambda > \lambda^*$ implies $T(B,E,\lambda) < 0$ for $E < E_B$. In this case, one can follow the suggestion in the text and extend the definition of the arctangent to its next determination.

The following outlines the method employed by Wood to solve C-33. With the operator $B = \int_0^\infty K(E',E)\, dE$, we can rewrite the eigenvalue problem as

$$B\chi_o = w(\lambda)\chi_o . \qquad \text{(C-37)}$$

We now replace the integral in B by the finite sum $\sum_{j=1}^{N} a_j K(E_j \rightarrow E_i)\chi_o(B,E_j)$ where a_j and E_j are dependent on the quadrature scheme. Thus, B becomes a matrix and we have

$$[B(\lambda) - w(\lambda)I]\chi_o = 0 \qquad \text{(C-38)}$$

With some manipulation, we can obtain an expression for the rate of change of $w(\lambda)$ with λ, namely, $\frac{dw}{d\lambda} = \frac{\chi_o^T \frac{dB}{d\lambda} \chi_o}{\chi_o^T \chi_o}$. An iteration scheme on λ is now used until the value of w is sufficiently close to 1. Doing this for several B^2 generates the λ_o-vs-B^2 curve.

Rather sophisticated scattering kernels have been coded for use with these multi-group theories. The most widely used is the

Summit code[47] which uses the incoherent approximation to evaluate the inelastic scattering cross sections. For graphite, a model due to Parks is employed which assumes that all the information required is contained in the phonon frequency spectrum. Since graphite is highly anisotropic, it is assumed that the vibration of atoms in the basal planes of the lattice are not coupled to vibrations perpendicular to the planes. Thus, a frequency spectrum is obtained for each type of vibration. This model was used by Ghatak and Honeck[21] in their graphite calculations. For beryllium, the Summit code is used with the frequency spectrum of Young and Koppel[34] (see Lee and Daitch[43]). The elastic scattering which occurs in polycrystals is modeled separately and added on to obtain the total cross section. We should note that all existing scattering codes neglect inelastic, coherent scattering which is important in the sub-Bragg energy range. This probably accounts for the incorrect predictions of λ^*.

APPENDIX D

THE EFFECTS OF EXPANDING THE ELASTIC SCATTERING KERNEL IN LEGENDRE POLYNOMIALS

This appendix examines the effects of anisotropic elastic scattering on the structure of the λ-plane. Begin with the Boltzmann equation

$$\frac{\partial\varphi(\underline{r},v,\underline{\Omega},t)}{\partial t} + \underline{v}\cdot\nabla\varphi + v\Sigma_T(v)\varphi = S_i\varphi + S_e\varphi + q_o(\underline{r},\underline{v})\delta(t) \qquad \text{(D-1)}$$

where

$$S_i = \int_{v',\Omega'} v'\Sigma_{inel}(v'\rightarrow v)\,\varphi(\underline{r},v',\underline{\Omega}',t)\,dv'\,d\Omega' \qquad \text{(D-2)}$$

and

$$S_e = \int_{v',\Omega'} v'\Sigma_{el}^{coh}(v'\rightarrow v;\underline{\Omega}'\rightarrow\underline{\Omega})\varphi(\underline{r},v',\underline{\Omega}',t)\,dv'\,d\Omega' \qquad \text{(D-3)}$$

Assume that S_i is a completely continuous operator and thus does not effect the continuum regions of the λ-plane. Expand the elastic, coherent scattering kernel in Legendre polynomials and assume that the kernel depends only on the cosine of the scattering angle, $\mu_o \equiv \underline{\Omega}\cdot\underline{\Omega}'$.

$$\Sigma_{el}^{coh}(v'\rightarrow v;\underline{\Omega}'\rightarrow\underline{\Omega}) = \Sigma_{el}^{coh}(v'\rightarrow v;\mu_o)$$

$$= \delta(v'-v)\left\{\frac{(\Sigma_{el}^{coh}(v))_{P_o}}{4\pi}P_o(\mu_o) + \frac{3}{4\pi}(\Sigma_{el}^{coh}(v))_{P_1}P_1(\mu_o) + \ldots\right\} \qquad \text{(D-4)}$$

or

$$\Sigma_{el}^{coh}(v' \rightarrow v;\mu_o) = \frac{\delta(v'-v)}{4\pi} \sum_{\ell=0}^{\infty} (2\ell+1) a_\ell(v) P_\ell(\mu_o) \ . \qquad \text{(D-5)}$$

Here, $P_\ell(\mu_o)$ is the ℓth Legendre polynomial and

$$a_\ell(v) \equiv (\Sigma_{el}^{coh}(v))_{P_\ell} \qquad \text{(D-6)}$$

is the P_ℓ component of elastic coherent scattering kernel. The addition theorem for Legendre polynomials can be written in terms of the spherical harmonics, $Y_n^m(\mu,\phi)$.

$$\frac{(2\ell+1)}{4\pi} P_\ell(\mu_o) = \sum_{m=-\ell}^{\ell} Y_\ell^{m\,*}(\mu',\phi') Y_\ell^m(\mu,\phi) \qquad \text{(D-7)}$$

Hence,

$$S_e = \int_{v'} dv'\, \delta(v'-v)\, v' \sum_{\ell=0}^{\infty} \sum_{m=-\ell}^{\ell} a_\ell Y_\ell^m(\mu,\varphi) \int_{-1}^{1} \int_{o}^{2\pi} Y_\ell^{m\,*}(\mu',\phi') \varphi(\underline{r},v',\mu',t) \cdot d\mu' d\phi' \qquad \text{(D-8)}$$

But $\varphi(\underline{r},v',\mu',t)$ does not depend on ϕ' so

$$\int_o^{2\pi} Y_\ell^{m\,*}(\mu',\phi')\, d\phi' = \begin{cases} 0 & m \neq 0 \\ 2\pi Y_\ell^o(\mu') & m = 0 \end{cases} \qquad \text{(D-9)}$$

Since $Y_\ell^o(\mu') = \sqrt{\frac{(2\ell+1)}{4\pi}}\, P_\ell(\mu')$, we have

$$S_e\varphi = \sum_{\ell=0}^{\infty} a_\ell(v) \left(\frac{2\ell+1}{2}\right) P_\ell(\mu) \int_{-1}^{1} P_\ell(\mu') \varphi(\underline{r},v,\mu',t)\, d\mu' \qquad \text{(D-10)}$$

Using this in the Boltzmann equation gives

$$\left(\frac{\partial}{\partial t} + \underline{v}\cdot\nabla + v\Sigma_T(v)\right)\varphi(\underline{r},v,\mu,t)$$

$$= S_i\varphi + \sum_{\ell=0}^{\infty} \frac{2\ell+1}{2} a_\ell(v)P_\ell(\mu)\int_{-1}^{1} P_\ell(\mu')\varphi(\underline{r},v,\mu',t)\,d\mu' + q(\underline{r},\underline{v})\delta(t) \tag{D-11}$$

Laplace transform D-10 in t and use $e^{i\underline{B}\cdot\underline{r}}$ theory to find

$$(\lambda + v\Sigma_T(v) + iBv\mu)\tilde{\varphi}(B,v,\mu,\lambda)$$

$$= S_i\tilde{\varphi} + \sum_{\ell=1}^{\infty} \frac{2\ell+1}{2} a_\ell(v)P_\ell(\mu)\,\tilde{\psi}_\ell(B,v,\lambda) + Q(v,\mu) \tag{D-12}$$

where we define

$$\tilde{\psi}_\ell(B,v,\lambda) = \int_{-1}^{1} P_\ell(\mu')\tilde{\varphi}(B,v,\mu',\lambda)\,d\mu' \,. \tag{D-13}$$

As before, those regions of the λ-plane where $\lambda + v\Sigma_T(v) + iBv\mu = 0$ are excluded. We are interested in the effect on Γ_e of the inclusion of angle dependent terms in $\Sigma_{el}^{coh}(v'\to v;\mu_o)$. Assume $\lambda + v\Sigma_T(v) + iBv\mu \neq 0$, divide by it, multiply by $P_j(\mu)$, and integrate over μ.

$$\tilde{\psi}_j(B,v,\lambda) = \int_{-1}^{1} \frac{P_j(\mu)S_i\tilde{\varphi}(B,v,\mu,\lambda)\,d\mu}{\lambda + v\Sigma_T(v) + iBv\mu}$$

$$+ \sum_{\ell=0}^{\infty} \frac{2\ell+1}{2} a_\ell(v)\,\tilde{\psi}_\ell(B,v,\lambda)\int_{-1}^{1} \frac{P_j(\mu)P_\ell(\mu)\,d\mu}{\lambda + v\Sigma_T(v) + iBv\mu}$$

$$+ \int_{-1}^{1} \frac{P_j(\mu)\,Q(v,\mu)\,d\mu}{\lambda + v\Sigma_T(v) + iBv\mu} \tag{D-14}$$

Let

$$z = i\left(\frac{\lambda + v\Sigma_T(v)}{Bv}\right), \tag{D-15a}$$

$$b_{j\ell}(v) = \left(\frac{2\ell+1}{2}\right)\left(\frac{i}{Bv}\right) a_\ell(v) \int \frac{P_j(\mu)P_\ell(\mu)\, d\mu}{z - \mu} \tag{D-15b}$$

$$c_j(v) = \frac{i}{Bv}\int_{-1}^{1} \frac{P_j(\mu)(S_i\varphi)\, d\mu}{z - \mu} \tag{D-15c}$$

$$q_j(v) = \frac{i}{Bv}\int_{-1}^{1} \frac{P_j(\mu)Q(v,\mu)\, d\mu}{z - \mu} \tag{D-15d}$$

Then

$$\tilde{\psi}_j(B,v,\lambda) - \sum_{\ell=0}^{\infty} b_{j\ell}(v)\tilde{\psi}_\ell(B,v,\lambda) = c_j(v) + q_\ell(v) \tag{D-16}$$

The standard approach is to assume that the sum over ℓ can be truncated after $n+1$ terms and is called the P_n approximation to the kernel. If we do this, we find that, since S_i is completely continuous, $\tilde{\psi}(B,v,\lambda)$ will not be analytic at those λ for which the determinant, D_n,

$$D_n \equiv \begin{vmatrix} 1-b_{oo} & -b_{o1} & \cdots & -b_{on} \\ -b_{10} & 1-b_{11} & \cdots & -b_{1n} \\ \cdot & & & \cdot \\ \cdot & & & \cdot \\ \cdot & & & \cdot \\ -b_{nn} & -b_{n1} & \cdots & 1-b_{nn} \end{vmatrix} \tag{D-17}$$

is zero. For $n = 0$, we have the case of isotropic elastic scattering considered in the thesis and we find

$$\Gamma_e(B,v,\lambda) = 1 - b_{oo} \qquad \text{(D-18)}$$

For $n = 1$, we have

$$D_1 = (1 - b_{oo})(1 - b_{11}) - b_{10}b_{01}$$

and, with $\xi = -\frac{1}{iz}$,

$$D_1 = (1 - \frac{a_o(v)}{Bv}\tan^{-1}\xi)(1 - \frac{3a_1}{Bv}\tan^{-1}\xi) + \frac{3a_o(v)a_1(v)}{(Bv)^2}\left[1 - \frac{\tan^{-1}\xi}{\xi}\right]^2 \qquad \text{(D-19)}$$

The limit of D_1 as $\xi^2 \to 0$ (or as $B^2 \to 0$) is

$$D_{1_{\xi=0}} = \left(1 - \frac{a_o(v)}{\lambda + v\Sigma_T(v)}\right)\left(1 - \frac{a_1(v)}{\lambda + v\Sigma_T(v)}\right) = 0 \qquad \text{(D-20)}$$

Recalling that $a_o(v) \equiv \Sigma_{el}^{coh}(v)$ and $a_1(v) \equiv (\Sigma_{el}^{coh}(v))_{P_1}$, the P_1 component of the elastic scattering kernel, we find two solutions of D-20,

$$\lambda_1(B=0,v) = -v\Sigma_i(v) \qquad v \in (v_B, \infty) \qquad \text{(D-21a)}$$

and

$$\lambda_2(B=0,v) = -v(\Sigma_T(v) - (\Sigma_{el}^{coh}(v))_{P_1}) \quad v \in (v_B, \infty) \qquad \text{(D-21b)}$$

At $v = v_B$, $(\Sigma_{el}^{coh}(v_B))_{P_1}$ is negative[34] implying $\lambda_2(0, v_B)$ is in the area described in figure 7. Since $v_B\Sigma_i(v_B) = \lambda^*$, we have $\lambda_1(0, v_B) = -\lambda^*$. Thus, at $B^2 = 0$, $\lambda_1(B, v_B) = -\lambda_{el}$. Calculations indicate $|\Sigma_{el}^{coh}(v)|_{P_1} < \Sigma_{el}^{coh}(v)$ for all v which implies $\lambda_2(B=0,v) < \lambda_1(B=0,v)$

for all v.

To examine the behavior of $\lambda_1(B,v)$ and $\lambda_2(B,v)$ for small B^2 (small ξ^2), expand the functions in D_1 about $B^2 = 0$ ($\xi^2 = 0$).

$$D_1 = (\lambda + v\Sigma_T(v) - a_o + \frac{a_o}{3}\xi^2)(\lambda + v\Sigma_T - a_1 + \frac{3a_1}{5}\xi^2)$$

$$+ \frac{a_o a_1}{3}\xi^2 + O(\xi^4) = 0 \qquad \text{(D-22)}$$

$|\lambda_1(B,v) - \lambda_1(B=0,v)| = O(\xi^2)$ and $|\lambda_2(B,v) - \lambda_2(B=0,v)| = O(\xi^2)$ because $\xi^2 << 1$. Thus, near $\lambda_1(B,v)$ we find

$$\lambda_1(B,v) = -v\Sigma_i(v) - \frac{B^2}{3\Sigma_{el}^{coh}(v)}\left[1 + \frac{(\Sigma_{el}^{coh}(v))_{P_1}}{(\Sigma_{el}^{coh}(v))_{P_o} - (\Sigma_{el}^{coh}(v))_{P_1}}\right] + O(B^4) \qquad \text{(D-23)}$$

At $v = v_B$, we have

$$\lambda_1(B,v_B) = -\left(\lambda^* + \frac{B^2}{3(\Sigma_{el}(v))_{P_o}}\left\{1 + \frac{(\Sigma_{el}^{coh}(v_B))_{P_1}}{(\Sigma_{el}(v_B))_{P_o} - (\Sigma_{el}^{coh}(v_B))_{P_1}}\right\}\right) + O(B^4)$$

which is equation II-49 in the text. Analogously, we find

$$\lambda_2(B,v) = \lambda_2(0,v) - vB^2\left(\frac{(\Sigma_{el}^{coh}(v))_{P_1}}{(\Sigma_{el}^{coh}(v))_{P_o}}\left[\frac{3}{5(\Sigma_{el}^{coh}(v))_{P_o}}\right.\right.$$

$$\left.\left. - \frac{1}{3\left\{(\Sigma_{el}^{coh}(v))_{P_o} - (\Sigma_{el}^{coh}(v))_{P_1}\right\}}\right] + O(B^4) \qquad \text{(D-25)}$$

Since $\lambda_2(0,v)$ lies in the area in figure 7 and since

$\lambda_2(B,v) - \lambda_2(0,v) = 0(B^2)$, this root remains in the area.

For an n term expansion, we find that

$$\lambda_{i+1}(B=0,v) = -v(\Sigma_T(v) - (\Sigma_{el}^{coh}(v))_{P_i}), \quad i = 0,1,\ldots,n-1 \tag{D-26}$$

because the off-diagonal terms of D_n in equation D-17 are zero at B = 0. By examining the integrals in b_{ij}, we find that $1 - b_{ii}$ is $O(1)$, $b_{i,i+1}$ and $b_{i+1,i}$ are $O(B)$, $b_{i+2,i}$ and $b_{i,i+2}$ are $O(B^2)$, etc. Thus, we find the elements of D_n behavior, for small ξ, as

$D_n =$

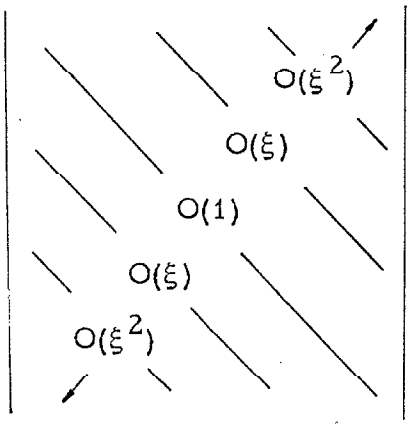

(D-27)

To see this, consider the integral

$$I_{j\ell}(z) = \frac{i}{Bv}\int_{-1}^{1} \frac{P_j(\mu)P_\ell(\mu)\, d\mu}{z-\mu} \tag{D-28}$$

which forms the core of $b_{j\ell}$. We are interested in the large $|z|$ (small B) behavior. Thus, rewrite $I_{j\ell}(z)$ as

$$I_{j\ell}(z) = \frac{1}{\lambda + v\Sigma_T(v)}\int_{-1}^{1} \frac{P_j(\mu)P_\ell(\mu)\, d\mu}{(1 - \frac{\mu}{z})} \tag{D-29}$$

and, for $\left|\frac{\mu}{z}\right| << 1$,

$$I_{j\ell}(z) = \frac{1}{\lambda + v\Sigma_T(v)} \int_{-1}^{1} P_j(\mu) P_\ell(\mu) \sum_{n=0}^{\infty} \left(\frac{\mu}{z}\right)^n d\mu \qquad \text{(D-29a)}$$

We can interchange the order of summation and integration because the series converges uniformly. Use now the orthogonality of the Legrende Legrendre polynomials,

$$\int_{-1}^{1} P_j(\mu) P_\ell(\mu)\, d\mu = \delta_{j\ell} \qquad \text{(D-30a)}$$

the recursion relation,

$$(2j+1)P_j(\mu) = (j+1)P_{j+1}(\mu) + jP_{j-1}(\mu) \qquad \text{(D-30b)}$$

and the formula

$$\int_{-1}^{1} \mu P_j(\mu) P_\ell(\mu)\, d\mu = 0 \qquad |j-\ell| > 1 \qquad \text{(D-30c)}$$

Thus, for $j \neq \ell$, D-29a is

$$I_{j\ell}(z) = \frac{1}{\lambda + v\Sigma_T(v)} \int_{-1}^{1} P_i(\mu) P_j(\mu) \left(\frac{\mu}{z} + \left(\frac{\mu}{z}\right)^2 + \ldots\right) d\mu \qquad \text{(D-31)}$$

Relation D-30c implies that terms of order $1/z$ (O(B)) are non-zero only if $|i-j| = 1$, i.e., that $b_{i,i+1}$ and $b_{i+1,i}$ are O(B). Thus, if $|j-\ell| > 1$, $b_{j\ell}$ is $O(B^2)$ or higher.

To illustrate how one determines the order of these terms, consider the coefficient of $1/z^2$.

$$\frac{1}{z^2} \int_{-1}^{1} \mu \cdot \mu^2 P_j(\mu) P_\ell(\mu)\, d\mu$$

Using D-30b and D-30c, we find this coefficient is non-zero only if $|i+1-j| = 0$ or 1 and $|i-1-j| = 0$ or 1. Thus, $b_{i+2,i}$ and $b_{i,i+2}$ are $O(B^2)$. If we write the coefficient of $1/z^n$ as

$$\int_{-1}^{1} \mu^{n-1}(\mu P_j(\mu))P_\ell(\mu)\, d\mu$$

and use D-30b successively until D-30c applies, we find $b_{i,i+n}$ and $b_{i+n,i}$ are $O(B^n)$. These order estimates imply that, for any order Legendre expansion n, the edge of the elastic continuum is, to terms of order B^2, given by equation D-24. This is the result presented in the text.

APPENDIX E

CONTINUITY OF THE SOLUTION IN B^2

To examine the question of the continuity of the neutron density in B^2, consider the Boltzmann equation in the form

$$\frac{\partial \chi(B,v,\mu,t)}{\partial t} + w(B,v,\mu)\chi(B,v,\mu,t)$$

$$= \int_0^\infty \int_{-1}^1 k(v',v)\chi(B,v',\mu',t)\, dv'\, d\mu' + \frac{Q(v)}{2\sqrt{M(v)}} \qquad \text{(E-1)}$$

where

$$w(B,v,\mu) = v\Sigma_T(v) + iBv\mu \qquad \text{(E-2)}$$

$$k(v',v) = v'\Sigma_s(v',v)\sqrt{\frac{M(v')}{M(v)}} = k(v,v'). \qquad \text{(E-3)}$$

Integrating E-1 directly gives

$$\chi(B,v,\mu,t) = \frac{Q(v)}{2\sqrt{M(v)}}\, e^{-w(B,v,\mu,t)}$$

$$+ \int_0^t \int_0^\infty \int_{-1}^1 e^{-w(B,v,\mu)(t-t')} k(v',v)\chi(B,v',\mu',t')$$

$$\cdot\, d\mu'\, dv'\, dt'. \qquad \text{(E-4)}$$

It follows from integration over μ that

$$n(B,v,t) = \frac{Q(v)}{\sqrt{M(v)}} K(B,v,t)$$

$$+ \int_0^t \int_0^\infty K(B,v,t-t')k(v',v)n(B,v',t')\, dv'\, dt' \qquad \text{(E-5)}$$

where

$$n(B,v,t) = \int_{-1}^{1} \chi(B,v,\mu,t)\, d\mu \qquad (E\text{-}6)$$

$$K(B,v,t) = e^{-v\Sigma_T(v)t} \frac{\sin(Bvt)}{(Bvt)} \qquad (E\text{-}7)$$

We will show that $n(B,v,t)$ is jointly continuous in B and t for any fixed v. We include isotropic, elastic scattering which implies that $\Sigma_T(v)$ has a finite number of finite discontinuities, i.e., it is piecewise continuous in v.

Let

$$f(B,v,t) = \frac{Q(v)}{\sqrt{M(v)}} K(B,v,t) \qquad (E\text{-}8)$$

The following conditions hold:

1. $f(B,v,t)$ is jointly continuous in B and t for any fixed v.
2. $K(B,v,t)$ is jointly continuous in B and t for any fixed v.
3. For reasonable $Q(v)$ (such as $Q(v) = M(v)$),
$$|f(B,v,t)| \le \frac{Q(v)}{\sqrt{M(v)}} e^{-v\Sigma_T(v)t} < N .$$
4. $|K(B,v,t)| \le e^{-v\Sigma_T(v)t} \le 1 .$
5. $\int_0^\infty k(v',v)\, dv' < M .$

The first four conditions are clear. The effect of elastic scattering on condition 5 is as follows:

$$\int_o^\infty k(v',v)\,dv' = \int_o^\infty k_i(v',v)\,dv' + \int_o^\infty v\Sigma_{el}(v)\sqrt{\frac{M(v')}{M(v)}}\;\delta(v'-v)\,dv' \tag{E-9}$$

$$\int_o^\infty k(v',v)\,dv' = \int_o^\infty k_i(v',v)\,dv' + v\Sigma_{el}(v)\ . \tag{E-10}$$

$v\Sigma_{el}(v)$ is bounded for all v. The work of Kuščer and Corngold[32] on the inelastic scattering kernel in solids indicates the integral of $k_i(v',v)$ is bounded.

We now construct the solution to equation E-5 by iteration, namely,

$$n(B,v,t) = \varphi_o(B,v,t) + \varphi_1(B,v,t) + \varphi_2(B,v,t) + \ldots \tag{E-11}$$

where

$$\varphi_n(B,v,t) = \int_o^t\int_o^\infty K(B,v,t-t')k(v',v)\varphi_{n-1}(B,v',t')\,dv'\,dt' \tag{E-12}$$

Here, $\varphi_o(B,v,t) = f(B,v,t)$ and is continuous, jointly, in B and t. Since $K(B,v,t-t')$ is jointly continuous in B, t and t', it follows that all the $\varphi_n(B,v,t)$ are jointly continuous in B and t.

We now show, using the Weierstrass M-test[38], that the series E-11 converges uniformly in B and t. To do this, proceed as follows:

$$|\varphi_o(B,v,t)| < N$$

$$|\varphi_1(B,v,t)| \le \int_o^t\int_o^\infty |K(B,v,t-t')|\,|k(v',v)|\,|\varphi_o(B,v',t')|\,dv'\,dt'$$

$$|\varphi_1(B,v,t)| < NMt$$

$$|\varphi_2(B,v,t)| < N\frac{(Mt)^2}{2!}$$

$$\vdots$$

$$|\varphi_n(B,v,t)| < N\frac{(Mt)^n}{n!} \quad .$$

N and M are independent of B, v, and t. Thus, on any bounded interval $[0,b]$, the moduli of the terms in the series E-11 do not exceed the positive numbers

$$N\frac{(Mb)^n}{n!}$$

which form a convergent series. Therefore, the series E-11 is absolutely and uniformly convergent in $[0,b]$. Since each term in the series E-11 is jointly continuous in B and t, it follows that the sum, $n(B,v,t)$, is a continuous function of B and t.

LIST OF REFERENCES

1. G. von Dardel, "A Study of the Interaction of Neutrons with Moderating Materials," Phys. Rev. 94, No. 5, 1272 (1954).

2. G. von Dardel and N. Sjostrand, "Diffusion Parameters of Thermal Neutrons in Water," Phys. Rev. 96, No. 5, 1245 (1954).

3. J. Dorning, "Time-Dependent Neutron Thermalization in Finite Media," BNL-11680, Brookhaven National Laboratory Report (1967).

4. K. H. Beckurts, "Transient Effects in Space, Time, and Energy," Proceedings of the Brookhaven Conference on Neutron Thermalization, Vol. III, RE-1 (1962).

5. A. V. Antonov et al., "A Study of Neutron Diffusion in Beryllium, Graphite, and Water by the Impulse Method," Int. Conf. on Peaceful Uses of Atomic Energy, V, 3 (Geneva, 1955).

6. M. Nelkin, "The Decay of a Thermalized Neutron Pulse," Nucl. Sci. & Eng. 7, 210 (1960).

7. J. Lehner and G. M. Wing, "Solution of the Linearized Boltzmann Transport Equation for the Slab Geometry," Duke Math. Journal 23, 125 (1956).

8. R. Van Norton, "On the Real Spectrum of a Mono-Energetic Neutron Transport Operator," Comm. Pure Appl. Math. IX, 487 (1962).

9. K. Jorgens, "An Asymptotic Expansion in the Theory of Neutron Transport," Comm. Pure Appl. Math. XI, 219 (1958).

10. N. Corngold, "Some Transient Phenomena in Thermalization, I. Theory," Nucl. Sci. & Eng. 19, 80 (1964).

11. M. Nelkin, "Asymptotic Solutions of the Transport Equation for Thermal Neutrons," Physica 29, 261 (1963).

12. L. Sirovich and J. Thurber, "Plane Wave Propogation in Kinetic Theory," J. Math. Phys. 8, 888 (1967).

13. S. Albertoni and B. Montagnini, "On the Spectrum of Neutron Transport Equation in Finite Bodies," J. Math. Anal. & Appl. 13, 19 (1966).

14. S. Ukai, "On the Initial-Value Problem of the Transport Equation for a Moderator Slab," J. Nucl. Sci. & Tech. 3, 430 (1967).

15. A. Mockel, "On the Disappearance of Discrete Decay Constants in Slabs," Nucl. Sci. & Eng. 26, 279 (1966).

16. W. M. Andrews, "Measurement of the Temperature Dependence of Neutron Diffusion Properties in Beryllium using a Pulsed Source Technique," University of California, Lawrence Radiation Laboratory Report UCRL-6083 (1960).

17. I. F. Zhezherun, "Pulsed Beam Method of Investigating Neutron Diffusion in Beryllium," J. Nucl. Energy Parts A/B 19, 284 (1965).

18. F. A. Kloverstrom and T. T. Komoto, "Diffusion Cooling in Beryllium and Graphite," Trans. Am. Nucl. Soc. 1, 94 (1958).

19. H. Klose, M. Küchle, and W. Reichardt, "Pulsed Neutron Measurements in Graphite," Proceedings of the Brookhaven Conference on Neutron Thermalization, Vol. III, 935 (1962).

20. A. I. M. Ritchie and M. T. Rainbow, "Some Measurements of Decay Constants Close to $(v\Sigma_{inel})_{min}$ in Pulsed BeO Assemblies," Nuc. Sci. & Eng. 28, 306 (1967).

21. A. K. Ghatak and H. C. Honeck, "On the Feasibility of Measuring Higher Time Decay Constants," Nucl. Sci. & Eng. 21, 227 (1965).

22. L. S. Kothari, "Decay Constant of a Neutron Pulse Inside a Finite Solid Moderator Assembly," Nucl. Sci. & Eng. 23, 402 (1965).

23. I. C. Goyal and L. S. Kothari, "The Decay of Equilibrium Neutron Flux Inside Beryllium Blocks at Different Temperatures," Nucl. Sci. & Eng. 23, 159 (1965).

24. I. C. Goyal, A. K. Ghatak, and L. S. Kothari, "On the Persistant Change in the Measured Values of the Decay Constant in Beryllium," J. Nucl. Energy Parts A/B 20, 667 (1966).

25. N. Corngold and K. Durgun, "Analysis of Pulsed-Neutron Experiments in Moderators via a Simple Model," Nucl. Sci. & Eng. 29, 354 (1967).

26. N. Corngold, "Theoretical Interpretation of Pulsed Neutron Phenomena," IAEA. Symp. on Pulsed Neutron Research, Vol. I, 199 (I.A.E.A., Vienna, 1965).

27. M. Borysiewicz and J. Mika, "Time Dependent Thermalization with Elastic Scattering," IAEA Symp. on Neutron Thermalization and Reactor Spectra (Ann Arbor, 1967).

28. I. Kuščer, "Advances in Neutron Thermalization Theory," IAEA Symp. on Neutron Thermalization and Reactor Spectra, (Ann Arbor, 1967).

29. A. Weinberg and E. Wigner, The Physical Theory of Neutron Chain Reactors (The University of Chicago Press, Chicago, 1958).

30. M. M. R. Williams, The Slowing Down and Thermalization of Neutrons (John Wiley and Sons, Inc., New York, 1966).

31. R. Dorfman, "Note on the Linearized Boltzmann Integral Equation for Rigid Sphere Molecules," Proc. N.A.S. 50, 804 (1963).

32. I. Kuščer and N. Corngold, "Discrete Relaxation Times in Neutron Thermalization," Phys. Rev. 139A, A981 (1965).

33. L. Kothari and K. Singwi, "Interaction of Thermal Neutrons with Solids," in Solid State Physics Vol. 8, 110, F. Seitz and D. Turnbull, eds. (Academic Press, New York, 1959).

34. J. Young and J. Koppel, "Scattering Kernel for Beryllium," Nucl. Sci. & Eng. 19, 367 (1964).

35. J. R. Beyster, J. M. Neill, and J. C. Young, "Recent Developments in Integral Neutron Thermalization," in Reactor Physics in the Resonance and Thermal Regions, vol. I, 151 (The M.I.T. Press, Cambridge, 1966).

36. K. M. Case, "Elementary Solutions of the Transport Equation and their Application," Ann. Phys. 9, 1 (1960).

37. N. I. Muskhelishvili, Singular Integral Equations (P. Noordhoff N.V., Groningen, Holland, 1953).

38. E. Hille, Analytic Function Theory (Ginn and Company, New York, 1959).

39. N. Corngold, P. Michael, and W. Wollman, "The Time Decay Constants in Neutron Thermalization," Nucl. Sci. & Eng. 15, 13 (1963).

40. F. G. Tricomi, Integral Equations (Interscience Publishers, Inc., New York, 1957).

41. C. S. Shapiro and N. Corngold, "Time Eigenvalues and Degenerate Kernels in Neutron Thermalization," Phys. Rev. 137A, A1686 (1965).

42. M. M. R. Williams, "The Energy-Dependent Milne Problem with a Simple Scattering Kernel," Nucl. Sci. & Eng. 18, 260 (1964).

43. R. R. Lee and P. B. Daitch, "An Analysis of Neutron Thermalization in Beryllium," Nucl. Sci. & Eng. 28, 247 (1967).

44. J. Wood, "Pseudo-Exponential Decay of a Neutron Pulse in Small Beryllium Systems," J. Nucl. Energy Parts A/B 20, 649 (1966).

45. G. De Saussure, "A Note on the Measurement of Diffusion Parameters by the Pulsed Source Technique," Nucl. Sci. & Eng. 12, 433 (1962).

46. J. Wood, "Time and Space Eigenvalues of the Boltzmann Equation," IAEA Symp. on Pulsed Neutron Research, Vol. I, 219 (I.A.E.A., Vienna, 1965).

47. J. Bell, "Summit, An IBM-7090 Program for the Computation of Crystalline Scattering Kernels," General Atomic Report, GA-2492 (1962).

48. D. E. Parks, "The Calculation of Thermal Neutron Scattering Kernels in Graphite," General Atomic Report, GA-2438 (1961).

49. R. R. Fullwood et al., "The Effects of Coherent Scattering on the Thermalization of Neutrons in Beryllium," Nucl. Sci. & Eng. 18, 138 (1964).

50. V. Ardente and G. Rossi, "The Decay of a Thermal Neutron Pulse in a Finite Coherent Moderator," IAEA Sump. on Neutron Thermalization and Reactor Spectra, (Ann Arbor, 1967).

51. K. H. Beckurts and W. Wirtz, Neutron Physics (Springer-Verlag, New York, 1964).

52. C. H. Reed, C. N. Henry, and A. A. Usner, "Decay of Thermalized Neutron Fields in Graphite," Nucl. Sci. & Eng. 30, 362 (1967).

53. E. G. Silver, "Experimental Investigation of Persisting Changes in the Thermal Neutron Decay Constant in Finite Media of Ice and Beryllium as a Function of Temperature and Buckling," Proceedings of the Brookhaven Conference on Neutron Thermalization, Vol. III, 981 (1962).

54. C. Cercignani, "Unsteady Solutions of Kinetic Models with Velocity-Dependent Collision Frequency," Ann. Phys. 40, 454 (1966).

55. J. J. Duderstadt, "The Theory of the Propogation of Plane Wave Disturbances in a Distribution of Neutrons," submitted for publication to J. Math. Phys. (Dec., 1967).

56. M. M. R. Williams, "Space, Time and Energy Separability in the Pulsed Neutron Experiment," Nukleonik 10, 252 (1967).

57. I. N. Vekua, Generalized Analytic Functions (Pergamon Press, Oxford, 1962).

58. E. Starr and G. A. Price, "Measurement of the Diffusion Parameters of Graphite and Graphite-Bismuth by Pulsed Neutron Methods," Proceedings of the Brookhaven Conference on Neutron Thermalization, Vol. III, 1034 (1962).

59. S. K. Davis, J. A. DeJuren, and M. Reier, "Pulsed-Decay and Extrapolation-Length Measurements in Graphite," Nucl. Sci. & Eng. 23, 74 (1965).

60. K. Serdula and J. Young, "Neutron Thermalization Studies in Graphite," Nucl. Sci. & Eng. 22, 40 (1965).

61. D. J. Hughes, Pile Neutron Research (Addison-Wesley Publishing Company, Inc., Cambridge, Mass., 1953).

62. G. E. Bacon, Neutron Diffraction (Claredon Press, Oxford, Second Edition, 1962).

63. P. A. Egelstaff, "The Slow-Neutron Cross-Section of Graphite," J. Nuclear Energy 5, 203 (1957).

64. P. G. Khubchandani, L. S. Kothari, and K. S. Singwi, "Thermal Inelastic Scattering of Cold Neutrons in Polycrystalline Graphite. II," Phys. Rev. 110, 70 (1958).

65. R. Bednarz, "Spectrum of the Boltzmann Operator with an Isotropic Thermalization Kernel," IAEA Sym. on Pulsed Neutron Research, Vol. I, 259 (Karlsruhe, 1965).

66. N. Corngold, "Some Recent Results in the Theory of the Transport of Thermal Neutrons," AMS Sym. on Transport Theory (1967).

67. E. Barnard et al., "Thermalization of Neutrons in Graphite," Proceedings of the Brookhaven Conference on Neutron Thermalization, Vol. III, 805 (1962).

68. Charles Kittel, Introduction to Solid State Physics (John Wiley and Sons, Inc., New York, Third Edition, 1966).

69. J. Arkuszewski, "Milne Problem for Thermal Neutrons with Absorption," Nucl. Sci. & Eng. 27, 104 (1967).